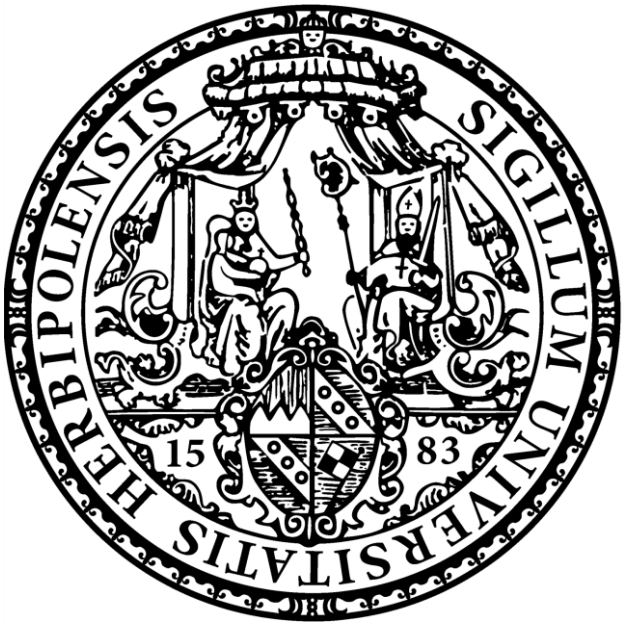

The role of WASH complex subunit Strumpellin in platelet function

Die Rolle der WASH-Komplexuntereinheit Strumpellin in der Thrombozytenfunktion

Doctoral thesis for a medical doctoral degree
at the Graduate School of Life Sciences,
Julius-Maximilians-Universität Würzburg,
Section Biomedicine

submitted by

Lucy Honor Reil
from Forchheim, Germany

Würzburg, 2021

Submitted on: .....

Office stamp

Members of the Thesis Committee:

Chairperson:	Prof. Dr. Alma Zernecke-Madsen
Primary Supervisor:	Dr. Markus Bender
Supervisor (Second):	Prof. Dr. Antje Gohla
Supervisor (Third):	Prof. Dr. Andreas Beilhack

Date of Public Defence: .....

Date of Receipt of Certificates: .....

Summary

Strumpellin is a member of the highly conserved pentameric WASH complex, which stimulates the Arp2/3 complex on endosomes and induces the formation of a branched actin network. The WASH complex is involved in the formation and stabilisation of endosomal retrieval subdomains and transport carriers, into which selected proteins are packaged and subsequently transported to their respective cellular destination, e.g. the plasma membrane. Up until now, the role of Strumpellin in platelet function and endosomal trafficking has not been researched. In order to examine its role, a conditional knockout mouse line was generated, which specifically lacked Strumpellin in megakaryocytes and platelets.

Conditional knockout of Strumpellin resulted in only a mild platelet phenotype. Loss of Strumpellin led to a decreased abundance of the αIIbβ3 integrin in platelets, including a reduced αIIbβ3 surface expression by approximately 20% and an impaired αIIbβ3 activation after platelet activation. The reduced surface expression of αIIbβ3 was also detected in megakaryocytes. The expression of other platelet surface glycoproteins was not affected. Platelet count, size and morphology remained unaltered. The reduction of αIIbβ3 expression in platelets resulted in a reduced fibrinogen binding capacity after platelet activation. However, fibrinogen uptake under resting conditions, although slightly delayed, as well as overall fibrinogen content in Strumpellin-deficient platelets were comparable to controls. Most notably, reduced αIIbβ3 expression did not lead to any platelet spreading and aggregation defects *in vitro*. Furthermore, reduced WASH1 protein levels were detected in the absence of Strumpellin.

In conclusion, loss of Strumpellin does not impair platelet function, at least not *in vitro*. However, the data demonstrates that Strumpellin plays a role in selectively regulating αIIbβ3 surface expression. As a member of the WASH complex, Strumpellin may regulate αIIbβ3 recycling back to the platelet surface. Furthermore, residual WASH complex subunits may still assemble and partially function in the absence of Strumpellin, which could explain the only 20% decrease in αIIbβ3 surface expression. Nonetheless, the exact mechanism still remains unclear.

Zusammenfassung

Strumpellin ist Teil des hoch konservierten, pentameren WASH-Komplexes, der den Arp2/3-Komplex auf Endosomen aktiviert und somit die Bildung eines verzweigten Aktinnetzwerkes ermöglicht. Der WASH-Komplex beteiligt sich an der Bildung und Stabilisierung von endosomalen Retrieval-Subdomänen und Transportvesikel. In letztere werden Proteine verpackt und anschließend zu ihrem Bestimmungsort innerhalb der Zelle, z.B. der Zellmembran, transportiert. Die Rolle von Strumpellin in der Thrombozytenfunktion und im endosomalen Transport wurde bislang noch nicht untersucht. Hierfür wurde eine konditionale Knockout-Mauslinie generiert, die weder in Megakaryozyten noch in Thrombozyten Strumpellin aufwies.

Der konditionale Knockout von Strumpellin hatte nur einen milden Thrombozytenphänotyp zur Folge. Der Verlust von Strumpellin resultierte in einem verminderten Gesamtproteingehalt von αIIbβ3-Integrin in Thrombozyten, einschließlich einer ca. 20-prozentigen Reduktion der Oberflächenexpression von αIIbβ3 und einer verringerten αIIbβ3-Aktivierung nach Thrombozytenaktivierung. Die reduzierte Oberflächenexpression von αIIbβ3 konnte auch in Megakaryozyten nachgewiesen werden. Die Expression anderer Oberflächenglykoproteine war nicht betroffen. Thrombozytenzahl, -größe und -morphologie blieben unverändert. Die reduzierte αIIbβ3-Expression in Thrombozyten führte zu einer verminderten Fibrinogenbindungskapazität nach Thrombozytenaktivierung. Die Fibrinogenaufnahme unter ruhenden Bedingungen, trotz initialer Verzögerung, und der Gesamtproteingehalt von Fibrinogen waren hingegen vergleichbar mit Kontrollproben. Interessanterweise verursachte die reduzierte αIIbβ3-Expression keine *in vitro* Spreading- und Aggregationsdefekte der Thrombozyten. Ein verminderter WASH1-Proteingehalt konnte ebenfalls nachgewiesen werden.

Abschließend lässt sich sagen, dass der Verlust von Strumpellin die Thrombozytenfunktion, zumindest *in vitro*, nicht beeinträchtigt. Die Daten zeigen jedoch, dass Strumpellin eine selektive Rolle in der Regulierung der αIIbβ3-Oberflächenexpression spielt. Als WASH-Komplexuntereinheit könnte Strumpellin möglicherweise das Recycling von αIIbβ3 zurück zur Thrombozytenoberfläche regulieren. Zudem könnten verbleibende WASH-Komplexuntereinheiten trotz fehlendem Strumpellin weiterhin einen funktionsfähigen Komplex bilden. Dies könnte unter anderem die nur 20-prozentige Reduktion der αIIbβ3 Oberflächenexpression erklären. Der genaue Mechanismus ist jedoch noch nicht bekannt.

Contents

List of tables

List of figures

List of abbreviations

ADP	Adenosine diphosphate
AP(s)	Adaptor protein(s)
APS	Ammonium peroxidsulfate
Arf	ADP-ribosylation factor
ARID	Autosomal-recessive intellectual disability
Arp2/3	Actin-related protein 2/3
ATP	Adenosine triphosphate
BAR	Bin-Amphiphysin-Rvs
bp	Base pair
BSA	Bovine serum albumin
C16orf62	Chromosome 16 open reading frame 62
$C_2H_7AsO_2$	Cacodylic acid
$CaCl_2$	Calcium chloride
CAV	Caveolin
CCC	COMMD/CCDC22/CCDC93
CCDC	Coiled coil domain containing
CIMPR	Cation-independent mannose-6-phosphate receptor
CLEC-2	C-type lectin-like type II transmembrane receptor
CLSM	Confocal laser scanning microscopy
COMMD	Copper metabolism MURR1 domain protein family
CRP	Collagen-related peptide
CVX	Convulxin
Da	Dalton
DAPI	4’,6-diamidino-2-phenylindole
DMS	Demarcation membrane system
DNA	Deoxyribonucleic acid
dNTP	Deoxynucleotide triphosphate
DSCR3	Down syndrome critical region 3
DTS	Dense tubular system
ECL	Enhanced chemiluminescence
ECM	Extracellular matrix
EDTA	Ethylene diamine tetra acetic acid
EE	Early endosome
EGFR	Epidermal growth factor receptor
EGTA	Ethylene glycol tetra acetic acid
ELISA	Enzyme linked immunosorbent assay
ER	Endoplasmic reticulum
ERC	Endosomal recycling compartment
ERGIC	ER-Golgi intermediate compartment
ES	Embryonic stem
ESCRT	Endosomal sorting complexes required for transport
FACS	Fluorescence-activated cell sorting
F-actin	Filamentous actin, also known as microfilaments
FAM21	Family with sequence similarity 21
FCS	Fetal calf serum
FERM	Four-point-one, ezrin, radixin, moesin
FITC	Fluorescein isothiocyanate
for	forward
FSC	Forward-scatter
G	Gauge
GAPDH	Glyceraldehyde 3-phosphate dehydrogenase
GBD	GTPase-binding domain
GP	Glycoprotein
H&E	Haematoxylin and eosin

HCl	Hydrogen chloride
HEPES	4-(2-hydroxyethyl)-1-piperazineethanesulfonic acid
HRP	Horseradish peroxidase
HSP	Hereditary spastic paraplegia
Ig(s)	Immunoglobulin(s)
ILV(s)	Intraluminal vesicle(s)
JMY	Junction-mediating regulatory protein
KCl	Potassium chloride
KH_2PO_4	Monopotassium phosphate
KO	Knockout
LDLR	Low-density lipoprotein receptor
LE	Late endosome
MAGE-L2	Melanoma antigen gene L2
MEFs	Mouse embryonic fibroblasts
MFI	Mean fluorescence intensity
$MgCl_2$	Magnesium chloride
MK(s)	Megakaryocyte(s)
MVB(s)	Multivesicular body/bodies
n.s.	Not significant
Na	Sodium
Na_2CO_3	Sodium carbonate
Na_2HPO_4	Disodium hydrogen phosphate
NaCl	Sodium chloride
NaH_2PO_4	Sodium dihydrogen phosphate
$NaHCO_3$	Sodium bicarbonate
NaOH	Sodium hydroxide
NES	Nuclear export signal
NLS	Nuclear localisation signal
NPF(s)	Nucleation promoting factor(s)
N-WASP	Neural-WASP
OCS	Open canalicular system
P	P-value
PAGE	Polyacrylamide gel electrophoresis
PBS	Phosphate buffered saline
PCR	Polymerase chain reaction
PE	Phycoerythrin
PF4	Platelet factor 4
PF4-Cre$^{-/-}$	PF4 negative
PF4-Cre$^{+/-}$	PF4 positive
PFA	Paraformaldehyde
PGI_2	Prostacyclin
PIP(s)	Phosphatidylinositol phosphate(s)
PLL	Poly-L-lysine
PVDF	Polyvinylidene difluoride
RE	Recycling endosome
rev	Reverse
Rhod	Rhodocytin
rpm	Rotations per minute
RSS	Ritscher-Schinzel syndrome
RT	Room temperature
s.d.	Standard deviation
SDS	Sodium dodecyl sulphate
SNARE	Soluble N-ethylmaleimide-sensitive factor attachment receptor
SNX	Sorting nexin
SPG8	Spastic paraplegia 8
Strumpellin$^{-/-}$	*Strumpellin*$^{flox/flox}$ *PF4-Cre*$^{+/-}$ (knockout)

Strumpellin$^{+/+}$	*Strumpellin*$^{flox/flox}$ *PF4-Cre*$^{-/-}$ (wild-type)
SWIP	Strumpellin and WASH-interacting protein
TAE	Tris acetate EDTA
TBC1D5	TBC1 domain family member 5
TBR	Tubulin-binding region
TBS	Tris-buffered saline
TBS-T	Tris-buffered saline containing Tween
TCR	T-cell receptor
TE	Tris EDTA
TEM	Transmission electron microscopy
TEMED	Tetraacetylethylenediamine ($C_3H_{16}N_2$)
TfnR	Transferrin receptor
TGN	*Trans*-Golgi network
Thr	Thrombin
TPO	Thrombopoietin
TRIM27	Tripartite motif-containing protein 27
Tris	Tris(hydroxymethyl)aminomethane
TXA_2	Thromboxane A_2
u	Unit
U46	U46619 (TXA_2 analogue)
USP7	Ubiquitin-specific protease 7
UV	Ultra-violet
VCA	Verprolin homology, central hydrophobic/ cofilin, acidic
VPS	Vacuolar protein sorting
vWF	*von Willebrand* factor
WASH	Wiskott-Aldrich syndrome protein and SCAR homologue
WASP	Wiskott-Aldrich syndrome protein
WAVE	WASP family verprolin homologue, also known as SCAR
WHAMM	WASP homologue associated with actin, membranes and microtubules
WRC	WAVE regulatory complex
WT	Wild-type
β2AR	β2-adrenergic receptor

1 Introduction

1.1 Platelet biogenesis and function

Platelets are small, anucleate and discoid-shaped cell fragments (diameter: 1-3 µm in humans, 1-2 µm in mice), which originate from mature megakaryocytes. Megakaryocytes are found primarily in the bone marrow. During early development, megakaryopoesis also takes place in the foetal liver, spleen and yolk sack (1). Megakaryocytes are large, highly polyploid cells, located near sinusoidal blood vessels, into which they extend long branched cytoplasmic extensions, so-called proplatelets (2). At the tips of proplatelets, shear forces lead to shedding of barbell-shaped proplatelets into the blood stream, where they fragment further into platelets (3-5). Furthermore, proplatelets release so-called preplatelets, an intermediate stage of platelet production. These large (diameter: ~2-10 µm), anucleate and discoid fragments convert reversibly into barbell-shaped proplatelets, which then undergo fission into platelets (5).

Before having the ability to produce platelets, megakaryocytes need to undergo a significant maturation process, which is promoted by thrombopoietin (TPO) binding to the megakaryocyte-specific receptor c-mpl (1, 6). In addition, they become highly polyploid (up to 128n) through endomitosis (DNA replication without cell division) and display an impressive cell growth (diameter: up to 100 µm in humans, 30-50 µm in mice) (1). During maturation, platelet-specific proteins, organelles and granules (e.g. α- and dense granules) are synthesised and are then transported to and packaged into nascent platelets (2, 7). In addition, an extensive internal network of interconnected cisternae and tubules, termed demarcation membrane system (DMS), develops, which serves as a membrane reservoir for proplatelets (2, 8). Each megakaryocyte emanates approximately 10 to 20 proplatelets, which elongate from the cell body, thin out and bifurcate repeatedly (1) (Figure 1A). The entire megakaryocyte is converted into proplatelets, eventually shedding up to 1,000 platelets (2, 4). Its nucleus is then extruded and degraded along with remaining cell material (2) (Figure 1B).

A highly organised cytoskeleton is crucial for proper platelet biogenesis. For instance, microtubules and associated molecular motor proteins dynein and kinesin provide the necessary force for proplatelet formation and extension, conversion of pre- into proplatelets as well as granule and organelle trafficking towards the tip (4, 5, 7, 9). The actin cytoskeleton also enables proplatelet formation as well as bending and branching of the shaft, which increases the number of platelet-forming tips (2, 4, 10) (Figure 1A).

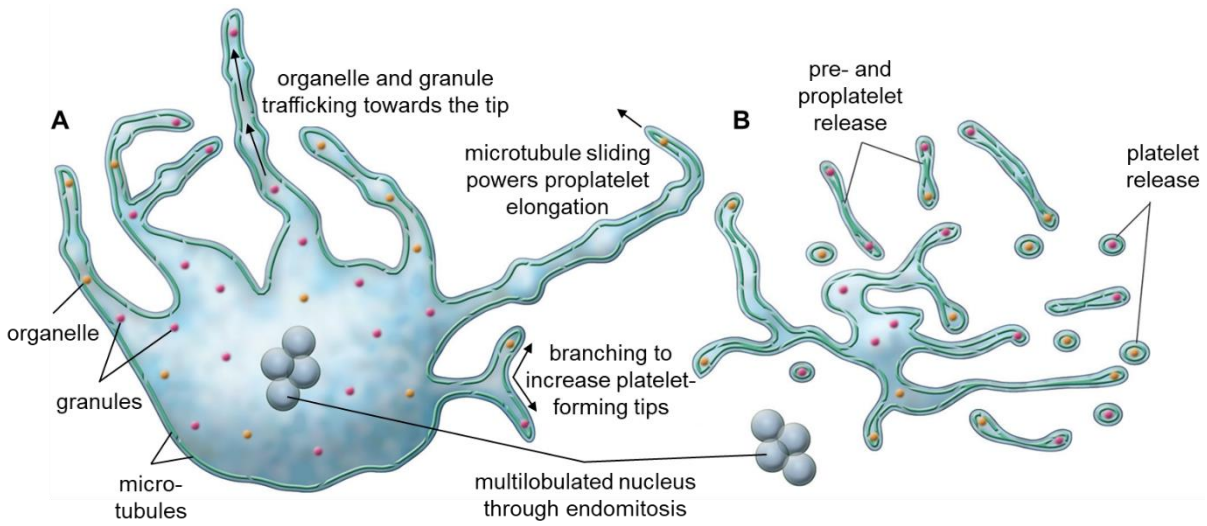

Figure 1: Schematic of platelet production from megakaryocytes
A) Microtubule sliding generates force for proplatelet formation and elongation into small vessels. It also allows for organelle and granule trafficking towards the proplatelet tip into nascent platelets. The actin cytoskeleton drives proplatelet formation as well as bending and branching of the proplatelet shaft to amplify platelet-forming tips. B) Barbell-shaped proplatelets and preplatelets are shed into the blood stream by shear forces and fragment further into platelets. Only the megakaryocyte's nucleus eventually remains and is degraded. Schematic adapted from (2).

Platelets are crucial for haemostasis and thrombosis. Human blood contains about 150,000 to 400,000 platelets per microliter (800,000 to 1,000,000 platelets/µl in mice). They circulate for roughly 10 days in the blood stream (for circa 5 days in mice) and, if unused, are then removed by macrophages in the liver and spleen (1, 11). However, upon vascular injury and ensuing exposure of subendothelial extracellular matrix (ECM), platelets adhere to the injured endothelium by binding ECM components, such as collagen, fibronectin, laminin and *von Willebrand* factor (vWF), via multiple ligand-specific receptors (11). Platelets rapidly become activated, dramatically change their shape, secrete their granule contents, and aggregate to form a haemostatic plug in order to seal the wound and minimise blood loss. Simultaneously, initiation of the coagulation cascade occurs. Both the extrinsic (via activated factor VII by exposed tissue factor) and the intrinsic (via sequential activation of factors XII, XI, IX and VIII) result in thrombin formation, which then converts fibrinogen to fibrin. A fibrin network is generated to form a more stable thrombus.

Initial platelet adhesion is mediated via the interaction of the glycoprotein (GP) Ib-V-IX receptor complex present on platelets and collagen-immobilised vWF at sites of vascular injury, especially at high shear rates (11, 12). This only transient interaction leads to an increasing deceleration and rolling of platelets on the endothelium (platelet tethering), which allows other platelet receptors to bind to their ligands (11). For instance, it enables the interaction between GPVI and collagen, which triggers signalling pathways resulting in platelet activation (11, 12). This leads to an upregulation of integrins on the platelet

surface by a change of affinity from low to high ('inside-out' signalling) (12, 13). This process facilitates integrins to bind to their ligands more effectively and thus, enforces stable and firm adhesion to the ECM via collagen through α2β1 and vWF through αIIbβ3 as well as platelet aggregation via fibrinogen through αIIbβ3 (11, 12). The latter contributes to the formation and growth of a stable thrombus (Figure 2).

Furthermore, platelets dramatically change their shape from discoid to a more spheric shape by reorganising their cytoskeleton. They extend finger-like and thin sheet-like protrusions, termed filopodia and lamellipodia, respectively (14). Platelet activation also leads to the secretion or incorporation into the surface membrane of platelet granule content. α-granules contain many adhesive proteins, such as fibrinogen and vWF, as well as coagulation factors. Dense granules release second-wave mediators adenosine diphosphate (ADP) and serotonin. Together with *de novo* synthesised thromboxane A_2 (TXA_2) and locally produced thrombin, ADP is essential for recruiting and activating further platelets to the growing thrombus (11, 12) (Figure 2).

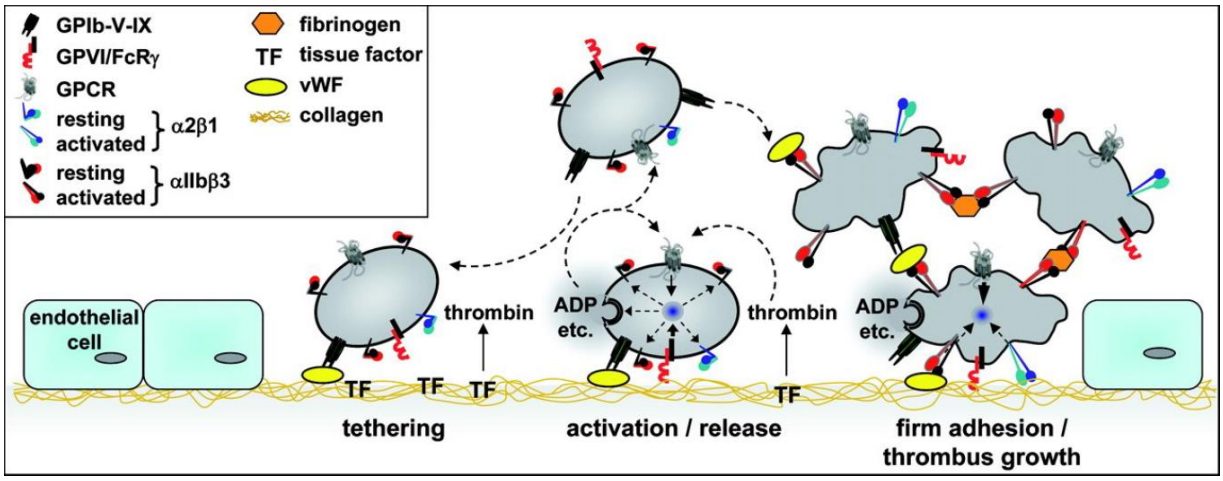

Figure 2: Depiction of thrombus formation
Platelet tethering is mediated by the GPIb-V-IX complex binding to immobilised vWF, which enables the interaction of GPVI with collagen. This triggers the activation of platelet integrins, resulting in firm adhesion to the ECM and platelet aggregation. Released ADP and TXA_2 and locally produced thrombin amplify platelet activation and recruit additional platelets. The reorganisation of the actin cytoskeleton leads to platelet shape change. Adapted from (11).

Pathological alterations to the endothelium, for instance atherosclerosis, can induce uncontrolled platelet activation and subsequent thrombus formation, which leads to vessel occlusion and insufficient blood and oxygen supply of the affected area resulting in stroke or myocardial infarction (12, 15).

1.2 Platelet ultrastructure

Transmission electron microscopy (TEM) can be used to visualise platelet ultrastructure (Figure 3). The ultrastructure of resting platelets is quite unique due to the fact that the plasma membrane contains an extensive reticular network of invaginations, termed the open canalicular system (OCS), which greatly enlarges the surface area of platelets (16). The OCS is connected to the outer milieu via pores and thus, may ensure uptake of plasma proteins as well as granule release after platelet activation (17). The OCS probably derives from the DMS and it is believed that it serves as a membrane reservoir during platelet spreading (18, 19). Platelets contain another specialised reticular membrane compartment – the internal dense tubular system (DTS). It originates from the smooth endoplasmic reticulum (ER) of megakaryocytes (18, 20). It is located near the peripheral microtubular ring in resting platelets and does not interact with the surface membrane (16, 17). The DTS stores calcium and other proteins involved in platelet activation (21). Both the OCS and the DTS are highly intertwined (20). Due to its electron-dense content, the DTS can be distinguished from the clear OCS in TEM images (21).

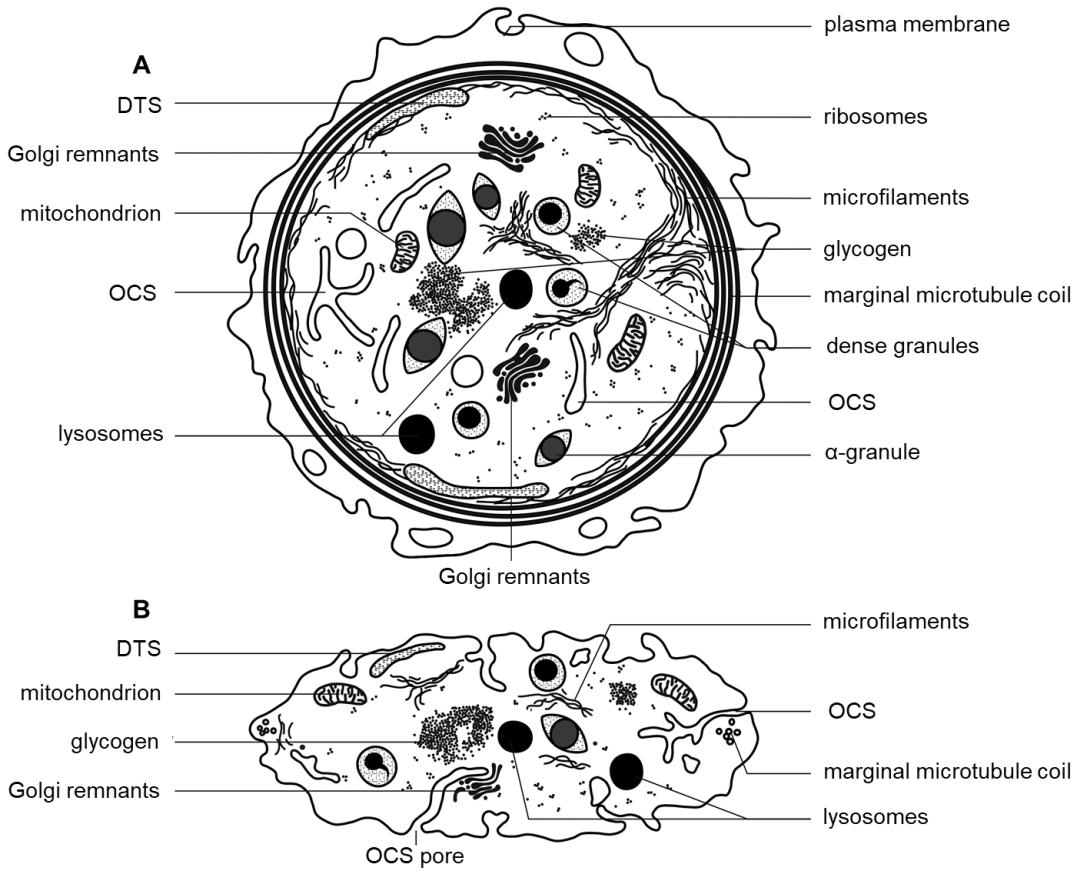

Figure 3: Schematic of platelet ultrastructure
A) Equatorial plane and B) cross-section of a resting platelet. Adapted from (17).

Resting platelets owe their discoid shape to their cytoskeleton, which consists of microfilaments (filamentous actin or F-actin), a peripheral band of microtubules and spectrin. The cytoskeleton also mediates the rapid shape change from discoid to spheric, which platelets undergo after activation. The membrane skeleton consists of a spectrin network, which lines the inner plasma membrane as well as the OCS (18, 22). It is connected to actin filaments radiating from the centre towards the plasma membrane (22, 23). Furthermore, microfilaments form a rigid cytoplasmic scaffold, arranged by filamin A (cross-links actin filaments at a 90° angle) and α-actinins (align actin filaments parallel to each other) (14). Overall, actin is the most abundant protein in platelets with approximately two million copies per platelet (22). Around 40% of total actin are assembled into actin filaments in resting platelets (14). The formation of microfilaments rapidly increases to ~80% after platelet activation, which drives platelet shape change and granule secretion (14). Microtubules are organised into the characteristic marginal ring, which maintains the discoid shape of resting platelets. It consists of multiple associated, short and highly dynamic microtubules of mixed polarity (18, 24). Approximately 40% of total tubulin are assembled into this microtubule coil (14). In general, microtubules consist of α- and β-tubulin heterodimers, which can reversibly assemble into polymers. β1-tubulin is the predominant isoform in megakaryocytes and platelets and may contribute to the coil's flexibility and structure (18).

At least three major types of secretory granules (α-, dense-granules and lysosomes) are found in the cytoplasm of resting platelets, which differ in their ultrastructure, content, rate of exocytosis and function. They are formed in megakaryocytes and transported along proplatelets into nascent platelets (7, 25). Upon platelet activation granule components are secreted or incorporated into the plasma membrane by exocytosis. α-granules are the most abundant (50-80 per platelet) as well as the largest granules (diameter: 200-500 nm, surface area: ~14 μm^2/platelet) (26, 27). They are quite heterogeneous in size, shape (round to ovoid and even tubular) as well as content and its distribution within the granule (20). α-granules contain many coagulation factors as well as adhesive proteins, such as Factor V, XI and XIII, fibrinogen and vWF (16, 28). They also contain numerous other proteins involved in inflammation and wound healing (16, 28). Integrin αIIbβ3 as well as P-selectin are expressed on the inner granule membrane (16, 26). Dense granules are small (~150 nm) and low in number (3-8 per platelet) (18, 21). Due to their high calcium und phosphate content, these granules appear as small, very dense bodies, surrounded by relatively clear cytoplasm and a single membrane (16, 21). Dense

granules contain, among others, the nucleotides ADP and adenosine triphosphate (ATP) as well as serotonin and histamine (21). And lastly, platelets comprise 200 to 250 nm sized lysosomes (0-3 per platelet) (27). These granules contain proteolytic enzymes, which may play a role in thrombus formation and ECM remodelling (16).

1.3 The endosomal network

1.3.1 The endosomal network in other cell types

The endosomal network is essential for maintaining cellular homeostasis and thus, guaranteeing proper cellular function, by sorting, recycling and degrading endocytosed proteins, such as adhesion molecules, ion and nutrient transporters and signalling receptors (29, 30). It is comprised of several interconnected and very dynamic membrane-bound compartments and serves as a major sorting machinery within the cell (29, 31).

Numerous proteins (further referred to as 'cargo') are endocytosed via clathrin-dependent or clathrin-independent pathways, e.g. via caveolin or ADP-ribosylation factor (Arf) 6 (32, 33). Endocytic vesicles then fuse with and incorporate their cargo into early endosomes (EE, also known as sorting endosomes), the first and main sorting station in the endocytic pathway (34, 35). EE mature through complex modifications into late endosomes (LE) (34). Both EE and LE target their cargo to specific subcellular destinations depending on the cellular function of the cargo protein (33). During this sorting process, endosomes assume a more tubular and vacuolar shape (34).

Cargo of both EE and LE can be either (Figure 4):

I) ubiquitinated and retained via internalisation into intraluminal vesicles (ILVs) to be delivered to lysosomes for degradation. For this to occur, EE need to undergo endosomal maturation. ILVs give LE their characteristic multivesicular body (MVB) appearance. MVBs/LE eventually fuse with lysosomes, forming so-called endo-lysosomes, where cargo is then degraded (33).

II) retrieved from the degradation pathway and subsequently recycled (back) to the plasma membrane for reuse, either directly or indirectly via recycling endosomes (RE) and the endosomal recycling compartment (ERC). Direct and indirect transportation to the plasma membrane is termed 'fast' and 'slow' recycling pathway, respectively (29, 33).

III) retrieved and targeted to other cell compartments, e.g. to the *trans*-Golgi network (TGN) or the ER via retrograde trafficking (29, 33).

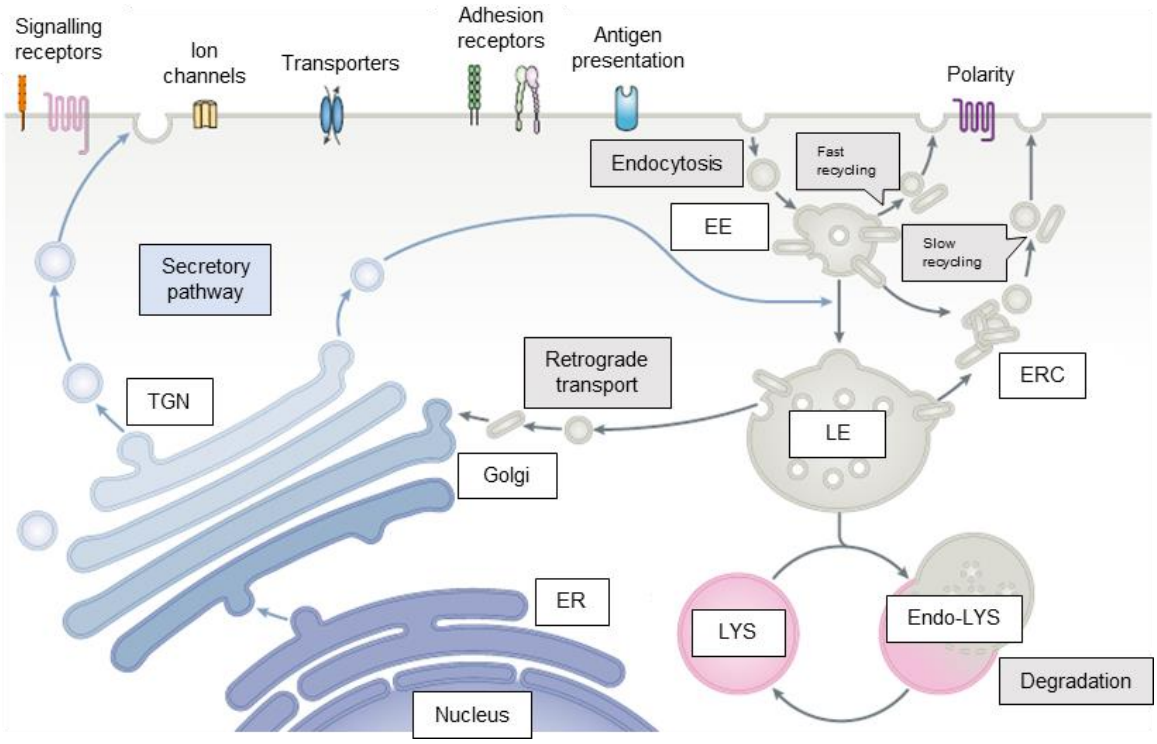

Figure 4: The endosomal network
Cargo is endocytosed and incorporated into EE, which gradually mature into MVBs/LE and later fuse with lysosomes (endolysosomes; Endo-LYS). Cargo destined for recycling is sorted into emerging endosomal tubulations and transported back to the plasma membrane via the fast or slow recycling pathway or transported to the TGN (retrograde transport). Cargo destined for degradation is internalised into ILVs and later degraded in lysosomes (LYS). Adapted from (33).

The maturation of EE to LE is coordinated by the family of Rab GTPases, distinct phosphatidylinositol phosphates (PIPs) and the vacuolar proton pump V-ATPase, among others. They also recruit effectors necessary for proper endosomal function. Main features of the maturation process are: 1) the replacement of Rab5 (EE marker) with Rab7 (LE marker), 2) the conversion of PI(3)P (EE) to PI(3,5)P_2 (LE), 3) the delivery of lysosomal hydrolases and protective membrane proteins, such as LAMP1 (lysosome marker), from the TGN, and 4) the increasing acidification of the maturing endosome via the V-ATPase (34, 36). Rab4 and Rab11 regulate the fast and slow recycling pathway, respectively, and are displaced during Rab5 to Rab7 conversion (36).

Increasingly, the intricate mechanisms for sorting cargo into its respective pathway and the necessary regulatory machinery are being explored. These regulatory machineries facilitate the formation, stabilisation, and segregation of different functional membrane domains on endosomes, including degradative and retrieval subdomains. Here, they control cargo selectivity, packaging into transport vesicles or ILVs, fission from or internalisation into the endosome as well as transportation to different cellular destinations.

Degradative subdomains are enriched with endosomal sorting complexes required for transport (ESCRT). Ubiquitinated cargo destined for degradation is recognised by the ESCRT machinery, which then mediates internalisation and formation of ILVs (33).

Retrieval and recycling of cargo are mediated by a number of (multi)protein complexes, including the retromer complex (in short retromer), the retriever complex (in short retriever) and the COMMD/CCDC22/CCDC93 (CCC) complex (Figure 5A). These cargo-retrieval complexes and their associated proteins recognise specific sequence motifs, so-called sorting motifs, in the cytosolic domain of their cargo (29). Retromer, retriever and the CCC complex localise to retrieval subdomains on EE and LE, which are distinct from the ESCRT enriched degradative subdomains (29, 33, 37).

The highly conserved retromer consists of a heterotrimer of vacuolar protein sorting (VPS) proteins 35, 29 and 26 (30, 38). In concert with various sorting nexin (SNX) adaptor proteins, retromer mediates retrieval of diverse cargo from degradation and selectively sorts it into emerging endosomal tubules destined for the TGN or the plasma membrane (30, 38). For instance, the retromer-SNX27-complex mediates endosome-to-plasma membrane recycling of the β2-adrenergic receptor (β2AR) and the glucose transporter GLUT1 (39, 40). The retromer-SNX3-complex regulates recycling of the divalent metal ion transporter Dmt1-II and the transferrin receptor (TfnR), among others (38). The SNX1/2-SNX5/6-complex can regulate retrograde transport of the cation-independent mannose-6-phosphate receptor (CIMPR) in concert or independently of retromer (29, 33). All SNX proteins contain a phox-homology (PX) domain, which allows interaction with PIPs (30). Some SNX proteins, such as SNX1/2/5/6, contain a C-terminal Bin-Amphi-physin-Rvs (BAR) domain, which induces and/or stabilises membrane bending and subsequently tubulation (30, 41). Retromer is recruited to EE and LE by SNX3 and Rab7, respectively (42-44). TBC1 domain family member 5 (TBC1D5), a GTPase-activating protein of Rab7, downregulates its recruitment (44, 45).

The conserved retromer-like retriever is a 171 kDa heterotrimeric complex, comprised of down syndrome critical region 3 (DSCR3; also known as VPS26C) protein, chromosome 16 open reading frame 62 (C16orf62; also known as VPS35L) protein and VPS29 (hence a member of both retromer and retriever) (37). It associates with the cargo adaptor SNX17, which regulates retrieval and recycling of integrins, including α5β1 integrin, and other proteins (37).

The CCC complex is composed of subunits: coiled-coil domain containing (CCDC) 22 and 93, C16orf62 and a member of the copper metabolism MURR1 domain protein family (COMMD1-10) (38, 46). It is required for endosomal sorting and recycling of the copper transporter ATP7A (46) as well as of the low-density lipoprotein receptor (LDLR) (47, 48). The latter regulates the level of circulating LDL cholesterol. The CCC complex also associates with retriever (37).

Numerous studies have demonstrated that the actin cytoskeleton is essential for endosomal function. It not only regulates endosomal biogenesis and maturation (49, 50), shape (51-54) and motility (31), but also the formation of endosomal subdomains (41, 55, 56) and sorting of cargo into distinct pathways (29, 57). The major actin-nucleation promoting factor on endosomes is the Wiskott-Aldrich syndrome and SCAR homologue (WASH) complex, where it mediates the generation of an actin-related protein 2/3 (Arp2/3) complex-dependant actin network (51, 52). The WASH complex interacts with retromer, and with retriever via the CCC complex (37, 45, 46, 58) (Figure 5B).

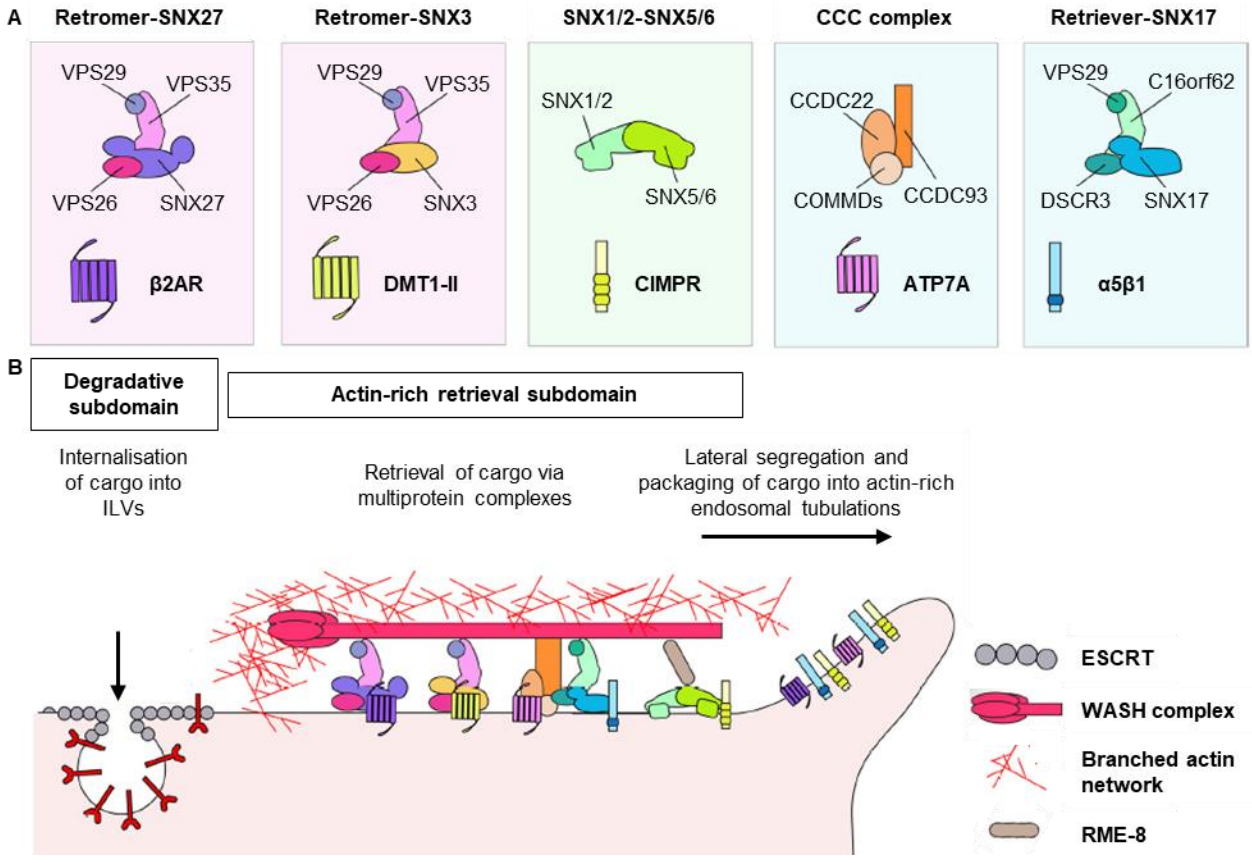

Figure 5: Cargo-retrieval and recycling complexes on endosomes
A) Schematic of structure of cargo-retrieval complexes retromer, CCC complex and retriever, their associated proteins and possible cargo proteins. B) The WASH complex acts as the major actin-nucleation promoting factor on endosomes. It associates with retromer, retriever and the CCC complex and mediates the generation of an Arp2/3-dependant actin network for cargo retrieval and recycling. Adapted from (29).

1.3.2 Endocytic trafficking in megakaryocytes and platelets

Endocytic trafficking in megakaryocytes and platelets is crucial for proper platelet function. It enables cargo uptake and packaging into platelet granules, recycling of platelet surface receptors and the release of bioactive proteins upon platelet activation and thus, plays an important role in haemostasis and thrombosis as well as regeneration and inflammation (59-61). Furthermore, endocytic trafficking is important for platelet granule biogenesis and maturation, which occurs in megakaryocytes and platelets, respectively (25, 61). However, the mechanisms of endocytic trafficking, its molecular machinery and possible trafficking routes in megakaryocytes and platelets remain poorly understood (Figure 6).

Platelets contain different endosomal compartments, including EE, RE and MVBs/LE, lysosomes, autophagosomes, ER (termed DTS in platelets), Golgi as well as platelet-specific α- and dense granules (59, 60, 62). Furthermore, proteomic analysis demonstrated that human platelets express key regulators for endocytosis, endocytic trafficking as well as for fusion and fission events, including clathrin-associated adaptor proteins (AP) 1-4, GTPases Arf1 and 3-6, caveolin (CAV) 1-3, clathrin, vesicle-scission-inducing GTPases dynamin 1-3, numerous Rab GTPases, retromer (VPS29 and 35) and retriever (C16orf62, DSCR3 and VPS29) subunits, SNARE proteins, sorting nexins (especially retromer- and retriever-associated SNX1, 2, 3, 5, 6, 17 and 27) and numerous others (59, 63).

It has been shown that platelets can endocytose plasma proteins, including albumin, fibrinogen and immunoglobulin (Ig) G (59, 64, 65). Furthermore, platelets internalise several of their surface receptors, such as αIIbβ3, C-type lectin-like type II transmembrane receptor (CLEC-2) and the purinergic receptors $P2Y_1$ and $P2Y_{12}$, which can then be degraded or recycled back to the plasma membrane (60, 66-68). Similar to other cells, endocytosis and intracellular transport in platelets can occur via clathrin-dependent or clathrin-independent pathways (59). Clathrin interacts with APs and other accessory proteins to recruit cargo to clathrin-coated pits, which line the plasma membrane, the OCS, vesicles, α-granules and lysosomes (59). AP2 localises to the plasma membrane, where it regulates endocytosis, whereas AP3 plays an important role in lysosomal and dense granule cargo trafficking (25). The GTPase dynamin promotes scission of clathrin-coated vesicles from membranes (59, 69). Clathrin-independent endocytosis can be divided into either: 1) a dynamin-dependent pathway, e.g. involving caveolae, or 2) a dynamin-independent pathway, via small GTPases like Arf6 (32, 59). Caveolae are small (diameter: 60-80 nm) invaginations of plasma and intracellular membranes with a specific

lipid and protein composition, including caveolins (70). They are important for endocytosis, exocytosis, lipid regulation and mechano-sensing (70). Arf6 mediates endocytosis, intracellular trafficking and receptor recycling, including of αIIbβ3 integrin in platelets (59, 60). It has been shown that after endocytosis, newly internalised cargo is trafficked to EE (Rab4-positive) before transportation to RE (Rab11-positive) for recycling to the plasma membrane or α-granules (vWF-positive) (60, 71).

Platelets also contain soluble N-ethylmaleimide-sensitive factor attachment receptor (SNARE) machinery, which enables membrane fusion during granulogenesis, granule secretion upon platelet activation and possibly during intracellular trafficking events (25, 59, 72). Platelet activation leads to granule contact with the OCS and the plasma membrane, membrane fusion and subsequent content secretion or incorporation into the plasma membrane (26, 73). Exocytosis of granules occurs at different rates, which are dependent on platelet agonist and stimulation strength (72). Dense granules are the most sensitive and secrete the fastest, whereas lysosome secretion is slower and dependent on a stronger agonist stimulation compared to α- and dense granules (72).

α- and dense granules are formed from the TGN and EE and mature from MVBs/LE in megakaryocytes (25, 74, 75). Hence, granules originate and obtain their content via the biosynthetic and endocytic pathway. After formation, maturing granules are transported through proplatelets into nascent platelets (7, 25). Granule maturation continues in circulating platelets (25). Although α- and dense granulogenesis show similarities, their formation requires distinct regulating and protein sorting machinery (25, 76). Overall, granule biogenesis is still not completely understood. Platelet α-granules obtain β-thromboglobulin, platelet factor 4 (PF4) and vWF, from biosynthesis; albumin, fibrinogen and IgG from endocytosis – occurring in megakaryocytes and platelets (18, 26). Sorting and packaging of proteins into α-granules occurs via different mechanisms. For instance, P-selectin contains a signal peptide, which directs it to the granule (25). vWF aggregates into large complexes, which are stored into distinct sub-compartments within α-granules (25). Exogenous proteins are endocytosed via receptor-mediated endocytosis or pinocytosis and trafficked via the endosomal network into α-granules (25). For example, fibrinogen is endocytosed via αIIbβ3 and subsequently stored in α-granules (77). Igs and vascular endothelial growth factor (VEGF) are taken up via pinocytosis (25).

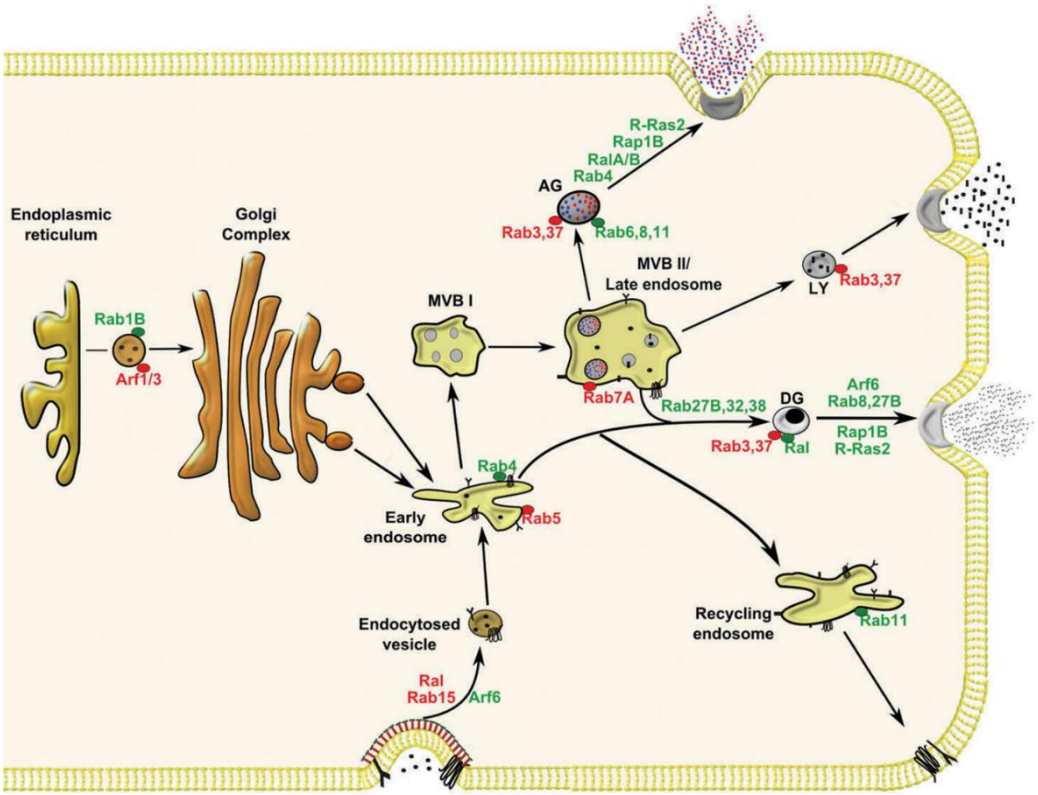

Figure 6: Schematic of endocytic trafficking in megakaryocytes and platelets
Platelet granules and their content derive from the biosynthetic and endocytic pathway. In megakaryocytes, cargo from both pathways is packaged into EE and either recycled to the plasma membrane via RE or retained in the endosome. EE mature into MVBs/LE from which α-granules, lysosomes and possibly dense granules originate. Granule cargo loading continues in platelets. Granules are recruited to the plasma membrane and their content secreted upon platelet activation. Vesicle trafficking is regulated by numerous Arf, Rab and Ras GTPases. GTPases studied in platelets and megakaryocytes are highlighted in green, GTPases studied in other cells are highlighted in red. Adapted from (61).

1.4 The WASp family

The actin cytoskeleton is essential for many different cellular processes. Its formation and continual rearrangement are regulated by F-actin nucleating factors. Depending on their subcellular location, these nucleating factors induce local actin polymerisation and thus, provide structural support, facilitate intracellular cargo trafficking and regulate membrane movement by generating mechanical force (52). For instance, the actin cytoskeleton facilitates endocytosis and phagocytosis at the plasma membrane as well as vesicle formation and transportation within the cell; it also allows for cell adhesion and migration by enabling filopodia and lamellipodia formation (78).

An important regulator of the actin cytoskeleton is the ubiquitous Arp2/3 complex. It has the ability to initiate the polymerisation of new actin filaments on already existing filaments in a 70°degree angle, thereby generating a network of branched actin filaments (79). Lacking activity on its own, the Arp2/3 complex needs to be recruited and activated by nucleation promoting factors (NPFs) (79). The most potent NPFs contain a conserved

C-terminal Arp2/3-activating domain, the so-called VCA (verprolin homology; central hydrophobic or cofilin homology; acidic) domain (51, 79, 80). This domain is also known as WCA (WASP homology domain 2 (WH2); connecting; acidic) domain. It is comprised of a verprolin homology motif to bind actin monomers and an acidic and a central hydrophobic domain to bind the Arp2/3 complex and to initiate the activating conformational change in Arp2/3 (79).

The Wiskott-Aldrich syndrome protein (WASP) family serves as an important NPF, containing a VCA domain. Due to their shared homology with WASP, the WASP family is comprised of WASP itself, N-WASP (neural-WASP), WAVE (WASP family verprolin homologue, also known as SCAR; isoforms 1-3), WHAMM (WASP homologue associated with actin, membranes and microtubules), JMY (junction-mediating regulatory protein) as well as WASH (81, 82) (Figure 7). They all contain a C-terminal VCA domain but differ in their N-terminal sequences, which allows inter- and intramolecular interactions. For example, WAVE and WASH are members of macromolecular complexes, which facilitate stability and subcellular localisation as well as regulate the activity of the VCA domain (82, 83). This allows for activity regulation of the Arp2/3 complex and thus, spatial and temporal formation of a branched actin network.

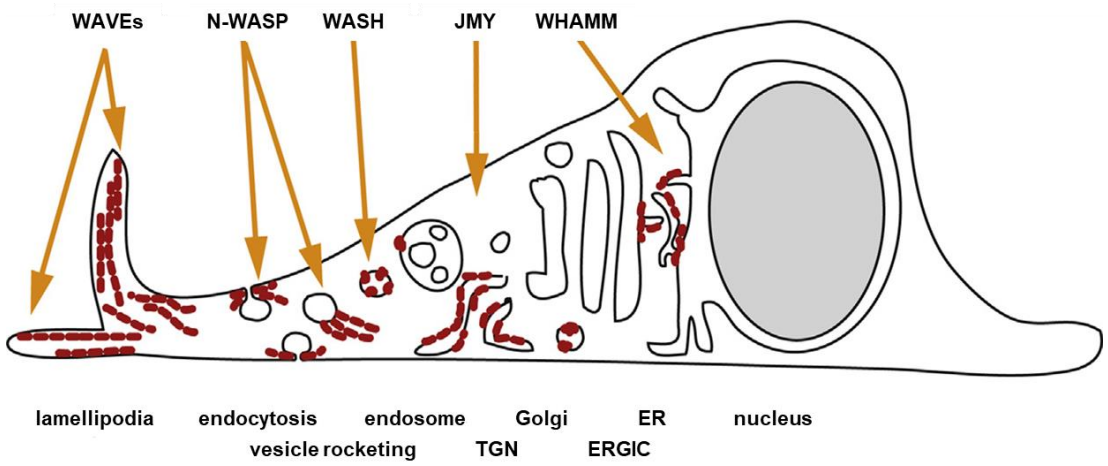

Figure 7: Schematic of main site of activity of WASP family members
WAVE localises to the leading edge of cells, where it stimulates Arp2/3 and establishes a branched actin network for lamellipodia and membrane ruffle formation. N-WASP is required for endocytosis and endosome motility. WASH plays a role in endosomal sorting and trafficking. JMY and WHAMM are involved in anterograde trafficking from the TGN and ER, respectively. Adapted from (84).

WASP and N-WASP contain a N-terminal GTPase-binding domain (GBD), which binds to the VCA domain and thus, autoinhibits its activity (80, 85). By binding the Rho GTPase Cdc42, the GBD releases the VCA domain, enabling it to bind to the Arp2/3 complex (82, 85). Both proteins are associated with the WASP-interacting protein (WIP) and WIP homologues, which contribute to complex stability and activity (80, 82). WASP is

restricted to hematopoietic stem cells, where it is required for phagocytosis and podosome formation (82). Mutations in the *WASP* gene cause the rare X-linked recessive Wiskott-Aldrich syndrome. Symptoms include eczema, severe immunodeficiency and microthrombocytopenia (86). The ubiquitous N-WASP plays a role in endocytosis, endosome motility and invadopodia formation (82, 85).

WAVE is part of a pentameric complex, named the WAVE regulatory complex (WRC). It is comprised of WAVE (isoforms 1-3), ABI1 or 2, NAP1 (also known as NCKAP1) or NCKAP1L (also known as HEM1), CYFIP1 or 2 (also known as SRA1/2) and HSPC300 (82). Binding of the GTPase Rac1 to the CYFIP subunit increases WAVE activity towards the Arp2/3 complex (82, 83). The WRC complex shows structural similarities to the WASH complex (see Chapter 1.5), especially in complex assembly, shape and size (83). The complex localises to the leading edge of migrating cells, where it is required for lamellipodia and membrane ruffle formation (79, 83). A recent study by *Schurr et al.* revealed that the WRC complex is also responsible for lamellipodia formation in murine platelets (87). Loss of the CYFIP1 subunit in platelets resulted in absent lamellipodia formation after platelet activation (87).

WHAMM localises to distinct domains of the *cis*-Golgi apparatus and the ER-Golgi intermediate compartment (ERGIC), where it facilitates membrane tubulation and transportation of vesicles between the ER and the Golgi (anterograde transport) (88). It is also involved in maintaining Golgi morphology and positioning as well as transportation of Golgi-cargo to the plasma membrane (88, 89). JMY has the ability to generate branched and unbranched F-actin via Arp2/3 complex-dependent and -independent mechanisms, respectively (90). It was first discovered as a transcriptional co-factor of the tumour suppressor p53 (91, 92). Furthermore, it can be detected at the leading edge of cells, where it plays a role in cell migration, and at the TGN, where it facilitates anterograde transport (84, 90, 93). In addition, both WHAMM and JMY have been implicated in autophagy (94-96).

1.5 The WASH complex and its subunit Strumpellin

The WASH complex (also known as the WASH regulatory complex; SHRC) is the major NPF on endosomes, where it regulates the formation of a branched actin network (51, 52, 97). It is a circa 500 kDa multiprotein complex consisting of five subunits: 1) WASH (also known as WASH complex subunit 1; WASHC1 or just WASH1), 2) FAM21 (family with sequence similarity 21; also known as KIAA0592), 3) CCDC53, 4) SWIP (Strumpellin

and WASH-interacting protein; also known as KIAA1033) and 5) Strumpellin (51, 52, 83) (Figure 8). The WASH complex is associated with numerous proteins, e.g. AP2 (98), actin-capping protein CAPZα/β (51, 83), CCDC22 and 93 (58), dynamin (51), FKBP15 (45, 99), B-type lamin (100), retriever (37), retromer (45, 58, 99), SNX1/2 (52, 58), SNX27 (39, 40), TBC1D5 (45) and tubulin (51, 52), among others.

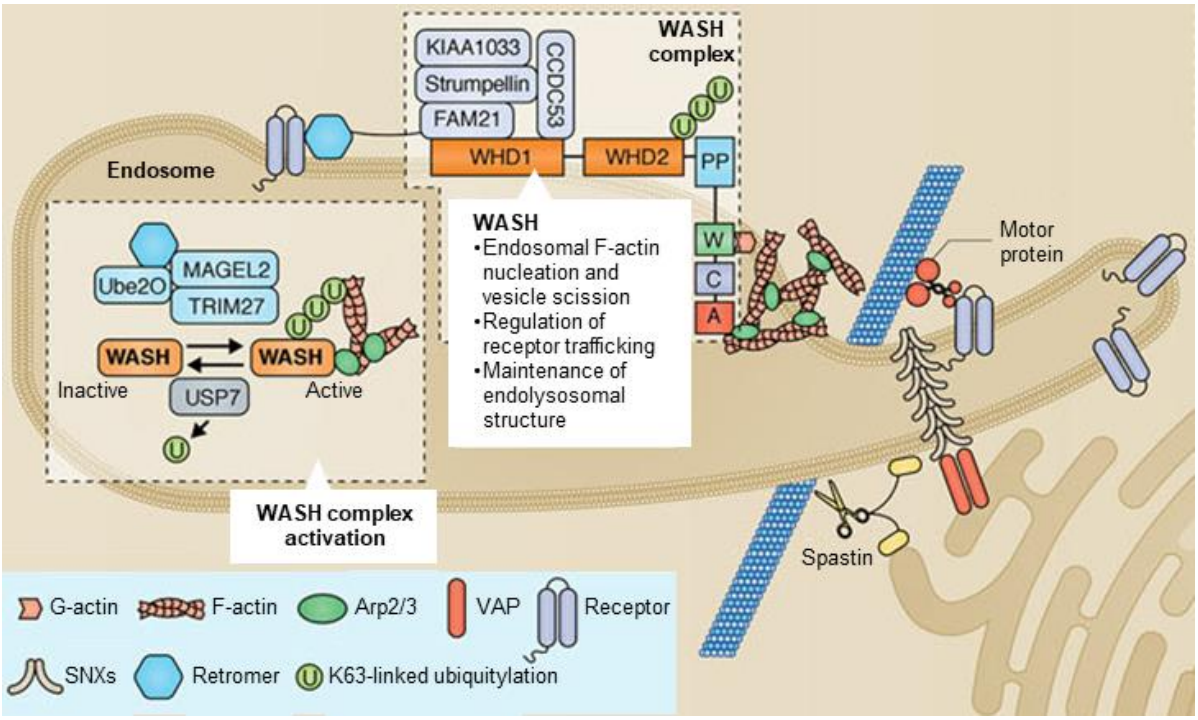

Figure 8: The WASH complex
The WASH complex is a pentameric complex, which consists of subunits WASH1, FAM21, CCDC53, SWIP (KIAA1033) and Strumpellin. It is activated via TRIM27/MAGE-L2/UBE2O complex-mediated polyubiquitylation. The WASH complex localises to endosomes, where it stimulates Arp2/3 and the subsequent formation of a branched actin network. This is essential for the formation and stabilisation of endosomal retrieval subdomains and transport carriers, into which selected proteins are packaged and subsequently transported to their respective cellular destination. Adapted from (82).

Human platelets express all five WASH complex subunits (63). In addition, WASH1, FAM21, SWIP and Strumpellin have all been detected in murine platelets (101) (Table 1). Total depletion of WASH1 in mice results in early embryonic lethality (around E7.5), possibly due to increased autophagy (53, 102).

Table 1: Proteomic studies of human and murine platelets
Approximate protein copy numbers of WASH complex members in human (63) and murine platelets (101).

	Human platelets [protein copy number]	Murine platelets [protein copy number]
WASH1	1,000	527
FAM21	930	339
CCDC53	900	Not listed
SWIP	1,000	379
Strumpellin	1,200	480

WASH1 (~55 kDa) is ubiquitously expressed and highly conserved (51, 54, 97, 103). It is predominantly found at restricted domains of EE and RE, moderately at MVBs/LE and sparsely at lysosomes, due to its co-localisation with EEA1 and Rab5, Rab4 and 11, CD63 and Rab7 as well as Lamp1, respectively (51, 52, 54, 104). WASH1 does not co-localise with the Golgi markers GM130 (*cis*-Golgi) and TGN38 (*trans*-Golgi) nor with clathrin-coated pits (51, 52).

It consists of a N-terminal WASH homology domain 1 (WAHD1, also known as WHD1; amino acids (aa): 1-167) and a tubulin-binding region (TBR, also known as WHD2; aa: 168-304) (52, 83). They are followed by a proline-rich region and a C-terminal VCA domain (52, 97). WAHD1 interacts with the other WASH complex subunits (52, 83). TBR binds to tubulin, whereas the VCA domain binds to actin monomers and the Arp2/3 complex (52) (Figure 9).

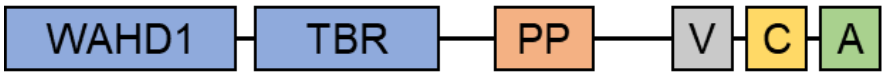

Figure 9: Domain structure of WASH1
WASH1 consists of a N-terminal WASH homology domain 1 (WAHD1), a tubulin-binding region (TBR), a proline-rich region (PP) and a C-terminal verprolin homology, central hydrophobic and acidic (VCA) domain.

WASH1 is intrinsically active *in vitro*, but its activity towards the Arp2/3 complex is inhibited by the WASH complex (51, 83). WASH1 activity is tightly regulated by alternating between K63-linked polyubiquitylation and deubiquitylation of a single lysine in the protein (K220) (105). This is mediated by E3 ubiquitin ligase tripartite motif-containing protein 27 (TRIM27) (105). Polyubiquitylation leads to a conformational change in WASH1, which exposes the VCA domain and enables actin polymerisation (30). The activity of TRIM27 is enhanced by melanoma antigen gene L2 (MAGE-L2), which is recruited to endosomes by retromer subunit VPS35 (105). In turn, the TRIM27/MAGE-L2 complex binds the deubiquitylating protein ubiquitin-specific protease 7 (USP7) (106). USP7 not only reduces WASH1 activity by direct deubiquitylation, but also promotes its activity by preventing auto-ubiquitylation and subsequent degradation of TRIM27 (106) (Figure 8).

With estimated 146 kDa, FAM21 (WASHC2) is the largest subunit of the WASH complex (107). It is comprised of two regions: 1) a N-terminal globular ‘head’ domain (~220 aa), which binds to subunits WASH1 and SWIP and is required for complex formation and stabilisation, and 2) a very long unstructured C-terminal ‘tail’ domain (~1,320 to 1341 aa) (58, 99, 108). FAM21 is less conserved, especially its tail, compared to other WASH complex members (45, 103). The tail domain contains 21 repeats of an acidic LFa motif (L-F-$[D/E]_{3\text{-}10}$-L-F; several acidic residues ($[D/E]_{3\text{-}10}$) flanked by leucine (L) and

phenylalanine (F)), which allow the interaction with various proteins important for WASH complex regulation (99). This includes multiple retromer complexes via its component VPS35 and the CCC complex subunits CCDC22 and 93 (46, 58, 99, 108). Retromer itself recruits the WASH complex to endosomes (45, 58, 99, 108). In addition, FAM21 has the ability to interact with several phospholipids and phosphatidylserines via its C-terminus, which include PI(3)P (enriched in EE), PI(3,5)P_2 (EE to LE transition), PI(4)P (enriched at the Golgi) and PI(5)P (39, 51, 83). Therefore, FAM21 can directly link the WASH complex to endosomes enriched in these phospholipids. *McNally et al.* demonstrated that a significant amount of FAM21 remains associated with endosomes in VPS35-knockout cells, suggesting a retromer-dependent and retromer-independent (e.g. via phospholipids) recruitment of the WASH complex to endosomes (37).

CCDC53 (WASHC3) is the smallest WASH complex subunit with approximately 22 kDa (107). Structurally, it is the second less conserved complex member after FAM21 with a predicted short coiled-coil shaped N-terminus (83, 103). CCDC53 may be important for complex assembly (83), however the precise function is currently unknown. Recently, HSF1 binding protein-1 (HSBP1) was identified as an assembly factor for the WASH complex (109). It plays a role in the dissociation of the homotrimeric precursor form of CCDC53 into monomers for WASH complex assembly (109).

SWIP (WASHC4), estimated to be 135 kDa, is a conserved and ubiquitously expressed protein (103, 110). It is predicted to have a small coiled-coil region at the N- and C-terminus (45). Mutations in the SWIP gene are associated with non-syndromic autosomal-recessive intellectual disability (ARID) (110, 111). Interestingly, a missense mutation in SWIP, which causes ARID, resulted in a significant decrease in SWIP, Strumpellin and WASH1 levels, destabilising the entire WASH complex (110). Hence, it is proposed that SWIP plays an important role in complex assembly (83, 110).

The WASH complex is recruited to the cytosolic side of endosomes by retromer via its subunit FAM21 (45, 58, 99, 108) or possibly binds directly to PIPs enriched in the endosomal membrane via FAM21 as well (37, 39, 51, 83). The WASH complex itself can recruit the CCC complex via FAM21 (46). In turn, the CCC complex can recruit retriever to the endosomal membrane (37). Hence, the WASH complex interacts with various cargo-retrieval complexes. After activation by ubiquitination, WASH1 recruits and stimulates the Arp2/3 complex to generate discrete patches of branched actin filaments (51, 52, 105).

By facilitating the formation of a branched actin network on endosomes, the WASH complex contributes to (Figure 10):

I) The formation and stabilisation of endosomal retrieval subdomains and their segregation from degradative subdomains (29, 41, 55, 56).

II) Cargo enrichment at the retrieval subdomains via associated cargo-retrieval complexes by restricting lateral mobility and diffusion into the degradative subdomain (29, 41, 55). By interacting with multiple retromers via FAM21, the WASH complex further increases the amount of retromer-associated cargo proteins at retrieval subdomains (99).

III) Membrane remodelling for transport carrier formation and their stabilisation (29). In concert with BAR-domain containing proteins, such as SNX-BARs, WASH1-mediated actin polymerisation induces tubulation of the endosomal membrane along microtubule tracks (29, 33). The continuous actin polymerisation generates a pushing force, whereas microtubules and associated motor proteins (e.g. dynein-dynactin complex) provide a pulling force, which contribute to the elongation of these tubulations (29, 51).

IV) Tubule fission from the endosome, making transportation of cargo to other cell compartments possible (51, 52). This is possibly mediated by GTPases (e.g. dynamin, a WASH complex-interacting protein) or ATPases (e.g. Eps15 homology domain-containing protein 1 (EHD1), a retromer-interacting protein) (35, 51). Tubule scission may be assisted by a preceding ER-endosome contact (33). Furthermore, the pushing force generated by the continuous actin polymerisation might contribute to tubule scission by inducing membrane tension (29).

V) Possible short-range motility of transport carriers towards their final destination (29).

Altogether, it has been shown that the WASH complex is involved in the sorting and trafficking of numerous cargo proteins. These include retromer-cargoes CIMPR (52), TfnR (51, 104), β2AR (40), GLUT1 and 2 (112, 113) and T-cell receptor (TCR) (112) as well as CCC complex-cargoes ATP7A (46) and LDLR (47, 48). The WASH complex is also involved in the delivery of epidermal growth factor receptor (EGFR) to lysosomes for degradation (53, 54). Therefore, the WASH complex plays a pivotal role in regulating endosomal sorting and trafficking of cargo into multiple pathways – from EE to RE, the plasma membrane, the TGN and even MVBs/LE.

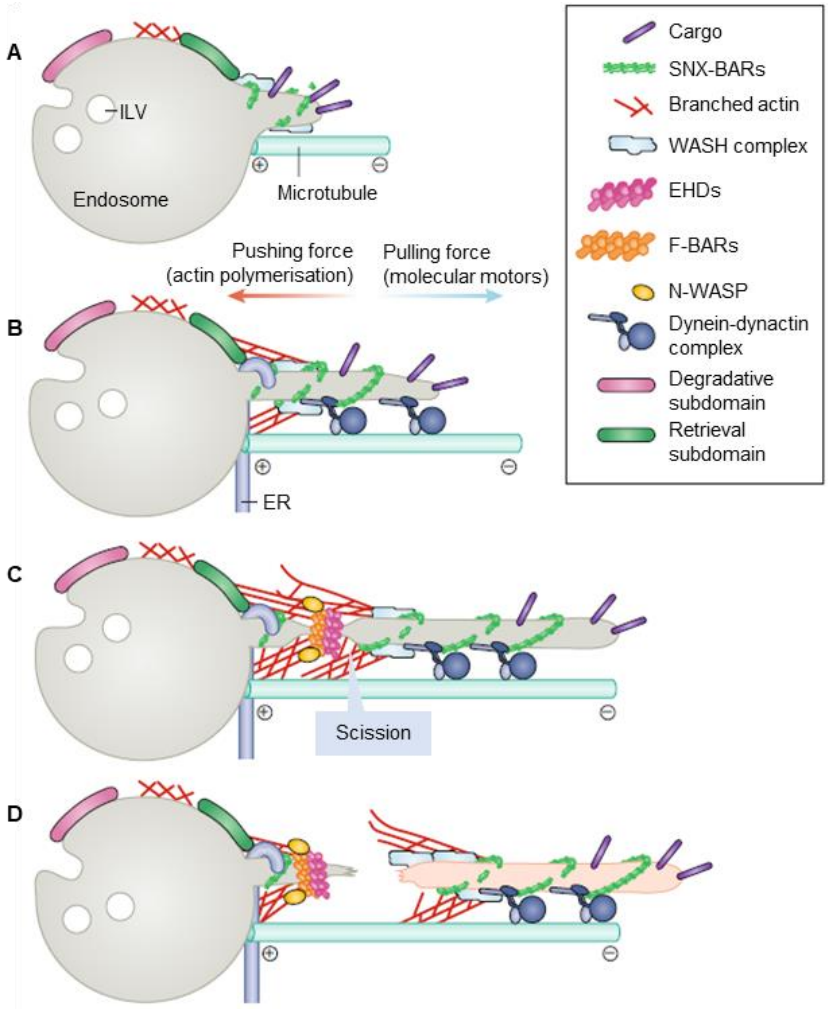

Figure 10: The WASH complex mediates endosomal tubulation and trafficking
A) The WASH complex is recruited to the cytosolic side of the endosomal membrane, where it stimulates Arp2/3 and the formation of a branched actin network. The actin network segregates retrieval from degradative subdomains, where cargo destined for degradation is internalised into ILVs. WASH1-mediated actin polymerisation stabilises retrieval subdomains, concentrates cargo destined for recycling via associated retrieval complexes and induces endosomal tubulation along microtubule tracks. B) The continuous actin polymerisation generates a pushing force, microtubules and associated motor proteins provide a pulling force, which leads to tubule elongation. C) Dynamin or EHD proteins in complex with F-BAR proteins are recruited to the tubule neck and induce membrane scission. This may be assisted by a preceding ER-endosome contact. D) The cargo-enriched carrier is transported to its respective cellular destination, e.g. the plasma membrane. Adapted from (33).

In humans, Strumpellin (WASHC5) is encoded by the *WASHC5* gene (also known as *KIAA0196* or *SPG8* gene) on chromosome 8q24.13, which is comprised of 29 exons (114, 115). Its estimated molecular size is 134 kDa (114). Strumpellin interacts with WASH1 via the C-terminus of SWIP (45, 83, 116). The highly conserved protein is ubiquitously expressed, with its highest expression in the brain and lungs, and mainly localises to the cytosol and ER (103, 114). It is estimated that there are approximately 1,200 copies in human platelets and circa 480 copies in murine platelets (63, 101).

Like WASH1, total loss of Strumpellin leads to embryonic lethality at a very early stage in murine development (before E13.5) (117). As no signs of terminated embryonic

development were detected *in utero*, *Jahic et al.* suggested that Strumpellin plays an essential role in the attachment of blastocytes to the epithelial lining of the uterus and/or very early embryonic development (possibly in motor-neuron outgrowth) (117, 118).

Strumpellin is still a relatively uncharacterised protein. It consists of 1,159 amino acids and can be divided into a N-terminal (aa: 1-240), a central (aa: 241-791) and a C-terminal domain (aa: 792-1,159) (114). The N-terminal domain is comprised of six α-helices and two short β-sheets and has no structural similarities or homology to any known domains (114). There are five spectrin-like repeats found in the central part, each consisting of three α-helices (114). Spectrin repeats can be found in several proteins involved in the cytoskeleton (116). The C-terminal domain displays a more α-helical formation and is structurally similar to exportin-5 and importin β1, which are important for transportation of microRNA precursors (114, 119).

Mutations in the *WASHC5* gene cause a rare motor form of hereditary spastic paraplegia (HSP), called spastic paraplegia 8 (SPG8) (OMIM #603563) (115, 118). HSP was first described by the German physician Adolf von Strümpell in 1904, after whom Strumpellin is named (103). Recently, it has also been associated with an ARID disorder known as Ritscher-Schinzel syndrome (RSS) or 3C (cranio-cerebello-cardiac) syndrome (OMIM #220210) (119).

Up until now, there are over 80 known genetic loci (SPG1-80 and others) and over 60 identified genes associated with HSP, making the disorder genetically very heterogeneous (120). Several of these genes encode proteins, which are involved in intracellular membrane shaping, remodelling and trafficking, including ER shaping (Spastin/SPG4, Reticulon 2/SPG12), endosomal tubulation and vesicle formation (Spastin/SPG4, Strumpellin/SPG8, Spartin/SPG20) and the formation and function of lysosomes (Spatacsin/SPG11, Spastizin/SPG15) (120). In the autosomal-dominant transmitted SPG8 upper motor neurons slowly, but progressively degenerate from distal to proximal. This eventually leads to relatively severe, mostly adult-onset paraplegia of the lower limbs (115). The symptoms include spasticity and weakness in the lower limbs as well as hyperreflexia, extensor plantar responses, a decrease in perception of vibration and urinary urgency (115). So far, there are 16 missense mutations, one large deletion and one frameshift nucleotide deletion identified in *WASHC5*, causing SPG8 (121). Interestingly, mutations in Strumpellin do not affect WASH complex assembly; mutated Strumpellin is folded differently but is still incorporated into a stable complex (83, 116, 122). Furthermore, it

does not influence the interaction of the WASH complex with retromer, thus the WASH complex still localises to endosomes (116). The exact molecular defect of mutated Strumpellin still remains unknown. A possibility might be that mutated Strumpellin has an impact on WASH complex activity or interaction with associated proteins, leading to defective activation of Arp2/3 and consequently disrupting endo-lysosomal function (116, 122, 123). Motor neurons may be especially susceptible to endosomal trafficking defects due to their long axons (up to 1 m in humans).

RSS is a clinically very heterogeneous disorder. Main symptoms are craniofacial abnormalities, cerebellar brain malformations and congenital heart defects (119). Patients affected by RSS show mutations in the *WASHC5* gene, which causes an approximate 60% decrease in Strumpellin levels, or in the *CCDC22* gene (CCC complex member) (119, 124).

1.6 Integrins

1.6.1 Platelet integrins

Integrins on the platelet surface serve as adhesion receptors by binding their respective ligand and enabling platelet adhesion to the ECM as well as platelet-platelet interaction (11). They are heterodimeric transmembrane proteins comprised of different α- and β-chains, which are non-covalently linked (11). Both chains contain a large N-terminal domain, a single-span transmembrane domain and a short C-terminal cytoplasmic domain (11). The latter interacts with numerous adaptor proteins, signalling proteins and cytoskeleton-associated proteins.

Integrins are able to signal bidirectionally. After platelet activation, the affinity towards their respective ligand shifts from low to high, enabling a stronger bond between receptor and ligand (12). This is termed ‘inside-out’ signalling (or integrin activation) and ensures proper integrin function solely at sites of vascular injury (12). In turn, ligand-bound integrins trigger inward signals, which lead to cellular responses, so-called ‘outside-in’ signalling (11, 12). This furthers additional integrin activation, granule secretion as well as cytoskeletal remodelling, including platelet spreading and clot retraction (12).

Platelets express the following integrins with their respective ligands enclosed in parentheses: α2β1 (collagen), α5β1 (fibronectin), α6β1 (laminin), αvβ3 (vitronectin, fibronectin and osteopontin) and αIIbβ3 (fibrin, fibronectin, fibrinogen and vWF) (12). Compared to αIIbβ3 (see Chapter 1.6.2) these integrins are all less expressed on human and murine platelets (63, 101). α2β1 has the ability to bind collagen type I-IV as well as XI, making it

important, but not essential, for firm platelet adhesion to the ECM (11). α5β1, α6β1 and αvβ3 also contribute to platelet adhesion, but are functionally redundant compared to the major platelet integrin αIIbβ3 (11, 125). Previous studies confirmed this by demonstrating that lack of α2- or β1-subunits in mice does not lead to any major haemostatic defects (125-127).

1.6.2 Integrin αIIbβ3

αIIbβ3 (also known as GPIIbIIIa) plays a pivotal role in platelet adhesion and aggregation, thus making it essential for haemostasis and thrombosis. It is the most abundant integrin on the platelet surface with approximately 80,000 copies and an additional intracellular pool (128, 129). Upon platelet activation and subsequent recruitment of platelet granules to the plasma membrane, most notably α-granules, internal αIIbβ3 is incorporated into the platelet membrane, adding to the already existing surface αIIbβ3 (130, 131). αIIbβ3 binds to ligands containing an arginine-glycine-aspartic acid (RGD) sequence (11). This includes fibrinogen, vWF, fibrin, fibronectin, thrombospondin and vitronectin.

αIIbβ3 is expressed in cells of the megakaryocyte lineage, where it is assembled in the rough ER from αIIb precursors and β3 and post-translationally processed in the Golgi complex (αIIb cleavage into a light and a heavy chain) (129, 132, 133). It has also been shown that platelets are able to synthesise αIIbβ3 *de novo* from mRNA (134).

αIIbβ3 is comprised of a large extracellular globular ‘head’, containing both N-terminal domains and the ligand-binding site, and two ‘tails’, containing both transmembrane and cytoplasmic domains (11). The extracellular ‘head’ domain of αIIb is composed of a N-terminal 7-bladed β-propeller followed by a ‘thigh’ and two ‘calf’ domains (11, 129). The β3 ‘head’ consists of a N-terminal βA domain followed by a hybrid domain, a PSI (plexin, semaphorin, integrin) domain, four EGF-like domains and a carboxy-proximal βTD domain (11, 129). The transmembrane domains of αIIb and β3 consist of α-helical coiled coil structures (11). The C-termini of both subunits make up their cytoplasmic tails. The αIIb cytoplasmic domain consists of a helical membrane-proximal and a more unstructured membrane-distal portion, whereas the β3 domain is composed of three helices (129) (Figure 11).

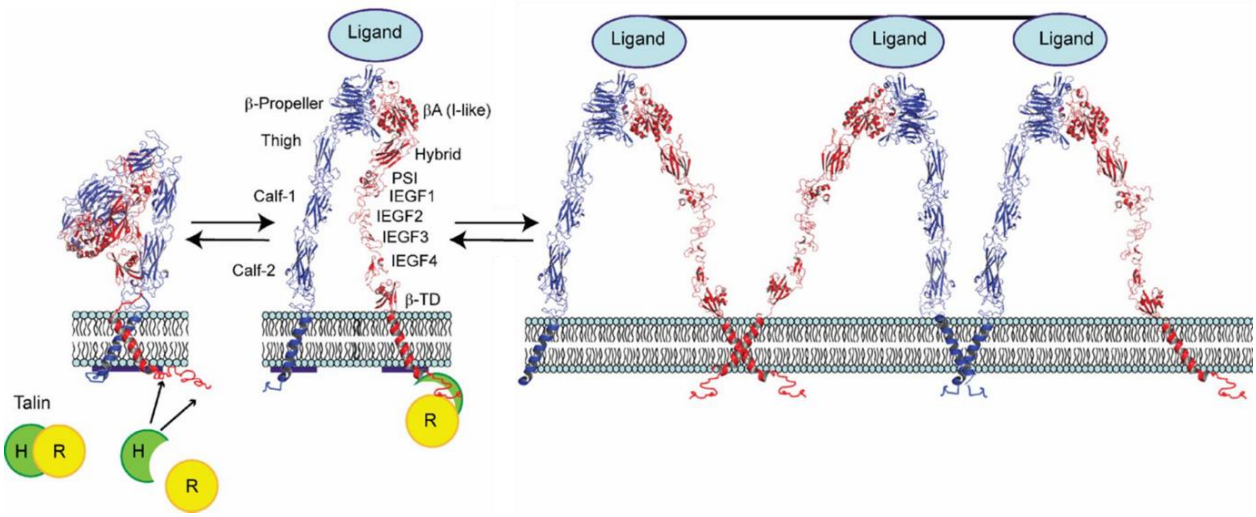

Figure 11: Depiction of αIIbβ3 integrin structure and activation
αIIbβ3 is maintained in a low-affinity, highly bent conformation on resting platelets. Upon platelet activation, inside-out signals result in talin-1 binding to β3, which triggers a conformational shift of the cytoplasmic domain. This is transmitted across the transmembrane domain and leads to an extended and open conformation of the extracellular domain with high affinity towards ligands, e.g. fibrinogen. Adapted from (135).

αIIbβ3 is maintained in its low-affinity state on circulating platelets, displaying a bent conformation of its extracellular domain (129). Upon platelet activation intracellular activators bind to the αIIbβ3 cytoplasmic domain and trigger a conformational change, which is transmitted across the integrin's transmembrane domain towards its extracellular head ("scissor"-like separation of the intracellular and transmembrane domain and "switch-blade"-like movement and extension of the head) (129). The unbent and open conformation of the head domain increases the affinity of αIIbβ3 towards its ligands. The main ligand of αIIbβ3 is fibrinogen, which is able to bind to activated αIIbβ3 on adjacent platelets, thereby, crosslinking platelets and facilitating the formation of platelet aggregates (129) (Figure 11). Ligand binding to and subsequent clustering of αIIbβ3 also triggers outside-in signalling by initiating trans-autophosphorylation of the β3-tail bound tyrosine kinase c-Src (129). Activated c-Src then triggers an intracellular signalling cascade, which leads to actin polymerisation and cytoskeletal reorganisation and thus, enables platelet adhesion, spreading, aggregation, clot retraction and subsequent thrombus growth (129).

Intracellular activators of αIIbβ3 include talin-1 and kindlin-3, among others. Both bind to distinct sites of the integrin's β3 cytoplasmic tail via their FERM (four-point-one, ezrin, radixin, moesin) domain (13, 136). Talin-1 is a 270 kDa adaptor protein, which binds to the β3 tail upon platelet activation, disrupts αIIb and β3 interaction and thus, induces the conformational shift (13, 129). It also links αIIbβ3 to the actin cytoskeleton via its actin binding site (13). Kindlin-3, a 76 kDa adaptor protein, is essential for αIIbβ3 integrin activation in concert with talin-1 (129, 136). Talin-1 and kindlin-3 also play a role in αIIbβ3

outside-in signalling, e.g. platelet spreading on fibrinogen and fibrin clot retraction (13, 136).

Qualitative or quantitative defects of αIIbβ3 affect platelet adhesion and aggregation and result in a severe, autosomal-recessive bleeding disorder called Glanzmann thrombasthenia (137). It has been shown that mice lacking subunit β3 display absent platelet aggregation, altered clot retraction and abnormal bleeding – similar to the human disease (138). These mice also displayed a decrease in fibrinogen uptake into platelets. Hence, αIIbβ3 is crucial for proper platelet function, enabling firm adhesion, aggregation and clot formation.

1.7 Aim of this study

Endocytic trafficking in megakaryocytes and platelets enables platelet granule biogenesis and packaging of granule content, uptake of plasma proteins, recycling of surface receptors and the release of bioactive proteins upon platelet activation. Therefore, endocytic trafficking is indispensable for platelet function. However, the underlying mechanisms of endocytic trafficking in megakaryocytes and platelets are poorly understood and key regulators of the endocytic machinery still need to be identified.

Strumpellin is a member of the highly conserved pentameric WASH complex, which serves as a major endosomal actin polymerisation-promoting complex. After recruitment to the endosomal membrane, it stimulates the generation of an Arp2/3-mediated actin network, thereby coordinating endosomal protein sorting and trafficking. Thus far, the WASH complex as well as Strumpellin have not been characterised in platelets and megakaryocytes. By generating a conditional knockout mouse, specifically lacking Strumpellin in platelets and megakaryocytes, its role was investigated.

The aim of this study was to elucidate the function of WASH complex subunit Strumpellin in murine platelets and megakaryocytes and consequently its effect on platelet biogenesis and function.

2 Material and methods

2.1 Material

2.1.1 Devices

Device	Manufacturer
APACT 4 fibrintimer	APACT (Hamburg, Germany)
Axiovert 200M inverted microscope	Zeiss (Oberkochen, Germany)
CoolSNAP EZ camera	Photometrics (Tucson, AZ, USA)
EM900 transmission electron microscope	Zeiss (Oberkochen, Germany)
FACSCalibur™	BD Biosciences (Heidelberg, Germany)
FluorChem® Q	Alpha Innotech (Kasendorf, Germany)
HEMAVET® 950	DREW (Miami Lakes, FL, USA)
HM 355S automatic microtome	Thermo Fischer (Schwerte, Germany)
LEICA ASP200S	Leica (Wetzlar, Germany)
Leica CM1900 cryostat	Leica (Wetzlar, Germany)
Leica DMI 4,000 B	Leica (Wetzlar, Germany)
MilliQ® integral water purification system	EMD Millipore (Billerica, MA, USA)
Sysmex KX-21N	Sysmex GmbH (Norderstedt, Germany)
TCS SP5 CLSM	Leica (Wetzlar, Germany)
TCS SP8 CLSM	Leica (Wetzlar, Germany)
UV transilluminator	Herolab GmbH (Wiesloch, Germany)

2.1.2 Materials

Material	Manufacturer
18 G x 1 ½", 20 G x 1 ½" needles	B. Braun (Melsungen, Germany)
26 G x 1 ½" needles	BD Biosciences (Heidelberg, Germany)
Cryofilm type 2C(9)	Section-Lab Co. Ltd. (Hiroshima, Japan)
EDTA-coated microvettes	Sarstedt (Nümbrecht, Germany)
Menzel-Gläser coverslips (24 x 50 mm)	Thermo Fisher (Schwerte, Germany)
Menzel-Gläser Superfrost® Plus microscope slides	Thermo Fisher (Schwerte, Germany)
Na-heparinised capillaries	Hartenstein (Würzburg, Germany)

2.1.3 Chemicals and reagents

Chemical/ Reagent	Manufacturer
2-propanol	Roth (Karlsruhe, Germany)
6x DNA loading dye	Thermo Fisher (Schwerte, Germany)
10x *Taq* buffer (+KCl, -$MgCl_2$)	Thermo Fisher (Schwerte, Germany)
Adenosine diphosphate (ADP)	Sigma-Aldrich (Schnelldorf, Germany)
Agarose standard	Roth (Karlsruhe, Germany)
Albumin fraction V	Roth (Karlsruhe, Germany)
Ammonium peroxidsulfate (APS)	Roth (Karlsruhe, Germany)
Apyrase (grade III)	Sigma-Aldrich (Schnelldorf, Germany)
BlueStar prestained protein marker	Nippon Genetics Europe (Düren, Germany)
Bovine serum albumin (BSA), low endotoxin	PAN Biotech (Aidenbach, Germany)
Calcium chloride ($CaCl_2$)	Roth (Karlsruhe, Germany)
Collagen-related peptide (CRP)	CRB Cambridge Research Biochemicals (Bil-lingham, UK)
Convulxin (CVX)	Axxora (Lörrach, Germany)
Deoxynucleotide triphosphates (dNTP)	Fermentas (St. Leon-Rot, Germany)

Chemical/ Reagent	Manufacturer
Dulbecco's phosphate buffered saline (PBS)	Sigma-Aldrich (Schnelldorf, Germany)
Eosin G	Roth (Karlsruhe, Germany)
Ethanol 100% denatured	Roth (Karlsruhe, Germany)
Ethanol 70% denatured	Roth (Karlsruhe, Germany)
Ethylene diamine tetra acetic acid (EDTA)	AppliChem (Darmstadt, Germany)
Eukitt® mounting medium	Sigma-Aldrich (Schnelldorf, Germany)
Fibrinogen from human plasma (#F13191), Alexa Fluor® 488 conjugated, for fibrinogen assay	Invitrogen (Waltham, MA, USA)
Fibrinogen from human plasma (#F4129), for aggregometry	Sigma-Aldrich (Schnelldorf, Germany)
Fibrinogen from human plasma (#F4883), for platelet spreading	Sigma-Aldrich (Schnelldorf, Germany)
Fluoroshield™	Sigma-Aldrich (Schnelldorf, Germany)
Fluoroshield™ with DAPI	Sigma-Aldrich (Schnelldorf, Germany)
GeneRuler DNA ladder mix	Thermo Fisher (Schwerte, Germany)
Glutaraldehyde ($C_5H_8O_2$)	Merck KGaA (Darmstadt, Germany)
Haematoxylin	Sigma-Aldrich (Schnelldorf, Germany)
Heparin sodium	Ratiopharm (Ulm, Germany)
Histosec® pastilles	Merck KGaA (Darmstadt, Germany)
Isofluran CP®	Cp-pharma (Burgdorf, Germany)
Magnesium chloride ($MgCl_2$) for PCR	Thermo Fisher (Schwerte, Germany)
Midori Green Advance DNA stain	Nippon Genetics Europe (Düren, Germany)
PageRuler™ Plus prestained protein ladder	Thermo Fisher (Schwerte, Germany)
Paraformaldehyde (PFA)	Sigma-Aldrich (Schnelldorf, Germany)
PF4_neu_for (primer forward)	Biomers (Ulm, Germany)
PF4_neu_rev (primer reverse)	Biomers (Ulm, Germany)
Phalloidin DyLight 650 (#21838)	Thermo Fisher (Schwerte, Germany)
Phalloidin-FITC	Enzo Life Sciences (New York, USA)
Poly-L-lysine solution	Sigma-Aldrich (Schnelldorf, Germany)
Powdered milk, fat-free	Roth (Karlsruhe, Germany)
Prostacyclin (PGI_2)	Sigma-Aldrich (Schnelldorf, Germany)
Protease inhibitor cocktail	Sigma-Aldrich (Schnelldorf, Germany)
Proteinase K	Thermo Fisher (Schwerte, Germany)
PVDF western blotting membranes	Roche Diagnostics (Mannheim, Germany)
Rhodocytin (Rhod)	Prof. Dr. J. Eble (University Hospital Frankfurt, Germany)
Roti® -phenol/chloroform/isoamyl alcohol (25:24:1)	Roth (Karlsruhe, Germany)
Rotiphorese® gel 30	Roth (Karlsruhe, Germany)
Sodium dodecyl sulphate (SDS)	Sigma-Aldrich (Schnelldorf, Germany)
Strump-for-U1 (primer forward)	Biomers (Ulm, Germany)
Strump-rev-D1 (primer reverse)	Biomers (Ulm, Germany)
Sucrose	Sigma-Aldrich (Schnelldorf, Germany)
Super cryoembedding medium (SCEM)	Section-Lab Co. Ltd. (Hiroshima, Japan)
Taq DNA polymerase	Thermo Fisher (Schwerte, Germany)
Tetraacetylethylenediamine (TEMED, $C_6H_{16}N_2$)	Roth (Karlsruhe, Germany)
Thrombin (Thr)	Roche Diagnostics (Mannheim, Germany)
Thrombopoietin (TPO)	Nieswandt laboratory (Würzburg, Germany)
Triton X-100	Sigma-Aldrich (Schnelldorf, Germany)
Trypan blue	Sigma-Aldrich (Schnelldorf, Germany)

Chemical/ Reagent	Manufacturer
Tween® 20	Roth (Karlsruhe, Germany)
U46619 (U46)	Enzo Lifesciences (Lörrach, Germany)
Uranyl acetate	Electron Microscopy Sciences (Hatfield, PA, USA)
Western Lightning® Plus-ECL – enhanced luminol reagent plus	PerkinElmer (Waltham, MA, USA)
Western Lightning® Plus-ECL – oxidizing reagent plus	PerkinElmer (Waltham, MA, USA)
Xylol	Roth (Karlsruhe, Germany)

All reagents and chemicals not listed above were obtained from AppliChem (Darmstadt, Germany), Roth (Karlsruhe, Germany) or Sigma-Aldrich (Schnelldorf, Germany).

2.1.4 Kits

Kit	Manufacturer	Catalogue Nr.
Mouse P-selectin enzyme linked immunosorbent assay (ELISA) kit	RayBio® (Peachtree Corners, GA, USA)	Q01102

2.1.5 Antibodies

2.1.5.1 Commercial primary and secondary antibodies

Antibody	Host	Manufacturer	Catalogue Nr.
Alexa Fluor® 488 anti-alpha-Tubulin	mouse	Thermo Fisher (Schwerte, Germany)	#322588
Alexa Fluor® 647 anti-CD105	rat	eBioscience (San Diego, CA, USA)	
Anti-Filamin A	rabbit	Cell Signalling (Danvers, MA, USA)	#4762
Anti-GAPDH	rabbit	Sigma-Aldrich (Schnelldorf, Germany)	#99545
Anti-Human Fibrinogen	rabbit	DAKO (Hamburg, Germany)	A0080
Anti-rabbit IgG-Cy3 linked	donkey	Jackson ImmunoResearch (West Grove, PA, USA)	#711-165-152
Anti-rabbit IgG-HRP linked	goat	Cell Signalling (Danvers, MA, USA)	#7074
Anti-Strumpellin	rabbit	Abcam (Cambridge, UK)	#101222
Anti-WASH1	rabbit	Atlas Antibodies (Bromma, Sweden)	HPA002698
FITC anti-CD29 (β1 integrin)	hamster	BioLegend (San Diego, CA, USA)	#102205

2.1.5.2 Non-commercial antibodies

Antigen	Antibody	Clone	Isotype
α2β1	LEN1	12C6	IgG2b
αIIbβ3	JON1	6C10	IgG2b
αIIbβ3	JON2	45A9	IgG2a
αIIbβ3	JON3	3F3	IgG1
αIIbβ3	JON6	14A3	IgG2b
αIIbβ3 (activated form)	JON/A	4H5	IgG2b
αIIbβ3	MWReg30	5D7	IgG1
β3	EDL-1	57B10	IgG2a
CD9	ULF1	96H10	IgG2a
CLEC-2	INU1	11E9	IgG1
Fcγ-RIIb/ RIII	HB.197™	2.4G2	IgG2b
GPIbα	p0p4	15E2	IgG2b
GPV	DOM2	89H11	IgG2a
GPVI	JAQ1	98A3	IgG2a
GPIX	p0p6	56F8	IgG2b
P-selectin	WUG 1.9	5C8	IgG1

The monoclonal rat antibodies listed above were generated and modified in the Nieswandt laboratory (Würzburg, Germany). They were either labelled with fluorescein isothiocyanate (FITC), phycoerythrin (PE) or DyLight-649 using commercially available antibody labelling kits.

2.1.6 Buffers and solutions

Blocking buffer

BSA (Albumin fraction V or BSA - low endotoxin)	1 or 5%
in PBS (1x or Dulbecco's PBS)	

Blocking buffer for western blotting

BSA or fat-free dry milk	5%
in TBS-T	

Cacodylate buffer for transmission electron microscopy, pH 7.2

$C_2H_7AsO_2$	0.1 M

CATCH buffer

BSA	3.5%
EDTA	3 mM
HEPES	25 mM
in PBS (1x)	
added prior to usage: fetal calf serum (FCS)	5%

Heparin

Heparin	20 U/ml
in TBS (1x)	

Laemmli buffer for SDS-PAGE

Glycine	0.95 mM
SDS	0.5%
Tris	40 mM

Lysis buffer for DNA isolation, pH 7.2

EDTA	5 mM
NaCl	200 mM
SDS	0.2%
Tris base	100 mM
added prior to usage: proteinase K (20 mg/ml)	100 µg/ml

Paraformaldehyde (PFA)

PFA	1, 2, 4 or 10%
in PBS (1x)	

Phosphate buffered saline (PBS), pH 7.14

KCl	2.7 mM
KH_2PO_4	1.5 mM
NaCl	137 mM
Na_2HPO_4	8 mM

Platelet lysis buffer (2x), pH 7.4

EGTA	10 mM
HEPES	15 mM
NaCl	150 mM
Triton X-100	2%
added prior to usage: protease inhibitor cocktail	0.01%

SDS sample buffer, 4x reducing

β-mercaptoethanol	20%
Bromophenol blue	0.04%
Glycerol	40%
SDS	8%
Tris-HCl	200 mM

Separating gel buffer for SDS-PAGE, pH 8.8

Tris-HCl	1.5 M

Stacking gel buffer for SDS-PAGE, pH 6.8

Tris-HCl	0.5 M

Tris acetate EDTA (TAE) buffer (50x), pH 8.0

Acetic acid	5.7%
EDTA	50 mM
Tris base	200 mM

Tank blot buffer for SDS-PAGE

Na_2CO_3	30 mM
NaHCO3	100 mM
to be used:	
H_2O	700 ml
Methanol	200 ml
Tank blot buffer	100 ml

Tris EDTA (TE) buffer, pH 8.0

EDTA	1 mM
Tris base	10 mM

Tris-buffered saline (TBS), pH 7.3

NaCl	137 mM
Tris-HCl	20 mM

Tyrode's buffer with or without Ca^{2+}, pH 7.4

$CaCl_2$	0 or 2 mM
HEPES	5 mM
KCl	2.7 mM
$MgCl_2$	1 mM
NaCl	137 mM
$NaHCO_3$	12 mM
NaH_2PO_4	0.43 mM
added prior to usage: BSA	0.35%
added prior to usage: Glucose	1%

Washing buffer (TBS-T)

Tween® 20	0.1%
in TBS (1x)	

If not stated otherwise all buffers were prepared with deionised water obtained from a MilliQ® integral water purification system. pH was adjusted using HCl or NaOH.

2.1.7 Mouse model

Conditional Strumpellin-deficient mice were generated by crossbreeding *Strumpellin*$^{flox/flox}$ mice with mice expressing the Cre-recombinase under the control of the *PF4* promoter (139). This enabled the generation of megakaryocyte and platelet specific knockout mice.

Strumpellin$^{flox/flox}$ mice were kindly provided by Dr. Laura M. Machesky (Cancer Research UK Beatson Institute, University of Glasgow, UK). The mouse line was generated by Sheila Bryson (Cancer Research UK Beatson Institute, University of Glasgow, UK) as follows (107): an embryonic stem (ES) cell clone (HEPD0534-7-C01) was obtained from the international knockout mouse consortium (IKMC) repository (140). The cells were then cultured on a monolayer of DR4 (4-drug resistant) irradiated mouse embryonic fibroblasts (MEFs) (141). Correct targeting of the *Strumpellin* gene (E430025E21Rik$^{tm1a(EUCOMM)Hmgu}$) in the ES cell clone was confirmed by polymerase chain reaction (PCR). The 5'-ends (GCTAGTGTCAGCGACAGAGTGCGCGCTC and CACAACGGGTTCTTCTGTTAGTCC) and 3'-ends (TCTATAGTCGCAGTAGGCGG and CAGGTTCACTGGCAGGTCGTGCTGTTAGAC) were screened using an expand long template PCR system (Roche Diagnostics, Mannheim, Germany) with the indicated oligonucleotides in accordance with the manufacturer's protocol. The presence of the isolated loxP site (TCATTCCCAGCACCTGTGTC and TGAACTGATGGCGAGCTCAG) was also confirmed by PCR. The mouse line was then derived by injecting ES cells into C57BL/6J blastocytes using standardised protocols (142). The resulting chimeric mice were identified by their agouti coat colour. Chimeric mice were bred and the germline transmitting chimeras were then identified by the coat colour of their offspring. The

presence of the modified allele was then confirmed by PCR using the aforementioned 3' loxP primers. Following this, heterozygous mice were crossbreed with a mouse line expressing Flpe (Tg(ACTFLPe)9205Dym) to eliminate the selectable marker by recombination at the FRT sites (143). The successful removal of the lacZ gene and the selectable marker cassette was confirmed by PCR across the remaining FRT site (CCAGAGGTGTGGCTCATAGG and TGACTGTTGGACAGGACACG). After the removal of the cassette exon, the modified allele had two remaining loxP sites flanking exon 12 of the *Strumpellin* gene. (Ensembl ID: ENSMUSE00000222520 in mouse genome assembly GRCm38.p4). Exon 12 was deleted following Cre recombination. This resulted in premature termination of mRNA translation, thus preventing the synthesis of the Strumpellin protein.

From here onwards the conditional mice will be referred to:

- *Strumpellin$^{flox/flox}$ PF4-Cre$^{-/-}$* as *Strumpellin$^{+/+}$* (control mice) and
- *Strumpellin$^{flox/flox}$ PF4-Cre$^{+/-}$* as *Strumpellin$^{-/-}$* (knockout mice).

All mice were maintained on a C57BL/6J background. If not stated otherwise, at least three independent experiments were conducted with sex-matched control and knockout mice aged six to twenty weeks. All animal studies were approved by the district government of Lower Franconia (Bezirksregierung Unterfranken).

2.2 Methods

2.2.1 Genotyping of mice

Mice were genotyped by PCR using DNA isolated from ear tissue.

2.2.1.1 Isolation of DNA from murine ear tissue

Murine ear tissue was lysed in 500 µl DNA lysis buffer for 3 hours at 1,400 rpm and 56°C. After lysis, 500 µl of phenol/chloroform/isoamyl alcohol were added. The well mixed samples were centrifuged for 10 minutes at 10,000 rpm and at room temperature (RT), thus separating each one into the nucleic acid containing upper aqueous phase and the lower organic phase. To precipitate the DNA, the upper phase was transferred to a new tube containing 500 µl 2-propanol. The samples were shaken well and centrifuged for 10 minutes at 1,400 rpm and 4°C. After removing the supernatant, 500 µl 70% ethanol were added to wash the DNA, followed by centrifugation (10 minutes, 1,400 rpm, 4°C). The supernatant was discarded, and the remaining DNA dried for 30 minutes at 37°C before solubilizing it in 50 µl TE buffer.

2.2.1.2 PCR

Apart from the primer set, assembly of all reaction components, as well as the PCR program were identical for both *Strumpellin* and *PF4* PCR.

PF4 primer set:

PF4_neu_for:	5'-CTCTGACAGATGCCAGGACA-3'	
PF4_neu_rev:	5'-TCTCTGCCCAGAGTCATCCT-3'	
predicted band size:	WT:	no PCR product
	PF4-Cre positive:	450 bp

Strumpellin primer set:

Strump-for-U1:	5'-GGGTAAGTGCTGGTCTCAAGTCAC-3'	
Strump-rev-D1:	5'-GCAAATCTAAGTGCTCAGGTGCTC-3'	
predicted band size:	WT:	481 bp
	KO:	618 bp

PCR mixture:

10x *Taq* buffer (+KCl, -$MgCl_2$)	2.5 µl
$MgCl_2$	2.5 µl
dNTP (10 mM)	1 µl
Primer for (1:10 dilution in H_2O of 100 pmol/µl stock)	1 µl
Primer rev (1:10 dilution in H_2O of 100 pmol/µl stock)	1 µl
Taq DNA polymerase	0.25 µl
H_2O	14.75 µl
Template DNA	2 µl

PCR program:

Table 2: PCR program for *Strumpellin* and *PF4-Cre*

Step	Temperature [°C]	Time [min]	
1	96	3:00	
2	94	0:30	35 cycles of steps 2 to 4
3	60	0:30	
4	72	0:45	
5	72	2:00	
6	22	∞	

2.2.1.3 Agarose gel electrophoresis

DNA bands were separated by agarose gel electrophoresis. A 2% agarose gel was prepared by dissolving 2 g agarose powder in 100 ml boiling 1x TAE buffer supplemented with 5 µl Midori Green Advance DNA Stain. The gel, equipped with a comb to create wells for sample loading, was left to set completely. It was then transferred into an electrophoresis chamber containing 1x TAE buffer. Wells were loaded with 20 µl PCR product mixed with 5 µl 6x DNA loading dye solution. 8 µl of 100-10,000 bp GeneRuler DNA ladder mix was loaded to later determine the size of the individual DNA bands under UV light. Previously ascertained samples from either *Strumpellin$^{flox/flox}$* or heterozygous *Strumpellin$^{wt/flox}$* as well as PF4 positive (*PF4-Cre$^{+/-}$*) or negative (*PF4-Cre$^{-/-}$*) mice were

used as control samples. Gel electrophoresis ran for 45 minutes at 140 Volt. DNA bands were visualised under UV light with a UV transilluminator.

2.2.2 Platelet isolation

Blood was drawn with Na-heparinised capillaries and collected in 300 µl heparin. After adding another 300 µl heparin, the samples were centrifuged for 6 minutes at 800 rpm. The platelet-rich upper layer was transferred into a new tube containing 300 µl heparin. After repeating the centrifugation step (6 minutes, 800 rpm), platelet-rich plasma was transferred into a new tube. The platelets were then pelleted by centrifugation (5 minutes, 2,800 rpm). After discarding the supernatant, the platelets were washed with 1 ml Tyrode's buffer. These steps were repeated three times in all. To prevent premature platelet activation, apyrase (0.02 U/ml) and PGI_2 (0.1 µg/ml) were added to the Tyrode's buffer of each washing cycle.

From here onwards isolated platelets will be referred to as 'washed platelets'. Platelet count per µl as well as subsequent preparation steps differed for each experiment. Details are given below for each method mentioned. Platelet count was determined by a Sysmex KX-21N cell counter.

2.2.3 Western blotting

2.2.3.1 Preparation of platelet lysates

To lyse the cells and solubilise proteins, washed platelets were pelleted by centrifugation for 5 minutes at 2,800 rpm. The supernatant was discarded and the platelets resuspended in platelet lysis buffer to achieve a platelet count of 1,000,000 platelets per µl. Samples were then put on ice for 30 minutes. To better detect Strumpellin, WASH1 and the three fibrinogen chains α, β and γ, disulphide bridges were cleaved. This was done by mixing the platelet lysates with 4x reducing SDS sample buffer.

2.2.3.2 Immunoblotting

Table 3: SDS-PAGE mixtures

SDS-mixture per 1 gel	4% stacking gel	10% separating gel	12% separating gel
30% Acrylamide	300 µl	2,000 µl	2,400 µl
APS (1:100)	20 µl	60 µl	60 µl
Buffer	500 µl	1,500 µl	1,500 µl
H_2O	1,000 µl	2,500 µl	2,000 µl
10% SDS	20 µl	60 µl	60 µl
TEMED (1:1000)	2 µl	6 µl	6 µl

For SDS-PAGE, platelet lysates were boiled for 5 minutes at 95°C. 20 µl per sample were loaded onto a 4% stacking gel. The separating gels for the individual proteins differed from each other as follows: a 10% separating gel was used to detect Strumpellin and WASH1; a 12% gel was used to separate and detect the three fibrinogen chains. BlueStar prestained protein marker (10-180 kDa) or PageRuler™ Plus prestained protein ladder (10-250 kDa) were used as markers to later estimate the size of the proteins in question. The gels ran for approximately 1 hour at 120 Volt in gel chambers filled with 1x Laemmli buffer.

The separated proteins were then transferred onto PVDF membranes by blotting for 1 hour at 350 mA. Afterwards, the membranes were blocked with 5% BSA or 5% fat-free dry milk for 1 hour at RT. The membranes were then incubated with the indicated antibodies overnight at 4°C. The proteins were detected using anti-rabbit IgG conjugated with horseradish peroxidase (HRP) and ECL solution. The images were taken using a Fluor-Chem® Q camera. GAPDH or Filamin-A were used as loading controls.

2.2.4 Measurement of whole-blood parameters by Hemavet®

Approximately 20 µl of blood were collected in EDTA-coated microvettes. Blood parameters were measured using a Hemavet®.

2.2.5 Platelet count, size and glycoprotein expression by FACS

50 µl blood were collected in 300 µl heparin and further diluted (1:20) in Tyrode's buffer. Samples were then incubated for 15 minutes at RT as follows: 1) with a mixture (1:1) of fluorophore-conjugated antibodies (2 µg/ml each; PE-labelled JON6 and FITC-labelled DOM2) to assess platelet size as well as platelet count per µl, or 2) with FITC-conjugated antibodies (2 µg/ml each), directed against platelet surface proteins, including GPIb, GPV, GPVI, GPIX, α2, β1, αIIbβ3, CD9 and CLEC-2, to determine their surface expression. After 15 minutes, 500 µl of PBS buffer were added. Platelet size, count as well as glycoprotein expression were measured using a FACSCalibur™ flow cytometer.

2.2.6 Determination of platelet ultrastructure by TEM

Washed platelets were fixed with 2.5% glutaraldehyde in 50 mM cacodylate buffer and subsequently embedded in Epon 812. Ultra-thin slices were sectioned and stained with 2% uranyl acetate and lead citrate. Samples were visualised with an EM900 transmission electron microscope. Images were analysed by manually determining platelet size and shape as well as granule and microtubule content with Image J.

2.2.7 F-actin assembly in platelets by FACS

Washed platelets were pelleted by centrifugation (5 minutes, 2,800 rpm) and resuspended in Tyrode's buffer containing $CaCl_2$ (500,000 platelets/µl). They were then incubated with a DyLight 649-labelled anti-GPIX antibody derivative (20 µg/ml) for 3 minutes at 37 C. The platelets were either left unstimulated or were activated using thrombin (0.1 and 0.001 U/ml) or CRP (10 and 1 µg/ml) for 2 minutes. Platelets were fixed with 10% PFA and permeabilised with 1% Triton X-100. F-actin was stained for 30 minutes using FITC-labelled Phalloidin (10 µM). 500 µl of PBS buffer were added, before F-actin polymerisation was measured using a FACSCalibur™ flow cytometer.

2.2.8 Cold-induced microtubule disassembly in platelets

Menzel-Gläser coverslips were coated with 0.01% Poly-L-lysine (PLL) for 20 minutes at RT and washed once with deionized water. Washed platelets were pelleted by centrifugation (5 minutes, 2,800 rpm) and resuspended in Tyrode's buffer containing apyrase (0.02 U/ml) to achieve a count of 300,000 platelets per µl. Next, the platelets were incubated under the following conditions, either: 1) for 3.5 hours at 37°C, or 2) for 3.5 hours at 4°C to assess microtubule depolymerisation, or 3) for 3 hours at 4°C before being rewarmed to 37°C for half an hour to induce re-polymerisation of tubulin. Platelets were then fixed with 1.5% PFA and permeabilised with 0.075% IGEPAL® CA-630 in PBS and directly transferred onto the coverslips. They were left to adhere to PLL for 30 minutes. The samples were then blocked with 5% BSA and immuno-stained using Alexa Fluor® 488-conjugated anti-α-tubulin (1 µg/ml) and Phalloidin DyLight 650 (1 u/ml) for 1 hour at RT. Mounted with Fluoroshield™, the samples were imaged using a TCS SP8 confocal laser scanning microscope (CLSM).

2.2.9 *In vitro* analyses of platelet function

2.2.9.1 αIIbβ3 activation and P-selectin exposure

50 µl of blood were collected in 300 µl heparin. It was then centrifuged for 5 minutes at 2,800 rpm and washed three times with Tyrode's buffer. The remaining blood pellets were resuspended in Tyrode's buffer containing $CaCl_2$. The platelets were either kept resting or were activated by ADP (10 µM), U46 (1 µM), a mixture of ADP and U46 (10 µM/ 1 µM), thrombin (0.1, 0.01 and 0.001 U/ml), CRP (10, 1 and 0.1 µg/ml), convulxin (CVX, 0.5 µg/ml) or rhodocytin (Rhod, 1 µg/ml). The samples were incubated with a mixture (1:1) of two fluorophore-conjugated antibodies (2 µg/ml each; JON/A-PE against active αIIbβ3 and WUG 1.9-FITC against P-selectin), first for 7 minutes at 37°C and then for

7 minutes at RT. 500 µl of PBS buffer were added. αIIbβ3 activation and P-selectin exposure were analysed using a FACSCalibur™ flow cytometer.

2.2.9.2 αIIbβ3 expression on the surface of activated platelets

50 µl of blood were collected in 300 µl heparin. After three centrifugation (5 minutes, 2,800 rpm) and washing cycles with Tyrode's buffer, the remaining blood pellets were resuspended in Tyrode's buffer with $CaCl_2$. The platelets were either kept resting or were stimulated with either ADP and U46 (10 µM/ 1 µM), thrombin (0.02 U/ml), CRP (10 µg/ml) or CVX (1 µg/ml). They were incubated with FITC-labelled JON6 for 7 minutes at 37°C and subsequently for 7 minutes at RT. 500 µl of PBS buffer were added. αIIbβ3 expression of activated platelets was assessed by a FACSCalibur™ flow cytometer.

2.2.9.3 Fibrinogen binding capacity

Washed platelets were pelleted by centrifugation (5 minutes, 2,800 rpm) and resuspended in Tyrode's buffer containing $CaCl_2$ (18,000 platelets/µl). The platelets were either kept resting or were activated with a mixture of ADP and U46 (10 µM/ 1 µM), CVX (0.5 µg/ml) or Rhod (1 µg/ml). The samples were then incubated with Alexa Fluor® 488-conjugated fibrinogen (50 µg/ml) for 5 minutes at 37°C. 500 µl PBS buffer were added. The fibrinogen binding capacity of resting and activated platelets after the indicated time point was measured by a FACSCalibur™ flow cytometer.

2.2.9.4 Fibrinogen uptake into platelets

Washed platelets were pelleted by centrifugation (5 minutes, 2,800 rpm) and resuspended in Tyrode's buffer (18,000 platelets/µl). To analyse the uptake of fibrinogen, previously described by *Huang et al.* (60), platelets were incubated with Alexa Fluor® 488-conjugated fibrinogen (150 µg/ml) for 0, 5, 15 or 30 minutes at 37°C. After fixation with 2% PFA overnight at 4°C, 0.1% trypan blue was added to quench the signal of extracellular Alexa Fluor® 488-conjugated fibrinogen. The samples were incubated for 10 minutes before adding 500 µl PBS buffer. Intracellular Alexa Fluor® 488-fibrinogen levels were measured using a FACSCalibur™ flow cytometer.

2.2.9.5 Platelet spreading on fibrinogen

Menzel-Gläser coverslips were coated with fibrinogen from human plasma (100 µg/ml) overnight at 4°C. They were then blocked with 1% low endotoxin BSA in sterile PBS buffer for 1 hour at RT and washed twice with PBS buffer and once with Tyrode's buffer prior to the spreading assay. Washed platelets were centrifuged (5 minutes, 2,800 rpm) and resuspended in Tyrode's buffer containing apyrase (0.02 U/ml) to achieve a platelet count

of 300,000 per µl. The samples were left to rest for 30 minutes at 37°C. The platelets (20 µl in 70 µl Tyrode's buffer with $CaCl_2$) were then stimulated with thrombin (0.01 U/ml) and left to spread on the coated coverslips for 5, 15 or 30 minutes. After the indicated time points, they were fixed with 4% PFA and imaged with an Axiovert 200 inverted microscope (100x/1.4 oil objective) and digitalised with a CoolSNAP EZ camera. Adherent platelets were divided into four stages according to their spreading progress and quantified using Image J.

2.2.9.6 Platelet aggregometry

Washed platelets were pelleted by centrifugation (5 minutes, 2,800 rpm) and resuspended in Tyrode's buffer containing apyrase (0.02 U/ml) to achieve a platelet count of 500,000 per µl. Samples were pooled, if necessary, to ensure enough measurements using different agonists. Prior to the experiment, platelets rested for 30 minutes at 37°C. Agonists thrombin (0.05 and 0.005 U/ml), collagen (10, 5 and 2.5 µg/ml) and U46 (1, 0.5, 0.25 and 0.1 µg/ml) were used for platelet stimulation. Platelets were prepared as follows: 1) for collagen and U46 washed platelets were diluted in Tyrode's buffer containing $CaCl_2$ and 70 µg/ml fibrinogen from human plasma; 2) for thrombin fibrinogen was excluded. To determine platelet aggregation, light transmission was assessed on an APACT 4 fibrintimer aggregometer. Transmission was recorded for 10 minutes. It was expressed as arbitrary units with transmission-through-buffer defined as 100% transmission.

2.2.10 P-selectin content by quantitative ELISA

A commercial mouse P-selectin enzyme linked immunosorbent assay (ELISA) kit was purchased from RayBio®. The experiment was performed according to the manufacturer's protocol to determine P-selectin content of platelet lysates (lysate dilutions: 1:1,200 to 1:4,800). An antibody specific to murine P-selectin, coated on a 96-well plate, was used in the assay. If present in the sample, immobilised P-selectin was detected using a biotinylated anti-mouse P-selectin antibody, HRP-labelled streptavidin and TMB substrate solution. Platelet lysates from P-selectin-deficient mice were used as negative controls.

2.2.11 Megakaryocytes

2.2.11.1 Megakaryocyte analysis in bone marrow and spleen histologic sections

Control and knockout mice were killed by cervical dislocation under isoflurane anaesthesia. The spleen as well as both femora were harvested and fixed in 4% PFA overnight at RT. Bones were decalcified using 10% EDTA in PBS buffer for at least 3 days at RT.

Subsequently, bones and spleen were dehydrated using a LEICA ASP200S tissue processor and embedded in paraffin. Five-micrometre-thick spleen and bone sections were prepared using a HM 355S automatic microtome. The sections were transferred onto *Menzel-Gläser* coverslips and subsequently deparaffinized, rehydrated, stained with haematoxylin and eosin (H&E) and dehydrated again as follows:

Deparaffination:	
Xylol I	3 minutes
Xylol II	3 minutes
Rehydration:	
100% ethanol	2 minutes
96% ethanol	2 minutes
90% ethanol	2 minutes
80% ethanol	2 minutes
70% ethanol	2 minutes
Deionised water	2 minutes
Staining:	
Haematoxylin	30 seconds
Sections were thoroughly washed under running tap water for 5 to	10 minutes
0.05% eosin in deionised water	2 minutes
Sections were washed once in deionised water	
Dehydration:	
70% ethanol	2 minutes
80% ethanol	2 minutes
90% ethanol	2 minutes
96% ethanol	2 minutes
100% ethanol	2 minutes
Xylol I	3 minutes
Xylol II	3 minutes

The sections were mounted with Eukitt® and left to dry overnight at RT. The samples were visualized using a Leica DMI 4,000 B inverted microscope.

2.2.11.2 Megakaryocyte analysis in whole femora cryosections

Femora of control and knockout mice were removed, cleaned and fixed with 4% PFA and 5 mM sucrose in PBS buffer for 1 hour under agitation. For dehydration, the bones were transferred into tubes containing a graded series of, in the following order, 10%, 20% and 30% sucrose in PBS buffer. Each dehydration step lasted for 24 hours at 4°C. The samples were then embedded in super cryoembedding medium (SCEM) and frozen for at least 1 hour at -80°C. The bones were sectioned into seven-micrometre-thick slices onto cryofilm type 2C(9) using a Leica CM1900 cryostat (144). The femora sections were then transferred onto *Menzel-Gläser Superfrost® Plus* microscope slides. After rehydration with PBS buffer for 20 minutes, the sections were blocked using 5% BSA for 1 hour at RT. Depending on the antibody's host, 5% goat serum, 5% rat serum or a mixture of both

were added to the BSA. To stain endothelium, the sections were incubated with Alexa Fluor® 647-conjugated anti-CD105 antibody (3.33 µg/ml) for 1.5 hours at RT. Megakaryocytes and platelets were labelled with an anti-αIIbβ3 antibody (JON6, 3.33 µg/ml). Cyanine 3 (Cy3)-linked anti-IgG was used as the necessary secondary antibody. Nuclei were stained and the sections mounted with Fluoroshield™ containing DAPI. After each staining process, the sections were washed twice using TBS-T and once with PBS buffer. Images were taken with a TCS SP5 CLSM. Megakaryocyte number, morphology and localisation to blood vessels were analysed.

2.2.11.3 Determination of bone marrow megakaryocyte ploidy and αIIbβ3 surface expression

Femora of control and knockout mice were harvested, and the bone marrow was flushed out into 2 ml CATCH buffer using a syringe. A single cell suspension was prepared using a syringe first and then differently gauged needles (18 G, 20 G and lastly 26 G). The suspension was passed through a cell strainer (pore size: 100 µm) to remove any bone or tissue parts. The samples were centrifuged for 5 minutes at 1,200 rpm at RT. After discarding the supernatant, the pellets were resuspended in 400 µl CATCH buffer and PBS (1:1) supplemented with 5% FCS. To saturate unspecific binding sites of the anti-αIIbβ3 antibody, the cells were incubated with an anti-Fcγ-RIIb/ RIII antibody (0.02 µg/µl) for 15 minutes. Megakaryocytes were then stained with a FITC-conjugated anti-αIIbβ3 antibody (MWReg30, 10 µg/µl) for 20 minutes. After three washing cycles using CATCH buffer, the cells were fixed with 250 µl 1% PFA and permeabilised with 500 µl 0.1% Tween in PBS buffer for 10 minutes each. During incubation, fixation and permeabilization the cells were kept on ice. Following three washing cycles, DNA was stained with propidium iodide (final concentration: 25 µg/ml) in H_2O supplemented with ribonuclease (final concentration: 100 µg/ml) overnight at 4°C. Megakaryocytes obtained from various control mice were mixed and served as an isotype control. Therefore, the cells were stained with an anti-rat FITC-conjugated IgG1 antibody (10 µg/µl) instead of the anti-αIIbβ3 antibody. All other steps were identical. The use of the anti-αIIbβ3 antibody also enabled the assessment of αIIbβ3 expression on the megakaryocyte surface. Data was measured by FACSCalibur™ and analysed using FlowJo software (FlowJo LLC, Ashland, OR, USA).

2.2.12 Measuring spleen to body weight ratio

Age and sex-matched mice were killed by cervical dislocation. Their bodies were weighed before harvesting the spleen. Spleens were also weighed. The weight of the spleen was plotted against the body weight for each individual mouse. The mean value for either control or knockout ± standard deviation (s.d.) was calculated and presented permille.

2.2.13 Statistical analysis

Results are shown as mean values ± s.d.. They represent independently conducted experiments on control and knockout mice. The respective number of conducted experiments is listed below the corresponding figure or table. Differences between controls and knockouts were analysed statistically using the (unpaired) Student's *t*-Test. Results with a *P*-value higher than 0.05 were considered as not significant (n.s.). *P*-values smaller than 0.05 were considered statistically significant: * $P < 0.05$; ** $P < 0.01$ and *** $P < 0.001$.

3 Results

To study the role of the WASH complex subunit Strumpellin in megakaryocytes and platelets, megakaryocyte and platelet specific *Strumpellin* knockout mice were generated by crossbreeding *Strumpellin*$^{flox/flox}$ mice with mice carrying the Cre-recombinase downstream of the *PF4* promoter. The conditional *Strumpellin* knockout mice were viable, healthy, fertile and born at a normal Mendelian ratio (data not shown).

Strumpellin$^{flox/flox}$ *PF4-Cre*$^{-/-}$ mice (controls) will be referred to as *Strumpellin*$^{+/+}$, *Strumpellin*$^{flox/flox}$ *PF4-Cre*$^{+/-}$ mice (knockout) as *Strumpellin*$^{-/-}$.

3.1 Platelet analysis of Strumpellin-deficient mice

3.1.1 Reduced WASH1 protein content in *Strumpellin*$^{-/-}$ platelets

To confirm the absence of Strumpellin in *Strumpellin*$^{-/-}$ platelets as well as investigate if Strumpellin deficiency has an impact on WASH1 protein levels, western blot assays were performed on platelet lysates of knockout and control mice. Strumpellin was detected at the expected size of 134 kDa in controls, but not in mutant platelets (Figure 12), confirming that the PF4-Cre/loxP system efficiently prevents Strumpellin expression. Western blot analysis also confirmed that Strumpellin deficiency leads to a reduction in WASH1 expression (75 kDa), suggesting an unstable WASH complex (Figure 12). GAPDH served as a loading control.

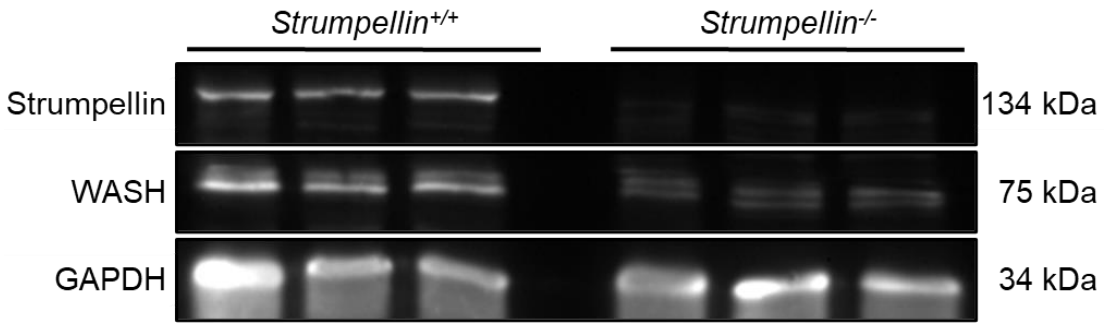

Figure 12: Strumpellin deficiency leads to a decrease in WASH1 expression in platelets
Western blot analysis confirmed the absence of Strumpellin and showed a decrease in WASH1 content in *Strumpellin*$^{-/-}$ platelets (n=3). GAPDH served as a loading control. The data represents one experiment. This experiment was performed with Dr. Yvonne Schurr and can also be found in her doctoral thesis (145).

3.1.2 Strumpellin deficiency does not affect platelet count and size

Next, whole-blood parameters of control and knockout mice were examined using a Hemavet®. No severe abnormalities in *Strumpellin*$^{-/-}$ mice were detected, as shown in Table 4. Especially platelet count and size were comparable to their littermate controls. White blood cell count as well as lymphocytes were slightly, but significantly increased in *Strumpellin*$^{-/-}$ mice, however, this result could not be reproduced.

Table 4: Normal blood parameters of *Strumpellin*$^{-/-}$ mice
Whole-blood parameters of *Strumpellin*$^{-/-}$ mice were determined by Hemavet®. Mean values ± s.d. (n=5), * $P < 0.05$, The data is representative of two independent experiments.

	***Strumpellin*$^{+/+}$**	***Strumpellin*$^{-/-}$**	**Significance**
Platelet count [592-2972 K/µl]	809±80	831±91	n.s.
Mean platelet volume [5.0-20.0 fl]	5.2±0.1	5.2±0.1	n.s.
White blood cells [1.8-10.7 K/µl]	8.7±2.5	12.7±2.2	*
Neutrophils [0.1-2.4 K/µl]	1.2±0.4	1.5±0.1	n.s.
Lymphocytes [0.9-9.3 K/µl]	7.2±2.1	10.8±2.1	*
Monocytes [0.0-0.4 K/µl]	0.3±0.1	0.4±0.1	n.s.
Eosinophils [0.0-0.2 K/µl]	0.0±0.0	0.0±0.0	n.s.
Red blood cells [6.36-9.42 M/µl]	9.8±0.4	9.7±0.5	n.s.
Haemoglobin [11.9-15.1 g/dl]	14.0±0.7	13.9±1.0	n.s.
Haematocrit [35.1-45.4%]	40.4±1.5	40.4±2.1	n.s.
Mean corpuscular volume [45.4-60.3 fl]	42.2±1.9	41.5±0.4	n.s.
Mean corpuscular haemoglobin [14.1-19.3 pg]	14.3±0.5	14.2±0.3	n.s.
Mean corpuscular haemoglobin concentration [30.2-34.2 g/dl]	34.6±0.7	34.3±0.7	n.s.
Red blood cell distribution width [12.4-27.0%]	17.0±0.3	16.8±0.4	n.s.

Unaltered platelet count (Figure 13A) and size (Figure 13B) were confirmed by flow cytometry. Count and size, the latter determined by the forward-scatter (FSC) signal, were measured using the PE-labelled JON6 antibody against αIIbβ3 and the FITC-labelled DOM2 against GPV. The results indicate functioning platelet production in the bone marrow of knockout mice.

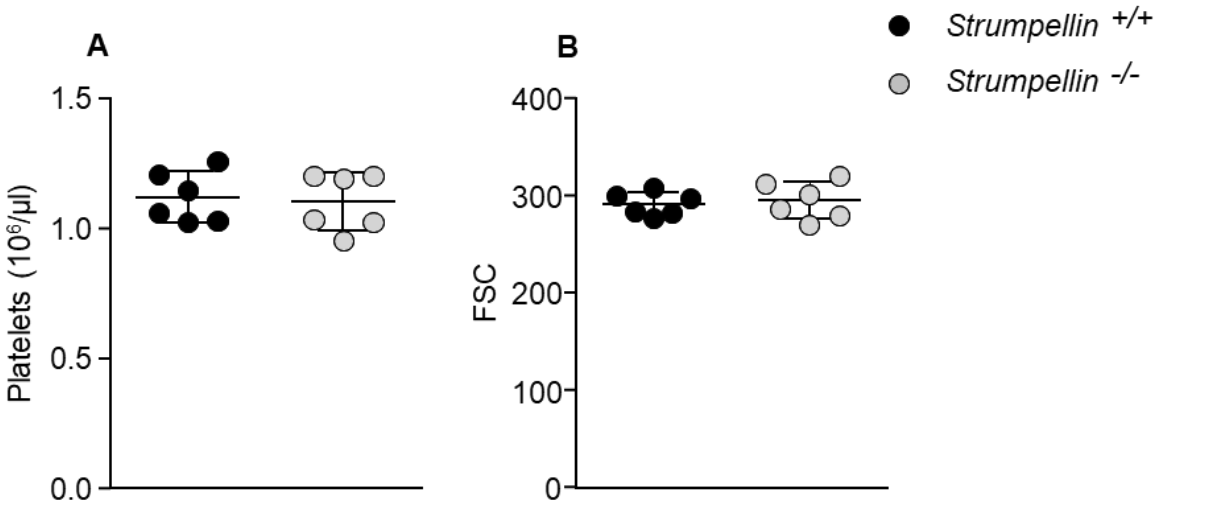

Figure 13: Unaltered count and size of *Strumpellin*$^{-/-}$ platelets
A) Platelet count per µl blood and B) size as mean FSC were measured by flow cytometry. Mean values ± s.d. (n=6). The data is representative of five independent experiments.

3.1.3 Increase in number, but unaltered size of α-granules in mutant platelets

Platelet granules are synthesised in megakaryocytes and derive from the endo-lysosomal system (25, 59). The major NPF on endosomes, the WASH complex and its subunit Strumpellin, may play a role in platelet granule biogenesis and affect ultrastructure, content and/or function.

Figure 14: Ultrastructure of resting platelets
Cross-section of a resting platelet. Platelets contain three major types of granules: α-granules, dense granules and lysosomes. Microtubules form a stabilising marginal ring. Due to its electron-dense content, the DTS can be distinguished from the OCS, which appears clear. Scale bar: 1 µm.

To detect possible alterations in the ultrastructure (Figure 14), caused by the loss of Strumpellin, platelet samples of *Strumpellin*$^{-/-}$ and control mice were prepared for TEM imaging. On analysing these images, no changes in platelet size were found, confirming Hemavet® and flow cytometry results. In addition, platelet shape remained unaltered (Figure 15A). The OCS and DTS appeared normal. Furthermore, no changes in micro-tubule number per platelet section were detected (Figure 15B). On analysing platelet granule content, a slight increase in dense granules as well as a slight, but significant increase in α-granule number in Strumpellin-deficient platelets were discovered (Figure 15C and D). However, the area of α-granules in *Strumpellin*$^{-/-}$ platelets was comparable to those in control platelets (Figure 15E and F). Although the increase in α-granule number is only moderate, it may indicate a role of Strumpellin in α- and possibly dense granule formation.

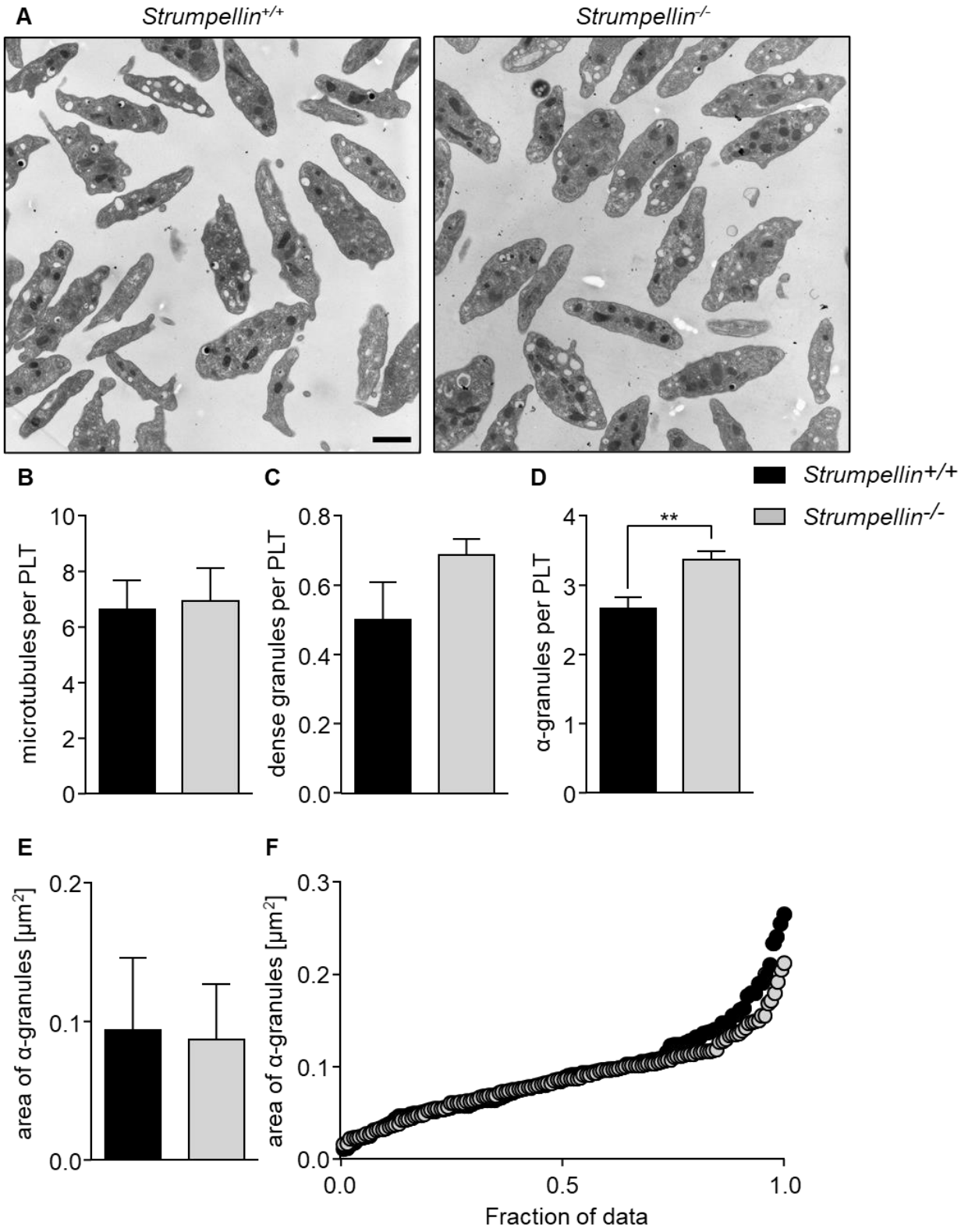

Figure 15: Increase in number, but unaltered size of α-granules in mutant platelets
A) Representative TEM images of washed platelets. Scale bar: 1 µm. B-C) Quantifications of microtubule, dense granule and α-granule number per platelet section. At least 489 platelets from three *Strumpellin*$^{+/+}$ mice and 472 platelets from three *Strumpellin*$^{-/-}$ mice were analysed. E) Determination of α-granule area in µm^2 from 121 *Strumpellin*$^{+/+}$ and 137 *Strumpellin*$^{-/-}$ platelets. F) Area of α-granules in µm^2 given as fraction of data. Values are mean ± s.d. (n=3), ** $P < 0.01$. The data represents one experiment.

3.1.4 Loss of Strumpellin does not alter F-actin assembly in platelets

Strumpellin deficiency resulted in reduced protein levels of actin-nucleation promoter WASH1 in murine platelets (Figure 12). To examine if Strumpellin deficiency or rather the decrease in WASH1 expression impacts overall F-actin polymerisation in platelets, an actin assembly assay was performed. Washed platelets were either left unstimulated or were activated using CRP or thrombin, before being fixed, permeabilised and stained for F-actin with FITC-labelled Phalloidin. The capacity of F-actin assembly was then measured by flow cytometry. Both *Strumpellin*$^{+/+}$ and *Strumpellin*$^{-/-}$ platelets displayed a similar increase in filamentous actin following platelet activation (Figure 16A). Furthermore, the ratio of F-actin in activated versus F-actin in resting platelets was determined for each agonist. Comparing them also showed a proportional increase of actin polymers in both *Strumpellin*$^{+/+}$ and *Strumpellin*$^{-/-}$ platelets (Figure 16B). This implies that loss of Strumpellin and/or the reduced amount of WASH1 does not affect overall F-actin polymerisation in platelets.

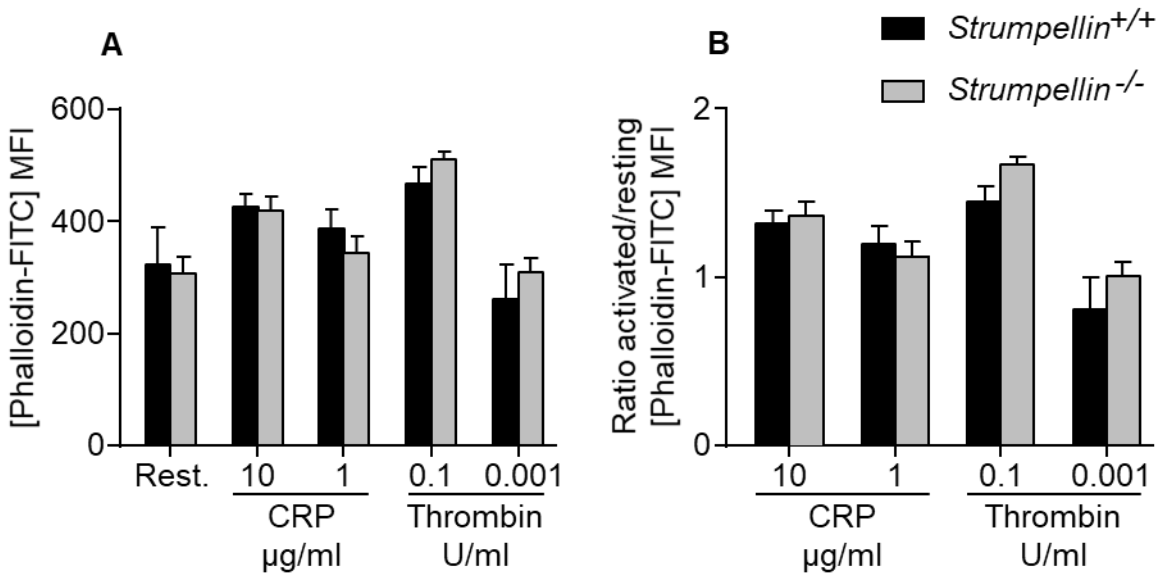

Figure 16: Strumpellin deficiency does not affect F-actin assembly in platelets
A) Resting and activated platelets, previously stimulated with CRP or thrombin, were permeabilised and stained for F-actin with FITC-labelled Phalloidin. Mean fluorescent intensity (MFI) was determined by flow cytometry and depicted as MFI ± s.d.. B) Ratios of F-actin in activated platelets vs. resting platelets are given for each agonist. Values are mean ± s.d. (n=3). The data is representative of two independent experiments. This experiment was performed with Dr. Yvonne Schurr and can also be found in her doctoral thesis (145).

3.1.5 Microtubules are stable in *Strumpellin*$^{-/-}$ platelets

The WASH complex mediates endosomal tubulation, which appear and elongate along microtubule tracks (29, 33). Furthermore, WASH1 directly interacts with α-tubulin via its TBR domain, possibly linking microtubules to retrieval subdomains where they assist in stabilisation and/or extension of forming tubules (29, 51, 52). This raised the question if loss of Strumpellin affects microtubule stability and its capacity to (de-)polymerise under certain conditions. Washed platelets were prepared and allowed to rest for 3.5 hours as follows: 1) at 37°C for microtubule assembly, 2) at 4°C for disassembly and 3) initially at 4°C, then the temperature was raised up to 37°C to induce re-assembly of tubulin. The fixed and permeabilised platelets were then stained for α-tubulin and F-actin and were left to adhere to PLL-coated coverslips. By assessing the microscopic images, no abnormalities in *Strumpellin*$^{-/-}$ platelets were found. At 37°C the platelets displayed the usual well-organised microtubule ring at the cell border, which dispersed and reappeared again at 4°C and 37°C, respectively (Figure 17A-C). This proves that Strumpellin deficiency does not alter microtubule dynamics in platelets. Microtubules are stable and can disassemble completely at lower and (re)assemble at higher temperatures. These results also coincide with the TEM findings, showing unaltered microtubule numbers per platelet section (Figure 15D).

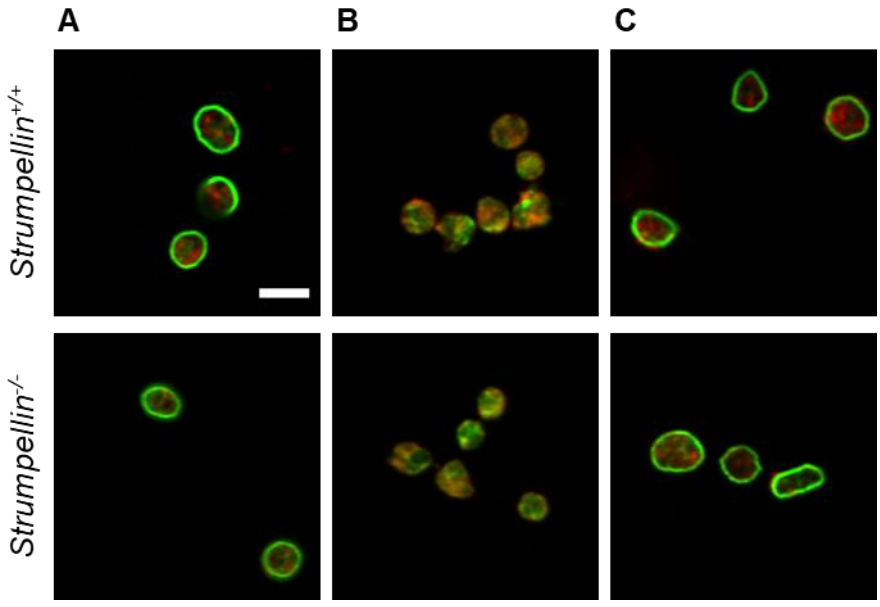

Figure 17: Unaltered microtubule stability in Strumpellin-deficient platelets
Washed platelets were left resting for A) 3.5 hours at 37°C, B) 3.5 hours at 4°C to depolymerise and C) 3 hours at 4°C before being rewarmed to 37°C for 0.5 hour to induce re-polymerisation of microtubules. They were stained with Alexa Fluor® 488-labelled anti-tubulin (green) and Phalloidin DyLight 650 (red). Representative images of the microtubule assembly assay (n=5). Scale bar: 2.5 µm. The data represents one experiment. This experiment was performed with Dr. Yvonne Schurr and can also be found in her doctoral thesis (145).

3.1.6 Decrease in αIIbβ3 expression on the surface of *Strumpellin*$^{-/-}$ platelets

Next, the surface expression of glycoproteins was examined on *Strumpellin*$^{+/+}$ and *Strumpellin*$^{-/-}$ platelets under resting conditions. The MFI of FITC-labelled antibodies against specific glycoproteins, listed in 2.1.5.1 and 2.1.5.2, was determined by flow cytometry. The MFI of GPIb, V and IX as well as CD9 and CLEC-2 was unaltered on Strumpellin-deficient platelets compared to controls. The MFI of integrin subunits α2 and β1 did not differ as well. The MFI of GPVI was slightly increased, however, this result could not be reproduced. Interestingly, a lower MFI of αIIbβ3 integrin was measured. Altogether there was an approximate decrease of 15% to 20% in αIIbβ3 expression on the surface of Strumpellin-deficient platelets under resting conditions (Table 5). The corresponding graph in Figure 18A gives a better overview of the glycoprotein surface expression.

Table 5: Strumpellin deficiency leads to a decreased αIIbβ3 surface expression in platelets
Diluted whole blood was incubated with FITC-labelled antibodies against indicated platelet glycoproteins. Surface expression, defined as MFI, was measured by flow cytometry. MFI is given as mean value ± s.d. (n=6), *** $P < 0.001$. The data is representative of five independent experiments.

	Strumpellin$^{+/+}$	*Strumpellin*$^{-/-}$	Significance
GPIb	339±8	343±13	n.s.
GPV	230±2	230±8	n.s.
GPVI	41±0.8	43±0.4	***
GPIX	418±6	409±10	n.s.
α2	45±0.7	46±3.0	n.s.
β1	153±5	149±8	n.s.
αIIbβ3	463±9	394±6	***
CD9	932±9	893±41	n.s.
CLEC-2	119±3	122±6	n.s.

Further flow cytometry assays confirmed the reduced αIIbβ3 surface expression by applying different antibodies against αIIbβ3 as well as one antibody against its subunit β3. *Strumpellin*$^{-/-}$ platelets displayed a decrease in αIIbβ3 surface expression of up to 20-22% with every antibody used (Figure 18B). The selected histograms of αIIbβ3 as well as of β3 surface expression, shown in Figure 18C, revealed that the entire population of mutant platelets shifted towards a lower MFI, suggesting a decrease in αIIbβ3 integrin on every single Strumpellin-deficient platelet and not only on a platelet subpopulation. These results suggest that Strumpellin selectively regulates αIIbβ3 surface expression.

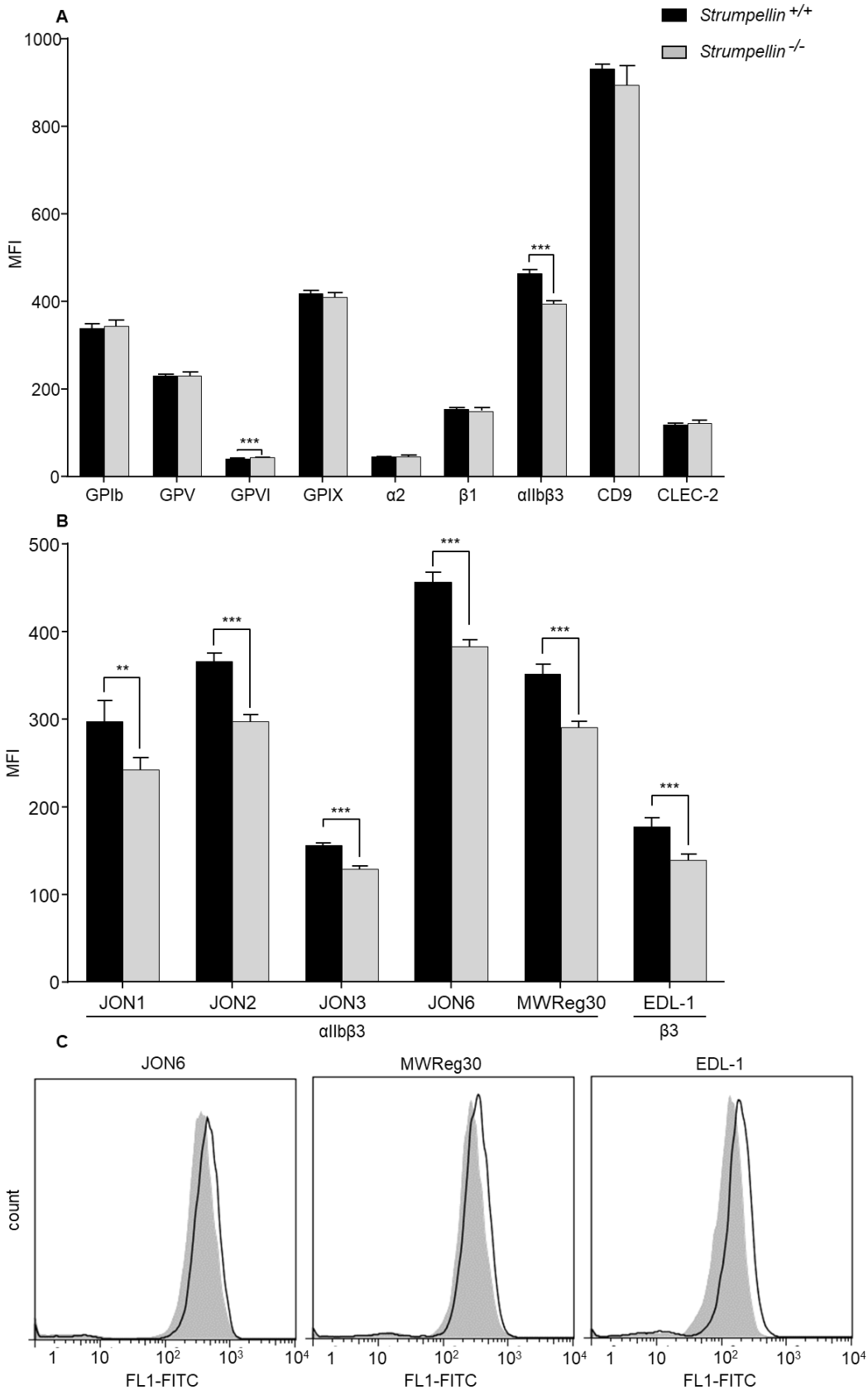

Figure 18: Decrease in αIIbβ3 surface expression in *Strumpellin*$^{-/-}$ platelets
Flow cytometric analysis of surface expression of A) indicated glycoproteins in platelets and B) αIIbβ3 and β3 determined by different antibodies. C) Selected histograms of flow cytometric measurements with indicated antibodies showed an αIIbβ3 and β3 decrease in the entire population of *Strumpellin*$^{-/-}$ platelets. Surface expression is given as MFI ± s.d. (n=6), ** $P < 0.01$, *** $P < 0.001$. The data is representative of five (A) and one (B and C) independent experiments. Ad B and C) this experiment was performed with Dr. Yvonne Schurr and can also be found in her doctoral thesis (145).

3.1.7 Impaired αIIbβ3 activation in *Strumpellin*$^{-/-}$ platelets

Upon platelet activation, intracellular signalling events lead to a conformational change of integrins and thus, higher affinity towards their ligands (12, 13). Furthermore, the internal pool of αIIbβ3 is exposed to the surface, adding to the already existing pool on the surface membrane (130, 131). Hence, determining the activated form of αIIbβ3 by flow cytometry can be used as a marker for platelet activation.

The applied agonists included ADP, U46619 (U46), thrombin, collagen-related peptide (CRP), convulxin (CVX) and rhodocytin (Rhod). ADP interacts with G-protein-coupled receptors $P2Y_1$ and $P2Y_{12}$ as well as calcium channel $P2X_1$ (146). $P2Y_{12}$ is the target of platelet aggregation inhibitors Clopidogrel, Prasugrel and Ticagrelor. U46619 acts as a TXA_2 analogue and binds to the G protein-coupled thromboxane receptor TP (146). Thrombin binds to the GPIb-V-IX complex as well as G protein-coupled protease-activated receptors (PARs) (146). CRP and CVX activate the GPVI-ITAM (immunoreceptor tyrosine-based activation motif) pathway (147). Rhod serves as a potent agonist of the hemITAM-containing CLEC-2 (148).

Using the PE-labelled JON/A antibody, directed specifically against activated αIIbβ3, a significant decrease in αIIbβ3 activation with almost every agonist was measured (Table 6 and corresponding Figure 19). This is possibly due to the already decreased level of αIIbβ3 expression on the platelet surface.

Table 6: Reduced αIIbβ3 activation in *Strumpellin*$^{-/-}$ platelets
Inside-out signalling of αIIbβ3 integrin was measured after platelet stimulation with indicated agonists using the PE-labelled JON/A antibody. MFI was measured by flow cytometry and is given as mean value ± s.d. (n=6), * $P < 0.05$, ** $P < 0.01$, *** $P < 0.001$. The data is representative of four independent experiments.

	***Strumpellin*$^{+/+}$**	***Strumpellin*$^{-/-}$**	**Significance**
Resting	22±2.1	19±1.3	*
ADP 10 µM	117±14	100±7	*
U46 1 µM	58±10.0	48±18.1	n.s.
ADP 10 µM/U46 1 µM	369±15	311±15	***
Thrombin 0.1 U/ml	493±40	419±32	**
Thrombin 0.01 U/ml	441±28	383±13	**
Thrombin 0.001 U/ml	76±4.2	66±15.5	n.s.
CRP 10 µg/ml	180±39	133±46	n.s.
CRP 1 µg/ml	123±33	90±35.2	n.s.
CRP 0.1 µg/ml	42±7.5	37±8.4	n.s.
CVX 0.5 µg/ml	273±44	203±48	*
Rhod 1 µg/ml	473±32	397±34	**

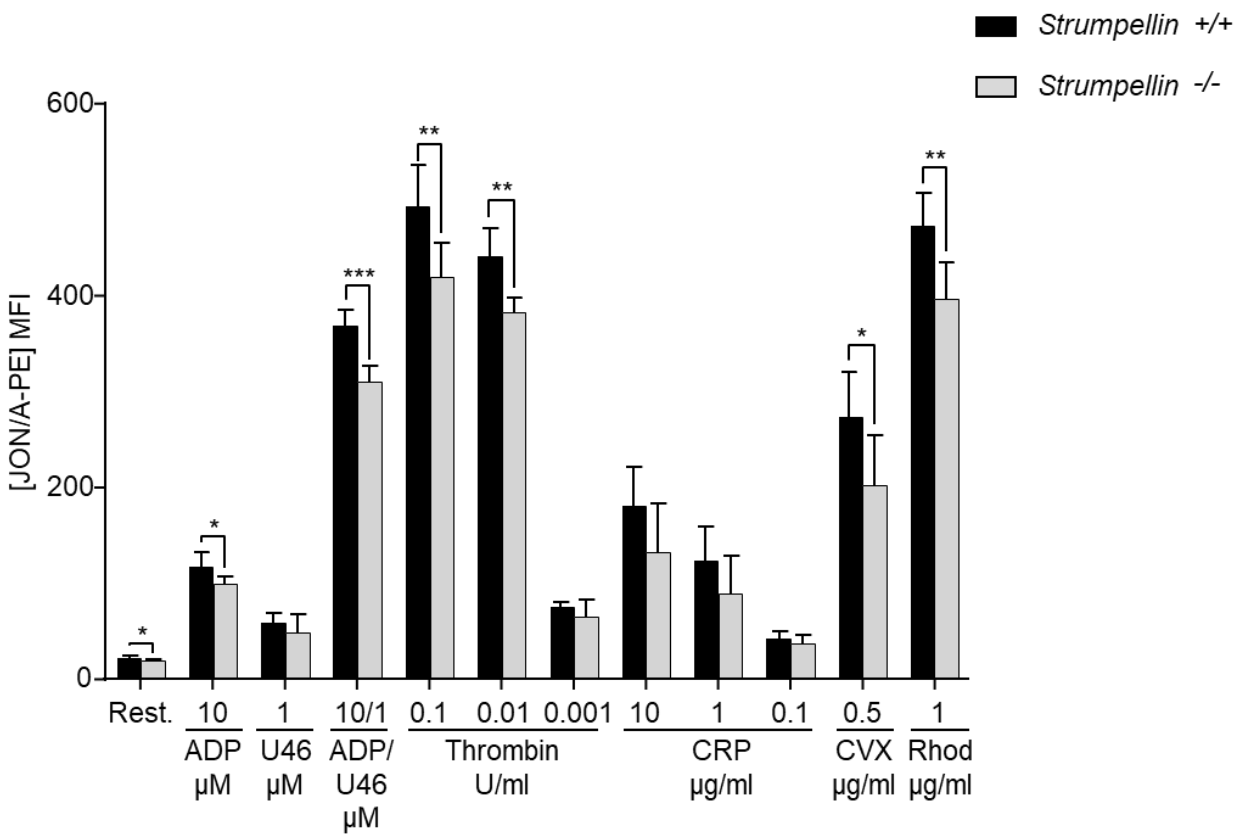

Figure 19: Strumpellin deficiency impairs αIIbβ3 activation
See Table 6.

3.1.8 Decrease in total αIIbβ3 content in mutant platelets

Next, it was assessed whether the entire αIIbβ3 content and not only its surface expression was affected by the loss of Strumpellin. The total αIIbβ3 surface expression, including the inactive and activated form, was measured by flow cytometry using the FITC-labelled JON6 antibody under resting conditions and after platelet activation. Platelets were activated using indicated agonists. This resulted in a persistent 20% decrease in total αIIbβ3 surface expression on Strumpellin-deficient platelets (Figure 20A). The ratio of αIIbβ3 surface expression after platelet activation to αIIbβ3 expression under resting conditions was then determined for each individual agonist. No significant changes were found after comparing ratios of *Strumpellin*$^{-/-}$ platelets to controls (Figure 20B). Similar results were obtained using the FITC-labelled JON1, 2 and 3 as well as MWReg30 against αIIbβ3 integrin (data not shown), thus confirming the findings so far. In addition, reduction of total αIIbβ3 in *Strumpellin*$^{-/-}$ platelets was also confirmed via FACS by permeabilising resting platelets and subsequently staining them with FITC-labelled JON6 (Figure 20C). This implies that lack of Strumpellin leads to a reduced total pool of αIIbβ3 integrin in platelets, but αIIbβ3 recruitment to the platelet surface after activation is still functional.

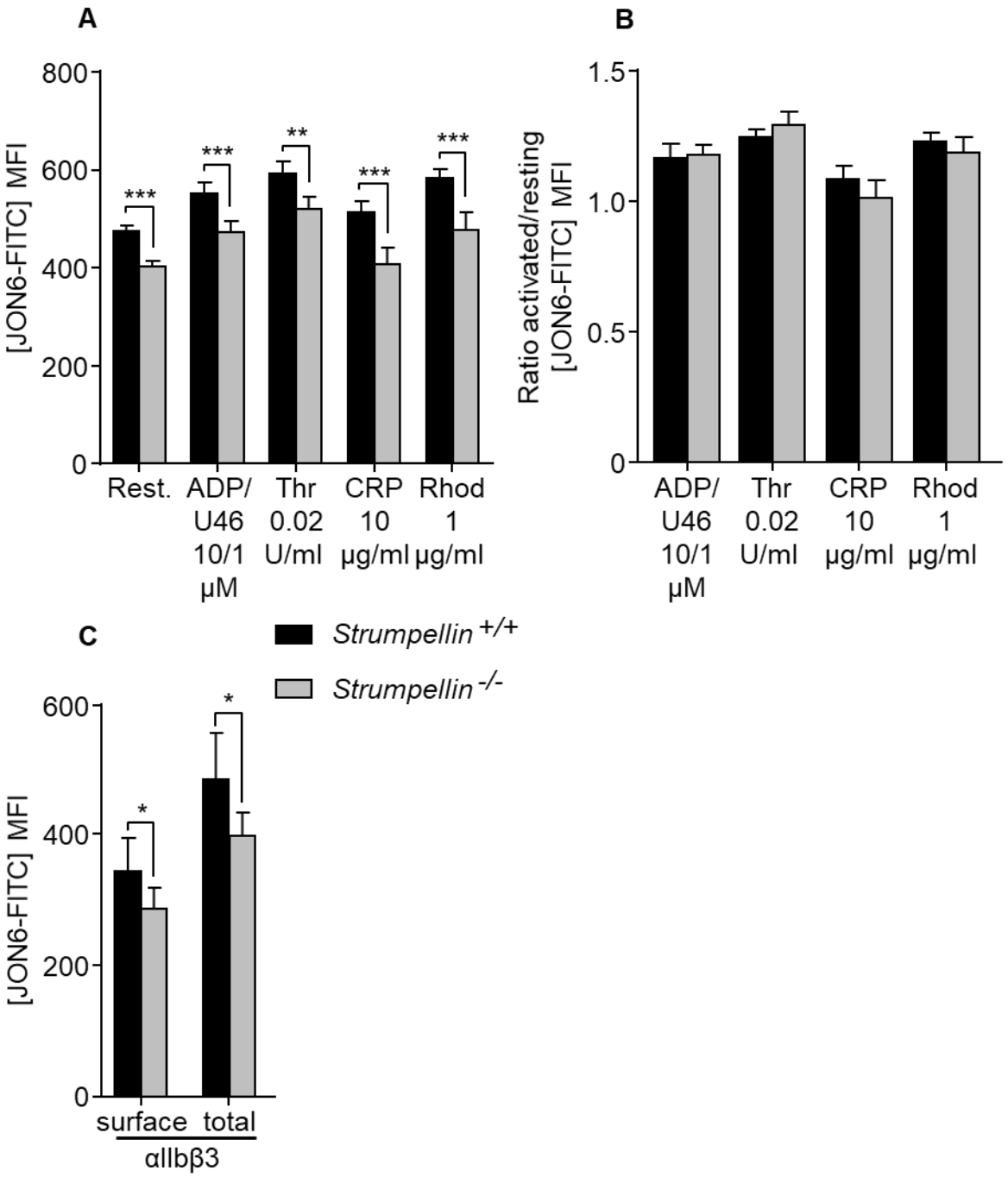

Figure 20: 20% decrease in total αIIbβ3 content in *Strumpellin*$^{-/-}$ platelets
A) Determination of total (inactive and activated) αIIbβ3 integrin on the platelet surface after platelet activation using indicated agonists. B) Ratios are given as total αIIbβ3 surface expression after platelet activation to total surface expression under resting conditions for each individual agonist. C) Analysis of αIIbβ3 surface expression and total content in permeabilised control and *Strumpellin*$^{-/-}$ platelets. MFI of FITC-labelled JON6-antibody against αIIbβ3 was measured by flow cytometry. Values are mean ± s.d. (n=6), * $P < 0.05$, ** $P < 0.01$, *** $P < 0.001$. The data is representative of three (A and B) and one (C) independent experiments. Ad C) this experiment was performed with Dr. Yvonne Schurr and can also be found in her doctoral thesis (145).

3.1.9 Unaltered fibrinogen content in *Strumpellin*$^{-/-}$ platelets

αIIbβ3 is essential for plasma fibrinogen uptake into platelets and subsequent storage into α-granules (77, 138). To ascertain whether the decrease in αIIbβ3 integrin in Strumpellin-deficient platelets had any effect on the abundance of fibrinogen, a western blot assay of platelet lysates was performed. *Strumpellin*$^{-/-}$ platelets did not show any striking differences compared to *Strumpellin*$^{+/+}$ platelets. Both control and mutant platelets contained three fibrinogen chains and a similar overall fibrinogen content, as seen in Figure 21. This suggests that the 20% reduction of αIIbβ3 is still sufficient for fibrinogen incorporation into Strumpellin-deficient platelets. Filamin A served as a loading control.

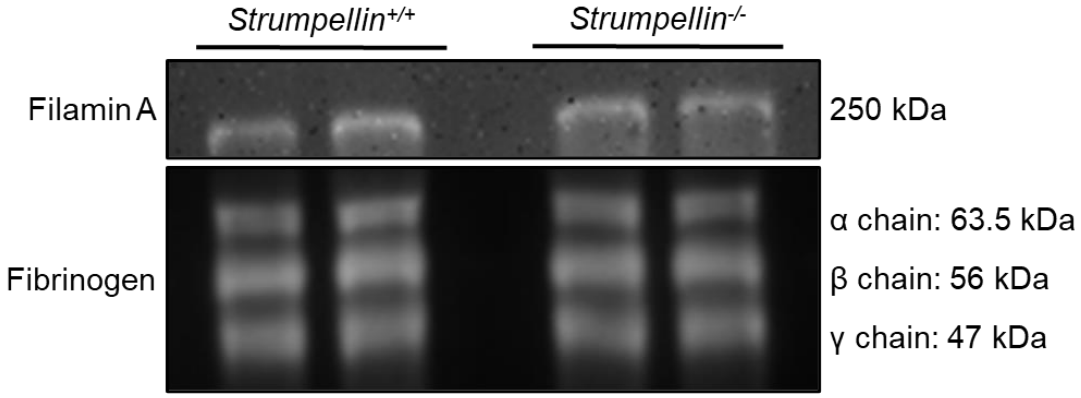

Figure 21: Unaltered fibrinogen content in *Strumpellin*$^{-/-}$ platelets
Western blot analysis of Strumpellin-deficient platelet lysates showed three fibrinogen chains. Fibrinogen content was normal (n=3). Filamin A served as a loading control. The data represents one experiment.

3.1.10 Mutant platelets with reduced αIIbβ3 binding capacity to fibrinogen and delayed fibrinogen uptake

Next, the functionality of αIIbβ3 was tested by performing cytometric analysis of αIIbβ3 binding capacity to fibrinogen as well as fibrinogen uptake into platelets.

To determine αIIbβ3 binding capacity to fibrinogen, *Strumpellin*$^{-/-}$ platelets as well as controls were incubated with Alexa Fluor® 488-conjugated fibrinogen for five minutes under resting and activated conditions using ADP/U46, CVX or Rhod. Subsequently, the binding capacity was measured by flow cytometry. Fibrinogen binding was significantly reduced after platelet activation (Figure 22A). This result is presumably due to the already decreased αIIbβ3 surface expression, leading to an overall reduced binding capacity.

To analyse fibrinogen uptake into platelets, Strumpellin-deficient platelets were incubated with Alexa Fluor® 488-conjugated fibrinogen for different time intervals under resting conditions. By adding trypan blue, extracellular Alexa Fluor® 488-fibrinogen fluorescence was minimised. This has been previously described by *Huang et al.* (60). Intracellular Alexa Fluor® 488-fibrinogen levels were then measured by flow cytometry. Strumpellin-

deficient platelets displayed an initial delay in fibrinogen uptake after five minutes. However, after 15 minutes, fibrinogen uptake into *Strumpellin*$^{-/-}$ platelets increasingly aligned with and after a time period of 30 minutes equalled fibrinogen uptake into *Strumpellin*$^{+/+}$ platelets (Figure 22B). This demonstrates that overall fibrinogen uptake into Strumpellin-deficient platelets is not impaired. However, the initial delay in fibrinogen internalisation may be the result of the reduced αIIbβ3 surface expression.

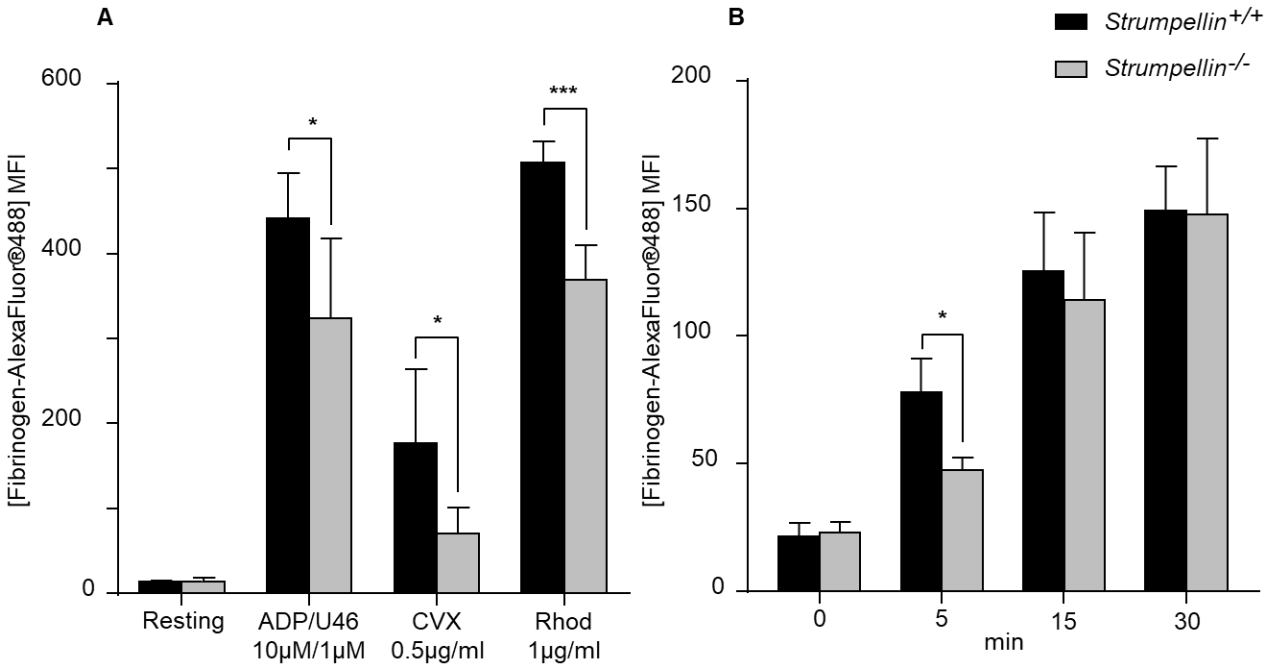

Figure 22: Fibrinogen-based analyses to determine αIIbβ3 functionality
A) Fibrinogen binding was determined after incubating washed platelets with Alexa Fluor® 488-labelled fibrinogen under resting and activated conditions using the indicated agonists. B) Washed platelets were incubated with Alexa Fluor® 488-fibrinogen for the indicated time intervals under resting conditions. After adding trypan blue to quench extracellular signals, fibrinogen uptake was determined. MFI of Alexa Fluor® 488-fibrinogen was measured by flow cytometry. Values are mean ± s.d. (n=5), * $P < 0.05$, *** $P < 0.001$. The data is representative of three independent experiments. These experiments were performed with Dr. Yvonne Schurr and can also be found in her doctoral thesis (145).

3.1.11 Unaltered spreading of *Strumpellin*$^{-/-}$ platelets on fibrinogen

To test αIIbβ3-dependent platelet spreading on fibrinogen, washed platelets were incubated with a low dose of thrombin to induce platelet activation. They were then left to spread on fibrinogen-coated coverslips for different time intervals before being imaged. During *in vitro* spreading, platelets undergo major shape changes, which can be divided into four consecutive phases, as depicted in Figure 23: I) platelet adhesion to the surface (roundish form), II) filopodia formation (finger-like protrusions), III) lamellipodia formation (sheet-like protrusions), both filopodia and lamellipodia can be observed, IV) fully spread platelet (‘fried egg’ resemblance).

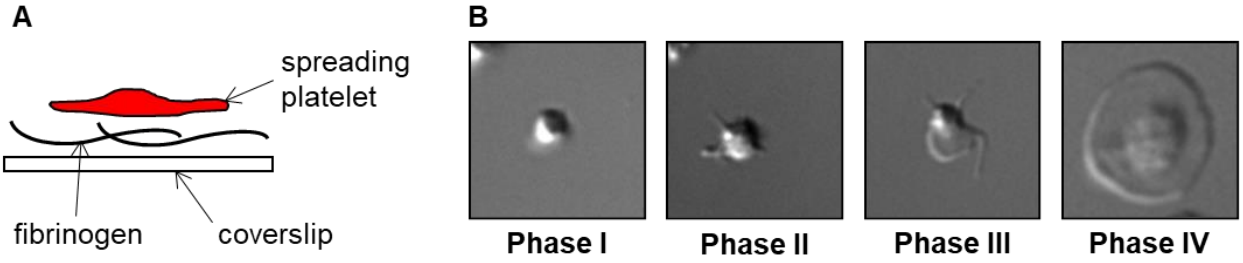

Figure 23: Shape change during platelet spreading
A) Illustration of a spreading platelet on a fibrinogen-coated coverslip. B) *In vitro* platelet spreading can be divided into four consecutive phases: I) platelets adhere to the fibrinogen-coated surface, II) platelets form filopodia, III) platelets form filopodia as well as lamellipodia, and IV) fully spread platelet (‘fried egg’).

Categorising *Strumpellin*$^{-/-}$ platelets according to their spreading progress and comparing them to control platelets, did not display any *in vitro* spreading defects nor a delay in spreading. Under static conditions Strumpellin-deficient platelets were able to adhere to fibrinogen-coated surfaces and form filopodia and lamellipodia (Figure 24A and B). *Hodivala-Dilke et al.* demonstrated that heterozygous β3-integrin mutant mice, which only express 50% of wild-type αIIbβ3 in platelets, do not develop a bleeding defect (138). This means that a reduction of up to 50% in αIIbβ3 expression does not necessarily lead to haemostasis defects even though the integrin is important for mediating platelet adhesion and aggregation. This supports the results obtained here, which showcase that a 20% decrease in αIIbβ3 is still sufficient to facilitate normal platelet spreading on fibrinogen.

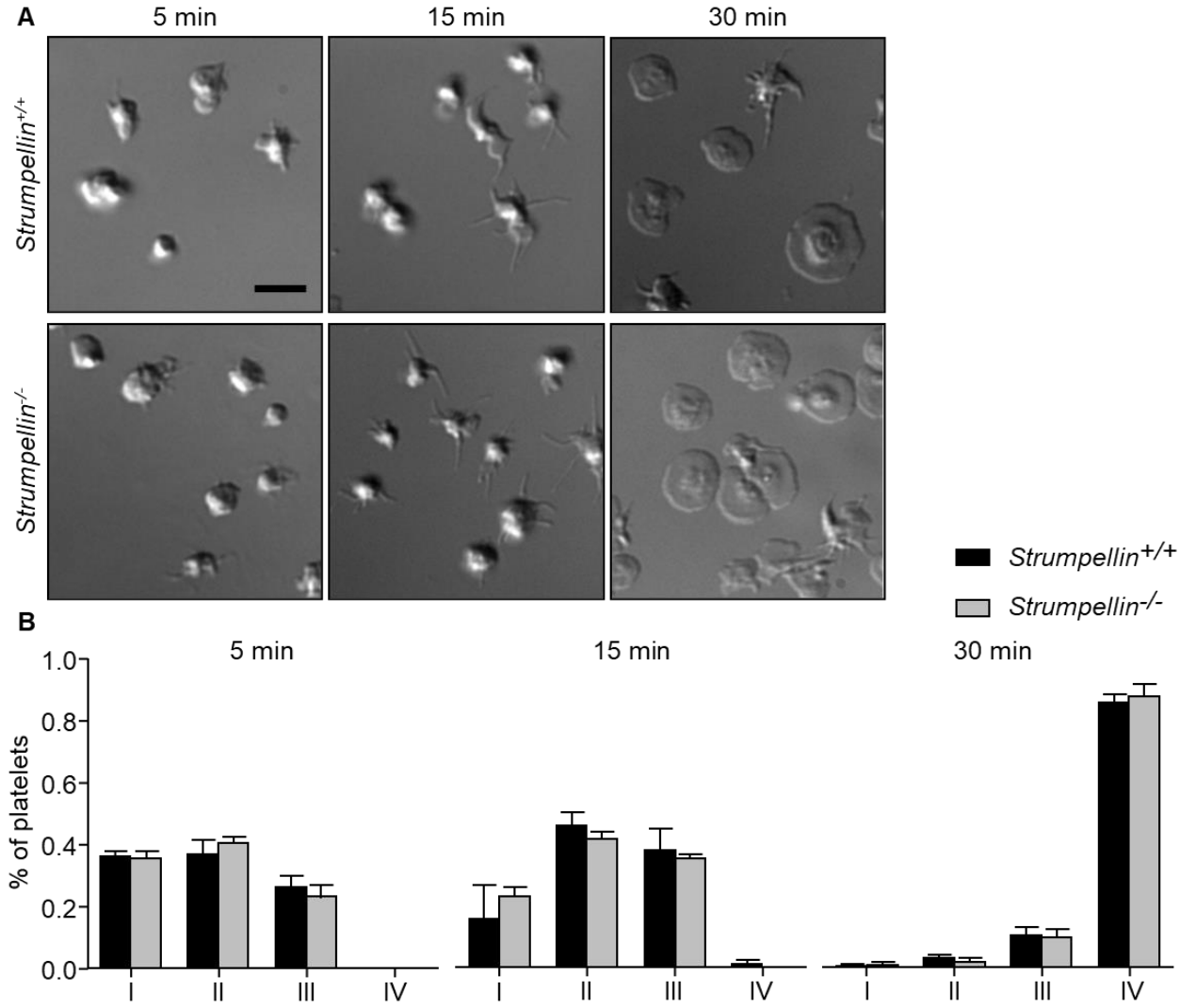

Figure 24: Unaltered spreading of *Strumpellin*$^{-/-}$ platelets on fibrinogen
A) Washed platelets, previously activated with 0.01 U/ml thrombin, spread on fibrinogen-coated coverslips for the indicated time intervals at 37°C. Representative images of the spreading assay after 5, 15 and 30 minutes. Scale bar: 5 µm. B) Quantification of individual spreading phases after indicated time intervals. Values are mean ± s.d. (n=3). The data is representative of two independent experiments.

3.1.12 Mutant platelets aggregate normally

Due to the overall decrease in αIIbβ3 in *Strumpellin*$^{-/-}$ platelets, an *in vitro* aggregation assay was performed using agonists thrombin, collagen and U46 in varying concentrations. Strumpellin-deficient platelets did not show any *in vitro* aggregation defects in response to all tested agonists (Figure 25). In addition to the unaltered spreading assay, this confirms that αIIbβ3 functions normally, at least *in vitro*.

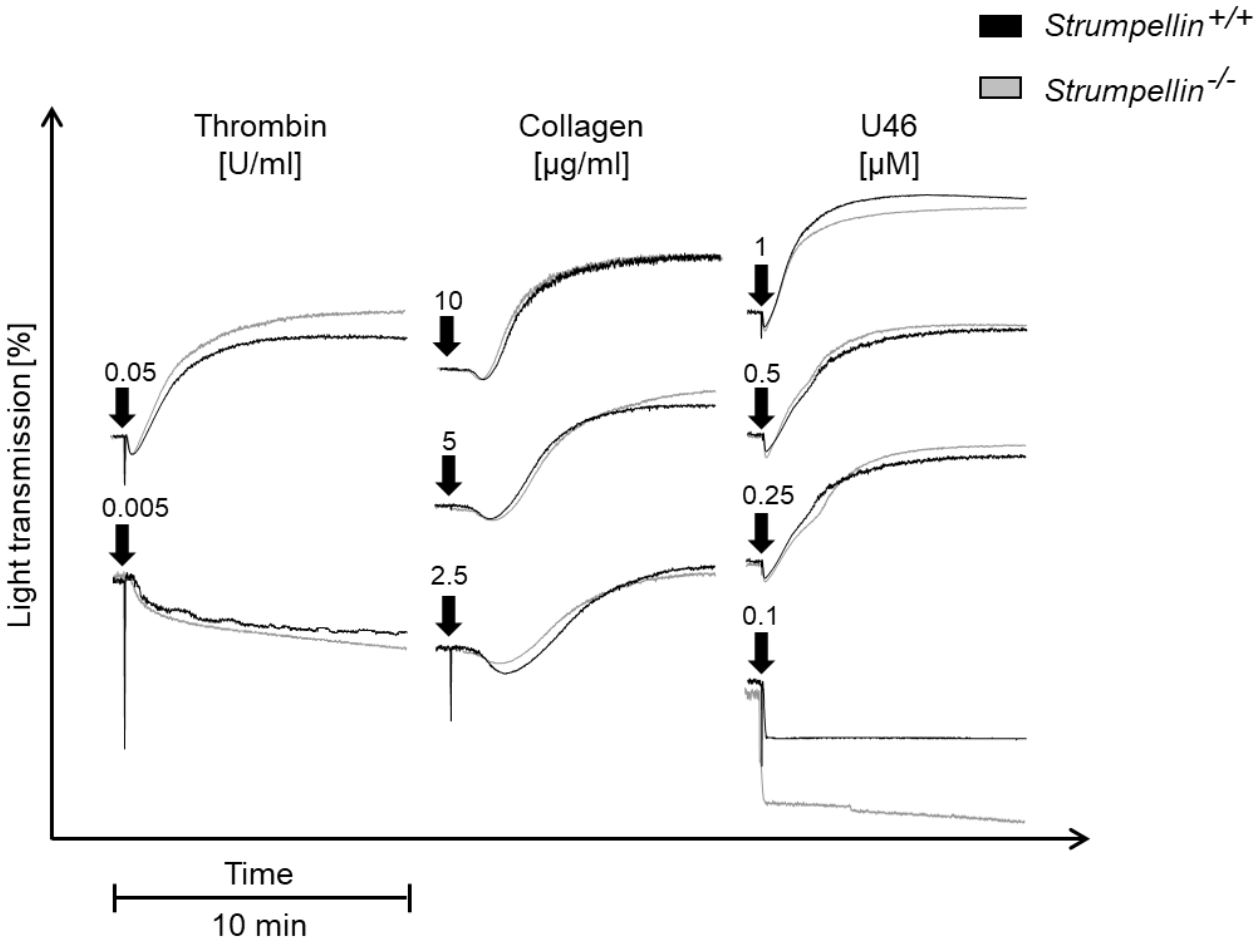

Figure 25: *Strumpellin*$^{-/-}$ platelets aggregate normally after activation
Washed platelets were activated by the indicated agonists. Aggregation capacity was then measured by determining light transmission in % for each sample for 10 min (n=4). The data represents one experiment.

3.1.13 Normal P-selectin exposure after platelet activation and overall unaltered P-selectin content in *Strumpellin*$^{-/-}$ platelets

Prior to platelet activation, P-selectin is stored in α-granules (16). It is then rapidly exposed to the surface following activation and subsequent degranulation. Hence, P-selectin can be used as a marker for α-granule release after platelet activation. To evaluate α-granule secretion in *Strumpellin*$^{-/-}$ platelets, flow cytometric measurements of P-selectin exposure after platelet activation using various agonists were performed. Strumpellin-deficient platelets did not display a significantly reduced P-selectin exposure after platelet stimulation with the indicated agonists (Table 7 and corresponding Figure 26).

Table 7: Unaltered P-selectin exposure in activated *Strumpellin*$^{-/-}$ platelets
P-selectin exposure was determined after degranulation following platelet activation using indicated agonists. MFI of the FITC-labelled WUG 1.9 antibody against P-selectin was measured by flow cytometry. MFI is given as mean value ± s.d. (n=6), * $P < 0.05$. The data is representative of four independent experiments.

	***Strumpellin*$^{+/+}$**	***Strumpellin*$^{-/-}$**	**Significance**
Resting	5.7±0.5	6.0±0.0	n.s.
ADP 10 µM	8.0±0.6	8.3±1.1	n.s.
U46 1 µM	7.3±1.3	9.3±1.6	n.s.
ADP 10 µM/U46 1 µM	80.5±6.2	82.8±6.7	n.s.
Thrombin 0.1 U/ml	125.8±7.3	118.2±3.5	n.s.
Thrombin 0.01 U/ml	113.5±16.3	98.8±9.9	n.s.
Thrombin 0.001 U/ml	6.2±0.4	6.0±0.0	n.s.
CRP 10 µg/ml	59.8±9.6	46.8±10.6	n.s.
CRP 1 µg/ml	41.3±10.5	31.2±10.0	n.s.
CRP 0.1 µg/ml	17.3±5.7	13.0±2.9	n.s.
CVX 0.5 µg/ml	56.0±9.4	51.8±6.5	n.s.
Rhod 1 µg/ml	122.6±8.7	90.5±19.0	*

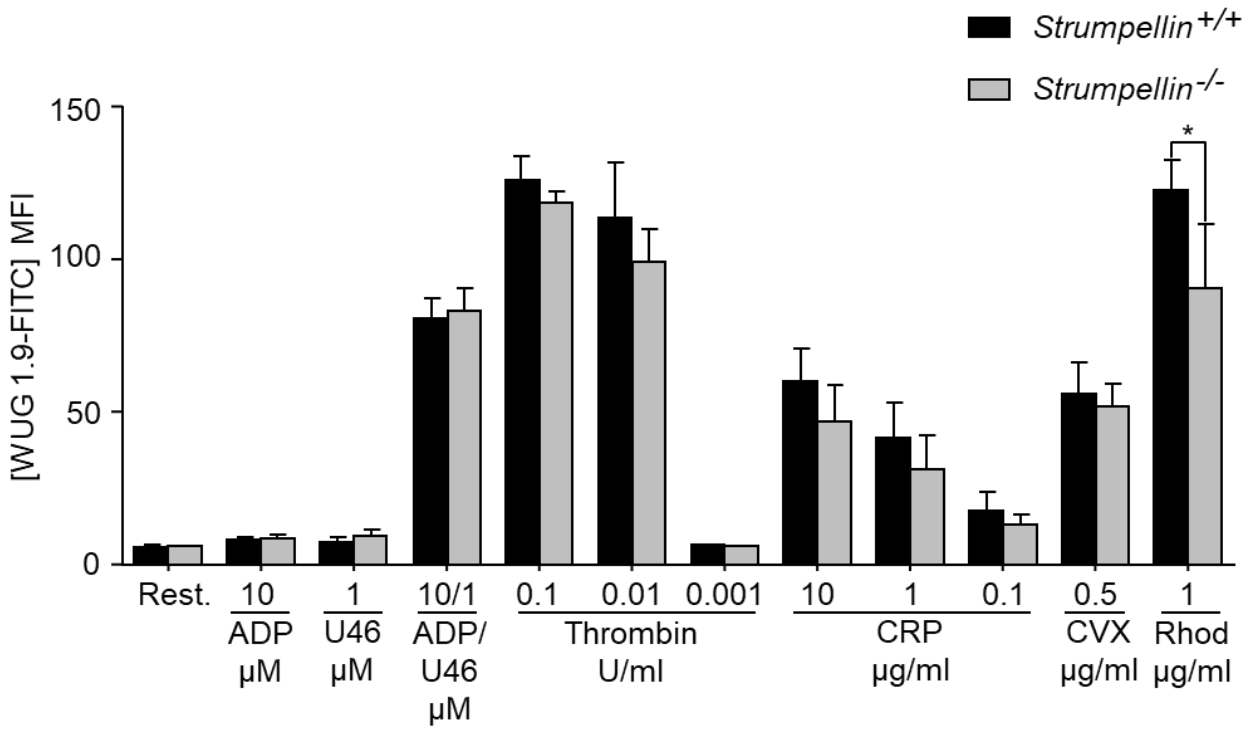

Figure 26: Normal P-selectin exposure in activated *Strumpellin*$^{-/-}$ platelets
See Table 7.

To analyse if loss of Strumpellin affected overall P-selectin abundance in platelets, P-selectin content was measured using a commercially bought mouse P-selectin ELISA kit from RayBio®. As shown in Figure 27, its concentration was unaltered in lysates of *Strumpellin*$^{-/-}$ platelets compared to *Strumpellin*$^{+/+}$. Mice deficient of P-selectin (referred to as *P-selectin*$^{-/-}$) were used as negative controls. This suggests that Strumpellin deficiency does not alter P-selectin translocation to the cell surface and thus, α-granule secretion, after platelet activation, nor total P-selectin content.

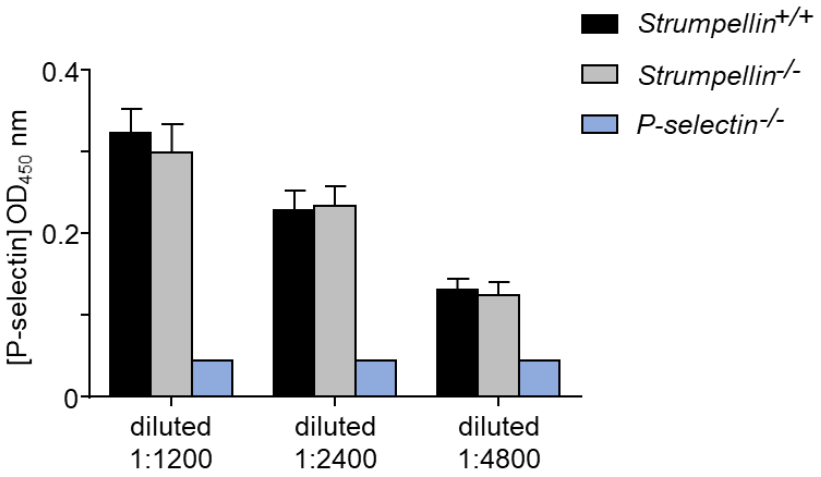

Figure 27: Unaltered P-selectin content in *Strumpellin*$^{-/-}$ platelets
Total P-selectin concentration in platelet lysates was determined by quantitative ELISA using a biotinylated anti-mouse P-selectin antibody as well as HRP-labelled streptavidin. Platelet lysates of *P-selectin*$^{-/-}$ mice served as negative controls. The colour intensity is depicted as optical density (OD) at a wavelength of 450 nm. Values are mean ± s.d. (n=6). The data is representative of two independent experiments. This experiment was performed with Dr. Yvonne Schurr and can also be found in her doctoral thesis (145).

3.2 Megakaryocyte analysis of Strumpellin-deficient mice

3.2.1 Unaltered appearance, localisation and number of megakaryocytes in bone marrow and spleen

Femoral bone and spleen histological sections were prepared and stained with H&E in order to examine megakaryocyte appearance, localisation and number in both bone marrow and spleen. Whilst preparing femora and the spleen, no abnormalities in bone and spleen size and structure were detected (data not shown). Apparent differences were also not observed comparing *Strumpellin*$^{-/-}$ to *Strumpellin*$^{+/+}$ histological sections: megakaryocytes appeared normal in size and structure and were evenly distributed throughout the organs (Figure 28A). No significant changes in megakaryocyte number in both the bone marrow (Figure 28B) and spleen (Figure 24C) of Strumpellin knockout mice were detected after quantifying them per field of view.

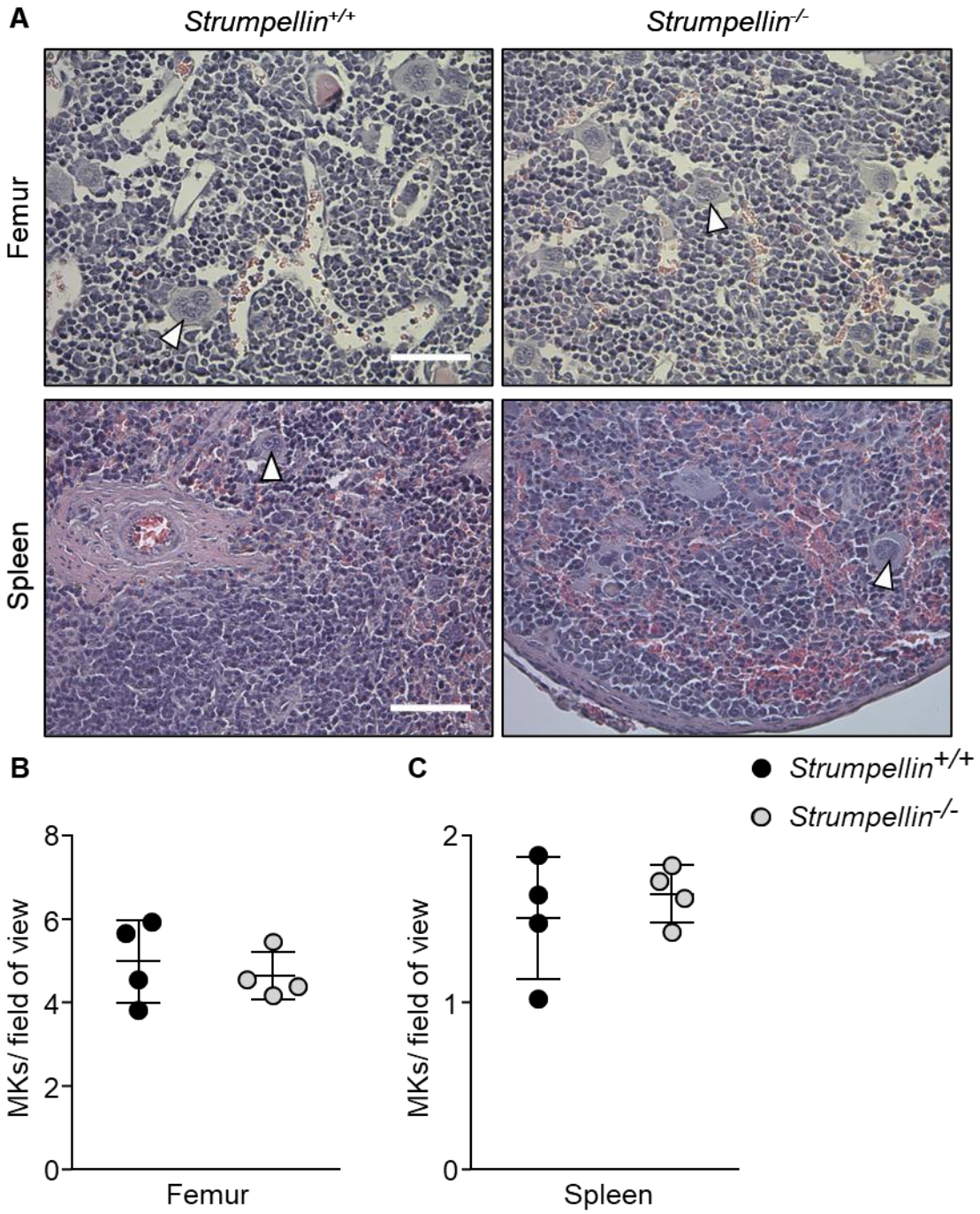

Figure 28: Normal mutant megakaryocyte appearance and number in bone marrow and spleen
A) Representative images of femur and spleen histological sections stained with H&E. White arrowheads indicate a megakaryocyte. Scale bar: 25 µm. Quantification of megakaryocyte number per field of view [294 x 220 µm] in B) femur and C) spleen. Values are mean ± s.d. (n=4). The data represents one experiment.

These results were supported by immunofluorescence studies on whole femora cryosections. Megakaryocytes were of normal morphology and localised near CD105-positive blood vessels (Figure 29). No aberrant release of platelet-like particles was detected in the bone marrow. Megakaryocyte numbers per field of view were comparable between *Strumpellin*$^{+/+}$ and *Strumpellin*$^{-/-}$ femora (data not shown). Taken together, these results

suggest that Strumpellin has no effect on megakaryocyte development nor on platelet production in the bone marrow.

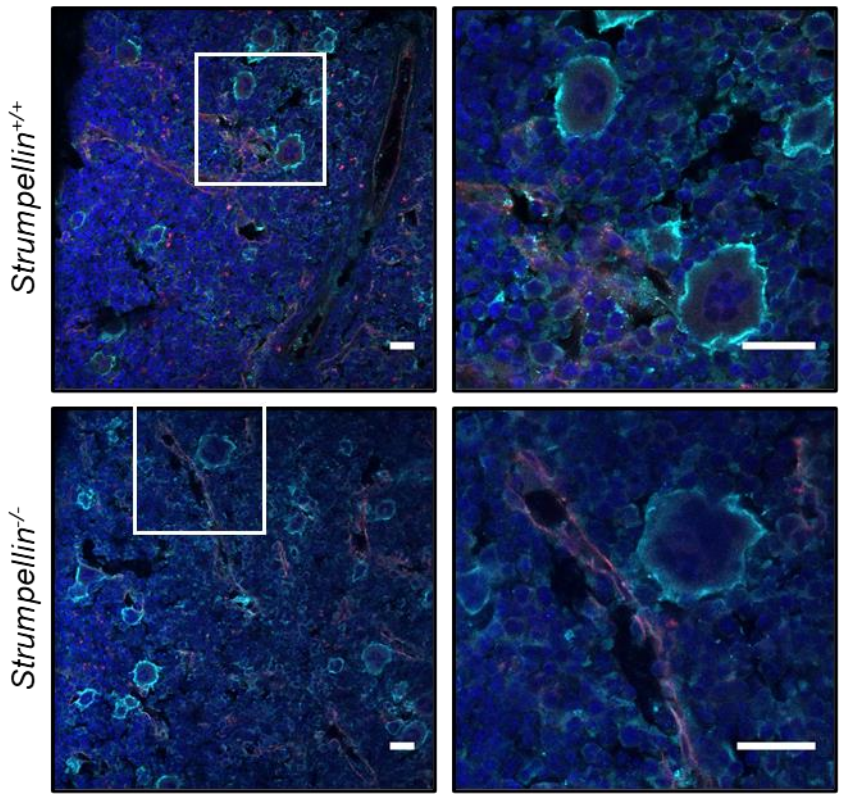

Figure 29: Mutant megakaryocytes appear normal in bone marrow
Representative images of whole femora cryosections stained for endothelium (CD105, red), nuclei (DAPI, blue) and megakaryocytes/ platelets (JON6, cyanine); magnified sections on the right. Scale bar: 25 µm. (n=4). The data represents one experiment.

3.2.2 Normal ploidy of *Strumpellin*$^{-/-}$ megakaryocytes

Megakaryocytes undergo a distinct maturation process during which they become polyploid by endomitosis in order to produce platelets (1). Megakaryocyte ploidy was measured using the MWReg30-FITC-labelled antibody to detect megakaryocytes and propidium iodide to stain DNA. The ploidy of *Strumpellin*$^{-/-}$ megakaryocytes was unaltered (Figure 30), suggesting a normal maturation process of megakaryocytes.

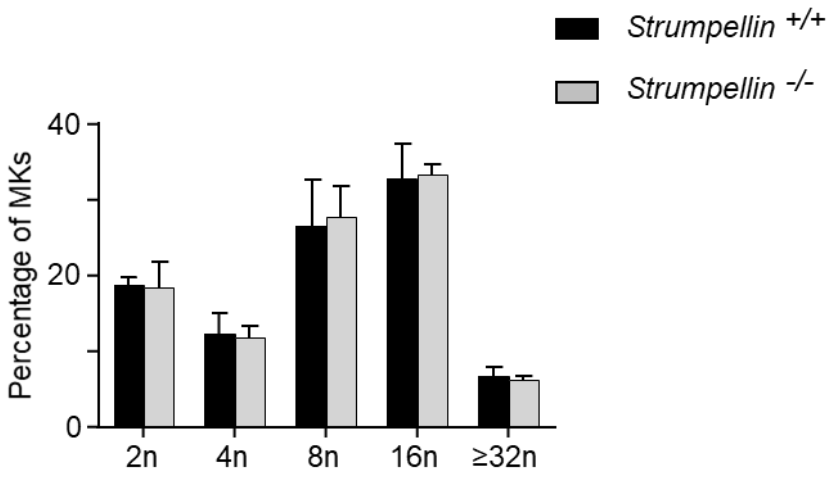

Figure 30: *Strumpellin*$^{-/-}$ megakaryocytes display normal ploidy
Ploidy of bone marrow megakaryocytes was determined by flow cytometry using FITC-labelled MWReg30 antibody (MK detection) and propidium iodide (DNA staining). Values are mean ± s.d. (n=3). The data is representative of three independent experiments.

3.2.3 Decreased αIIbβ3 surface expression in mutant megakaryocytes

A decrease of approximately 20% in αIIbβ3 surface expression was measured in Strumpellin-deficient platelets under resting conditions (Table 5, Figure 18). To detect a potential change in αIIbβ3 integrin expression at the megakaryocyte level, the MFI of αIIbβ3 in bone marrow megakaryocytes was determined by flow cytometry using the FITC-labelled MWReg30 antibody, specific to αIIbβ3 integrin. This resulted in a persistent 20% decrease in the integrin on the cell surface, indicating a decrease at the megakaryocyte level (Figure 31).

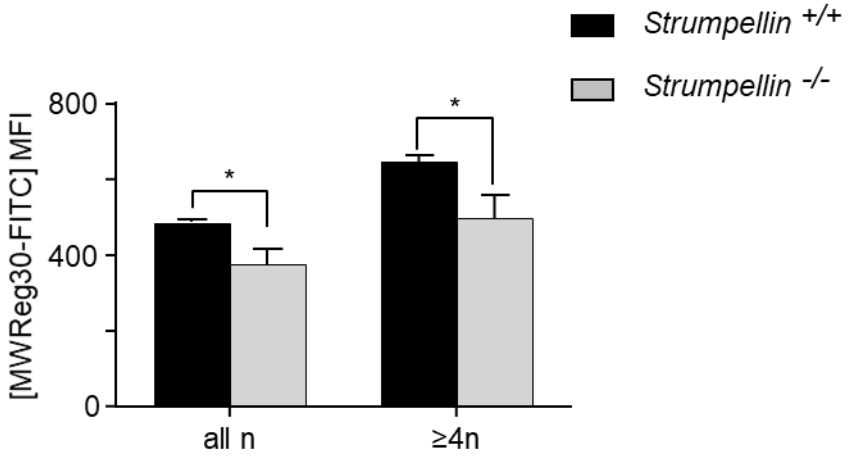

Figure 31: Decrease in αIIbβ3 surface expression in mutant megakaryocytes
Bone marrow megakaryocytes were stained for αIIbβ3 using the MWReg30 FITC-labelled antibody. Megakaryocytes were gated for every chromosome set (all n) or chromosome sets higher than 4 (≥4n). MFI was measured by flow cytometry and is given as mean value ± s.d. (n=3), * $P < 0.05$. The data is representative of three independent experiments.

3.3 Unaltered spleen to body weight ratio of *Strumpellin*$^{-/-}$ compared to *Strumpellin*$^{+/+}$ mice

To determine spleen to body weight ratios of *Strumpellin*$^{-/-}$ mice and their littermate controls, the mice were killed by cervical dislocation and their bodies weighed before harvesting and weighing the spleen. Preparing the organ, no macroscopic abnormalities in organ structure and size were observed (data not shown). Plotting spleen weight against body weight of each individual mouse showed that *Strumpellin*$^{-/-}$ mice have a normal spleen to body weight ratio (Figure 32).

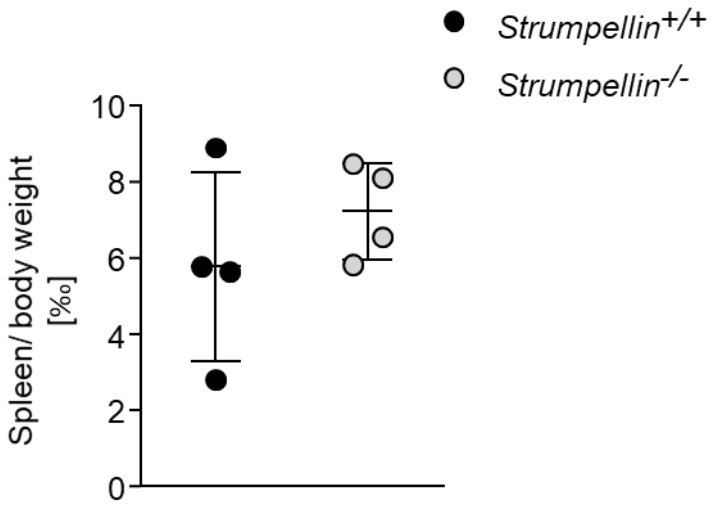

Figure 32: Normal spleen to body weight ratio of *Strumpellin*$^{-/-}$ mice
Spleen to body weight of *Strumpellin*$^{-/-}$ mice was determined and compared to their littermate controls (all male, 7 to 8 weeks). Values are mean ± s.d. and given permille (n=4). The data represents one experiment.

4 Discussion

The highly conserved Strumpellin protein is part of the pentameric WASH complex, which serves as the major actin-nucleation promoting factor on endosomes. It facilitates the formation of a branched actin network by stimulating the Arp2/3 complex and thus, plays an essential role in endosomal sorting and trafficking. However, endocytic trafficking in platelets and their precursors megakaryocytes remains understudied. To further identify key players of the platelet endocytic machinery, the role of Strumpellin in platelets and megakaryocytes was examined.

4.1 Deficiency of the WASH complex subunit Strumpellin leads to an unstable WASH complex

Megakaryocyte and platelet specific *Strumpellin*$^{-/-}$ mice were healthy, fertile and born at a normal Mendelian ratio. They displayed normal platelet, white blood cell and red blood cell count (Table 4, Figure 13A). Size and morphology of *Strumpellin*$^{-/-}$ platelets were comparable to control platelets (Table 4, Figure 13B, Figure 15A). Furthermore, an increase in spleen size or weight was not detected (Figure 32). Based on the unaltered blood cell count measured in *Strumpellin*$^{-/-}$ mice, an increase in spleen size and weight due to extramedullary haematopoiesis would not have been expected.

However, deficiency of Strumpellin probably leads to an unstable WASH complex. Western blot analysis of platelet lysates revealed that loss of Strumpellin resulted in reduced protein levels of WASH1 (Figure 12). Previous studies have shown that depletion of individual WASH complex subunits impacts overall stability of the complex. Nevertheless, some controversy exists concerning the destabilisation of the entire complex or only of specific subunits as well as the residual activity. *Jia et al.* performed RNAi-knockdown experiments on HeLa-cells and suggested that subunits FAM21, SWIP and Strumpellin serve as core subunits upon which WASH1 and CCDC53 assemble (83). WASH1 and CCDC53 expression was reduced by knockdown of all complex members, whereas FAM21, SWIP and Strumpellin expression was only affected by knockdown of each other (83). Similar results supporting this thesis were obtained by studies using different mammalian cell lines (39, 52, 123). However, complete knockout of WASH1 in MEFs caused a significant reduction in protein levels of all WASH complex subunits (53). Similar results were obtained in WASH1-deficient CD4-positive T-cells and hepatocytes (48, 112). Interestingly, residual FAM21, SWIP and Strumpellin still remained linked to each other in WASH1-deficient MEFs, also pointing towards the assembly of a WASH core complex

(53). Furthermore, studies proposed that remaining subunits still assemble and function, at least partially, after knockout of individual WASH complex subunits. For instance, complete loss of Strumpellin in mouse melanocytes caused a significant reduction in protein levels of WASH1, FAM21 and CCDC53 by ~30% and SWIP by ~20% (107). In the absence of Strumpellin remaining WASH complex members still associated and assembled into a complex (107). In addition, WASH1 as well as p34 (Arp2/3 complex) and cortactin (branched actin associated protein) still localised to EE and LE, though at a reduced level, indicating a partial function of WASH1 (107). In WASH1 knockout MEFs residual FAM21 and SWIP remained at endosomes (53). Similar results were obtained in knockdown experiments in hTERT-RPE1 cells, where FAM21 remained at endosomes (39). Altogether, these results suggest that depletion of subunits leads to an unstable WASH complex due to partial degradation of remaining subunits, which however, can still show residual activity. Furthermore, it has been shown that Strumpellin associates with spartin, a regulator of endosomal trafficking, as well as valosin-containing protein (VCP) independently of the WASH complex (114, 149). These results may indicate WASH-independent functions of individual WASH components. The immunoblot results obtained in this study also point towards a destabilisation of the WASH complex. However, remaining subunits may still assemble and operate on a lower level in the absence of Strumpellin. The effect Strumpellin deficiency has on WASH complex subunits FAM21, CCDC53 and SWIP in platelets was not analysed in this thesis. In order to examine the impact of Strumpellin on all complex members and really prove destabilisation of the WASH complex in platelets, further western blot analyses need to be performed.

Derivery et al. as well as *Gomez et al.* first demonstrated that WASH1 mainly localises to EE and RE, where it serves as a major actin-polymerisation promoter (51, 52). After RNAi-mediated silencing of WASH1, cells displayed exaggerated cargo-laden endosomal tubulations along microtubules, suggesting a defect in tubule scission from the endosome in the absence of actin polymerisation (51, 52, 54). WASH1 knockout in MEFs led to an enlarged and collapsed endo-lysosomal network, which accumulated in the juxtanuclear region of the cell, which was due to a completely absent WASH1-mediated actin network (53). Because Strumpellin deficiency resulted in reduced protein levels of WASH1 in murine platelets, the overall capacity of actin polymerisation in platelets after platelet stimulation was measured by flow cytometry. However, F-actin content in resting and activated *Strumpellin*$^{-/-}$ platelets was comparable to controls and it displayed a proportional increase after platelet activation (Figure 16). This implies that Strumpellin does not

affect or the amount of WASH1 in Strumpellin-deficient platelets is still sufficient for overall F-actin polymerisation after platelet activation. However, it is more likely that the WASH complex has no significant influence on overall F-actin assembly. Similar to other cell types, it may only play a role in actin polymerisation on the endosomal level in platelets. Flow cytometry measurements may not be sensitive enough to assess endosomal actin polymerisation. Further experiments, including immunofluorescence staining of platelets and megakaryocytes, are required to examine how the endosomal actin network is affected after loss of Strumpellin. So far, attempts to generate a functional antibody against Strumpellin for immunofluorescence studies of platelets and megakaryocytes have been unsuccessful.

Microtubule stability was also assessed in *Strumpellin*$^{-/-}$ platelets, because WASH1 is directly associated with α-tubulin via its TBR domain and WASH-mediated endosomal tubulations only appear and elongate along microtubule tracks (29, 51, 52). However, Strumpellin deficiency and/or WASH1 reduction had no effect on microtubule stability in platelets. Microtubules were stable and disassembled completely at 4°C and (re)assembled at 37°C (Figure 17). This is also in line with TEM analysis, which showed normal microtubule numbers per platelet section (Figure 15B).

4.2 Strumpellin selectively regulates αIIbβ3 integrin surface expression in platelets and megakaryocytes

Endocytic trafficking is an important regulatory mechanism to control integrin expression on the cell surface. Integrins can be internalised via clathrin-dependent or clathrin-independent endocytosis and subsequently undergo endosomal sorting into either the degradation or the recycling pathway (150, 151). Recycling of integrins back to the plasma membrane provides a constant fresh pool of integrins to generate new cell adhesions, which are essential for cell migration or invasion, cytokinesis, and other important cellular processes (150). Rab4-mediated fast recycling rapidly delivers integrins to the surface, whereas Rab11 mediates slow recycling. Over the last few years, numerous molecular pathways have been discovered, which differentiate between integrin subtype, activation state and trafficking route (151).

Thus far, receptor trafficking of αIIbβ3 has been primarily studied in platelets. Approximately 80,000 copies of αIIbβ3 are located on the platelet surface in resting platelets with an additional internal pool, which are always kept in a state of equilibrium (59, 128). αIIbβ3 is indispensable for platelet adhesion, aggregation and thus, thrombus formation. It is

also essential for plasma fibrinogen uptake and subsequent storage into α-granules (77, 138). Ligand-bound and -unbound αIIbβ3 can be endocytosed and recycled back to the plasma membrane, but the exact mechanisms are still unclear (59, 68, 152-154). Recent studies by *Banerjee et al.* and *Huang et al.* demonstrated that cellubrevin or vesicle-associated membrane protein (VAMP)-3, a v-SNARE, as well as Arf6 play an important role in regulating receptor-mediated endocytosis and endosomal trafficking in platelets and megakaryocytes, especially αIIbβ3-mediated endocytosis of fibrinogen and its subsequent uptake into α-granules (60, 71). This means that fibrinogen can be used as an indicator for αIIbβ3 movement through the cell (59). It binds to surface αIIbβ3, is internalised and transits through Rab4-, Rab11- and vWF-positive compartments (60, 71). Upon platelet activation, the internal pool of αIIbβ3 is exposed (130, 131). However, platelet activation, especially with ADP or thrombin, also increases fibrinogen-uptake into platelets and thus, αIIbβ3 internalisation (59, 153). Overall, flow cytometric analysis displays an increase in αIIbβ3 surface expression after platelet activation (compare Table 6, Figure 19, Figure 20A). This data suggests that platelet activation may also increase αIIbβ3 recycling back to the plasma membrane providing a constant fresh pool for platelet adhesion and aggregation.

Flow cytometric analysis of platelet glycoprotein expression detected an approximate 20% decrease in αIIbβ3 integrin surface expression on resting *Strumpellin*$^{-/-}$ platelets, which was confirmed by various antibodies against αIIbβ3 and β3 (Table 5, Figure 18). Interestingly, integrin subunits α2 and β1 were not affected by the loss of Strumpellin, neither were other platelet receptors. A persistent 20% decrease in total (inactive and active) αIIbβ3 surface expression on Strumpellin-deficient platelets under resting conditions and after platelet activation was measured (Figure 20A). Comparing ratios of αIIbβ3 expression after platelet activation to αIIbβ3 expression under resting conditions of *Strumpellin*$^{-/-}$ platelets to their controls did not display any significant changes (Figure 20B). This means that the additional exposure of internal αIIbβ3 did not compensate the decreased αIIbβ3 surface expression after platelet activation. FACS analysis of permeabilised platelets stained for αIIbβ3 confirmed that total αIIbβ3 abundance was significantly reduced in *Strumpellin*$^{-/-}$ platelets (Figure 20C). Furthermore, P-selectin exposure after platelet activation was normal, suggesting a functioning recruitment of α-granules and thus, the internal αIIbβ3 pool, to the platelet surface (Table 7, Figure 26). Remarkably, there was a persistent 20% decrease in αIIbβ3 surface expression on megakaryocytes, indicating a decrease at the megakaryocyte level (Figure 31). Further analysis of megakaryocytes,

including morphology, localisation and number in bone marrow and spleen (Figure 28, Figure 29) as well as ploidy (Figure 30) did not reveal any abnormalities.

In summary, these results indicate that: 1) WASH complex subunit Strumpellin selectively regulates αIIbβ3 integrin expression in platelets and megakaryocytes. 2) Strumpellin deficiency leads to a reduced surface and internal pool of αIIbβ3 integrin. And 3) even though total αIIbβ3 abundance is decreased in Strumpellin-deficient platelets, the recruitment of intracellular αIIbβ3 to the surface after platelets activation is possible and proportional to *Strumpellin*$^{+/+}$ platelets.

The following hypotheses could explain how Strumpellin influences αIIbβ3 surface expression:

I) Defective αIIbβ3 trafficking and recycling to the cell surface

Strumpellin deficiency may lead to a decreased or slower recycling rate of αIIbβ3, resulting in αIIbβ3 accumulation in endosomal compartments and eventual degradation in lysosomes. This might be due to the reduced WASH1 abundance and thus, decreased actin polymerisation activity on endosomes in *Strumpellin*$^{-/-}$ platelets and megakaryocytes.

The WASH complex plays an essential role in endosomal sorting and recycling of numerous cargo proteins as well as in maintaining endo-lysosomal integrity. Loss of WASH1 led to severe morphological changes of endosomes and lysosomes in different mammalian cell lines and resulted in defective cargo transport from all three endosomal trafficking pathways (degradation, recycling and retrograde trafficking) (51-54). Depletion of subunit Strumpellin also caused an enlarged and collapsed endo-lysosomal network with remaining WASH complex members aggregated at endosomes (39, 107, 116, 122).

The results obtained in this study are in agreement with previous findings suggesting a role of the WASH complex in integrin trafficking. *Zech et al.* demonstrated that the WASH complex plays an important role in recycling internalised α5β1 integrin in invasive ovarian (A2780) cancer cells, thus enabling invasive migration (104). In WASH1-depleted fibroblasts α5 barely localised to focal adhesions, which led to a decrease in focal adhesion number with subsequent cell adhesion and migration defects (155). In addition, α5β1 accumulated in CD63-positive MVBs/LE, hinting at a slower recycling rate or even increased lysosomal degradation (104). After WASH1 knockout in T-cells, surface expression and intracellular levels of

integrin LFA-1 (αL-β2) were significantly reduced, whereas integrins VLA-4 (α4-β1) and LPAM (α4-β7) were not affected (112). Very recently, *Lee et al.* published a paper also describing altered α5β1 integrin trafficking in Strumpellin-depleted hTERT-RPE1 cells and the discovery of a new Strumpellin-interacting partner – CAV1, an important component of caveolae (123). siRNA knockdown of Strumpellin or WASH1 greatly decreased total CAV1 protein levels (123). It also reduced CAV1 fluorescence signals at intracellular vesicles, whereas fluorescence signals at the plasma membrane remained steady (123). Furthermore, Strumpellin knockdown abolished α5 localisation to focal adhesions and increased intracellular α5 integrin, implying defective recycling back to the cell surface (123). Moreover, α5 predominantly co-localised with the lysosomal marker LAMP1 and overall α5 protein levels, like CAV1, were markedly reduced (123). After treatment with bafilomycin, an inhibitor of V-ATPase and thus lysosomal degradation, CAV1 and α5 protein levels were restored, which suggests enhanced lysosomal degradation in the absence of Strumpellin (123). Interestingly, Strumpellin containing a mutation in the CAV1-binding region (aa 241-790) did not rescue the reduced α5 protein levels, whereas wild-type Strumpellin did, which suggests that the interaction of CAV1 with Strumpellin is essential for α5 recycling (123).

This data, as well as the results obtained here, point towards a role of the WASH complex in selectively recycling specific integrins in different cell types from endosomal compartments to the plasma membrane. WASH1 possesses the ability to promote actin nucleation necessary for endosomal tubulation and thus, cargo trafficking. Complex members, like Strumpellin, may contribute either to: 1) complex stability and/or 2) WASH1 activity and/or 3) interaction with accessory proteins for cargo recognition or protection from being sorted into the degradation pathway, e.g. CAV1 and thus, integrin α5β1 (123). Next, it will be crucial to investigate the impact of lysosomal inhibitors, such as bafilomycin, on integrin degradation in Strumpellin-deficient platelets and megakaryocytes. Resulting normal αIIbβ3 surface levels in *Strumpellin*$^{-/-}$ platelets will support the hypothesis of a higher degradation rate of αIIbβ3 due to accumulation in the absence of Strumpellin.

II) Insufficient αIIbβ3 production

Another possibility could be that Strumpellin deficiency results in insufficient αIIbβ3 production by affecting transcription, translation and/or posttranslational modifications of αIIbβ3 in megakaryocytes and/or platelets. αIIbβ3 is mainly synthesised

and post-translationally processed in megakaryocytes (129, 132, 133). However, it has also been shown that αIIbβ3 can be *de novo* synthesised from mRNA in platelets (134).

Over the years, actin and actin-binding proteins have been found in the nucleus, where they are involved in gene expression by regulating transcription factors, chromatin remodelling and RNA polymerases as well as in mRNA processing and transport (156, 157). Several WASP family members have also been discovered in the nucleus, where they influence nuclear architecture as well as gene expression (91, 158-161).

WASH1 as well as SWIP and Strumpellin (then termed p63, p116 and p118, respectively) were originally found in the TATA-box-binding protein (TBP)-related factor 2 (TRF2) promotor transcription complex in *Drosophila*, which is involved in DNA replication and cell proliferation (158, 162). The complex also contains Nucleosome Remodelling Factors (NURF) 38 and 55, which have chromatin remodelling ability. In addition, *Verboon et al.* discovered that WASH1 plays an important role in maintaining the global nuclear architecture in *Drosophila* cells, including nuclear shape via B-type lamin interaction as well as organisation of chromatin and non-chromatin structures (e.g. nuclear organelles, protein machineries) (100).

All terminally differentiated haematopoietic cells, including megakaryocytes, originate from haematopoietic stem cells. *Xia et al.* demonstrated that in murine long-term haematopoietic stem cells (LT-HSCs), the predominantly nuclear WASH1 acts as a critical transcription co-factor for the proto-oncogene *c-Myc* (c-Myc promotes LT-HSC differentiation, among others) (163). WASH1 directly interacts with the Rbbp4 subunit of the NURF complex and through its actin nucleation-capacity, enables the complex to bind to and activate the *c-Myc* promoter (163). Conditional WASH1 knockout in hematopoietic stem cells resulted in severe anaemia, neutropenia as well as thrombocytopenia (platelet count: ~1,330,000/ml vs. ~126,000/ml) in mice due to defective LT-HSC differentiation (163). Approximately 60% of these mice died after eight weeks (163). These results showcase that WASH1 is essential for haematopoiesis. In this study analysis of general whole-blood parameters, especially platelet count and size, did not display any abnormalities in megakaryocytes and platelet specific knockout mice compared to

their littermate controls (Table 4, Figure 13). However, WASH1 localises differently in cells of the haematopoietic system: 1) in LT-HSCs mainly in the nucleus, 2) in short-term HSC (ST-HSCs) in the nucleus as well as in the cytoplasm, and 3) in multipotent progenitor cells (MPPs) predominantly in the cytoplasm (163). It needs to be further investigated how WASH1 as well as Strumpellin localise in nuclei-containing megakaryocytes. Depending on its subcellular location, the WASH complex may carry out different functions in different cells, including a role in regulating αIIbβ3 transcription.

Like WASP and N-WASP, WASH1 contains a highly conserved bipartite nuclear localisation signal (NLS) as well as a nuclear export signal (NES), which regulate nuclear and cytosolic localisation, respectively (97, 158). Furthermore, FAM21 contains functional NLS and NES motifs and it has also been predicted that the other WASH complex members, with the exception of CCDC53, have NLS motifs (158, 164). In addition, *Deng et al.* demonstrated that nuclear FAM21 regulates nuclear factor κB (NF-κB) gene transcription in pancreatic cancer cells – possibly independently of WASH1/ the WASH complex (164). Could this mean that other complex members, including Strumpellin, display WASH1-dependent or -independent nuclear functions?

Altogether, this data points to diverse functions of WASH1 and/or the entire WASH complex in the nucleus. Although a recycling defect in Strumpellin-deficient megakaryocytes and platelets seems more likely due to numerous corroborative studies, a role of Strumpellin in αIIbβ3 gene expression in megakaryocytes and/or platelets, via yet unknown mechanisms, may also be possible.

III) Defective αIIbβ3 storage into α-granules

Strumpellin deficiency may lead to altered α-granule formation with defective storage of αIIbβ3 into these organelles.

Platelet granules are synthesised in megakaryocytes before they are transported and packaged into nascent platelets (7, 25). They originate from the TGN and EE and mature from MVBs/LE (25, 74). This means that platelet granules obtain their content via the biosynthetic as well as the endocytic pathway. Granule maturation continues in circulating platelets, which includes endocytosis and trafficking of cargo to granules for storage (25, 59). Numerous studies have shown that WASH1

and Strumpellin deficiency lead to an abnormal endo-lysosomal system (51-54, 107).

This prompted the question whether the major NPF on endosomes, the WASH complex and its subunit Strumpellin, somehow affects platelet ultrastructure and thus, may indicate a role in platelet granule formation. To assess whether the lack of Strumpellin has an influence on granule morphology and number, α-granules as well as dense granules were quantified via TEM. Interestingly, the number of α-granules (*Strumpellin*$^{+/+}$: 2.66, *Strumpellin*$^{-/-}$: 3.36, $P = 0.004$) and dense granules (*Strumpellin*$^{+/+}$: 0.50, *Strumpellin*$^{-/-}$: 0.69, $P = 0.08$) per platelet section, albeit the latter statistically not significant, was slightly increased (Figure 15C and D). However, the area of α-granules in *Strumpellin*$^{-/-}$ platelets remained unaltered (Figure 15E and F). Although the increase in α-granule number is only moderate, the results imply that loss of Strumpellin somehow influences granule number. Could this also mean that Strumpellin affects αIIbβ3 packaging into α-granules? It is not possible to precisely distinguish between α-granules and lysosomes in routine TEM due to their similar density (16, 21). This makes it difficult to accurately quantify α-granule number in platelets in routine TEM. However, it is possible to identify lysosomes by specific cytochemical stains, which are directed at lysosomal proteins, e.g. acid phosphatase and arylsulfatase (165). Further experiments are needed to examine the underlying mechanism of this observation.

Very little is known about key regulators of the endocytic machinery in platelets and megakaryocytes. Studies have shown that αIIbβ3 is endocytosed and subsequently localises to Rab4-, Rab11- or VWF-positive endosomal compartments (60, 71). The findings of this thesis indicate that Strumpellin is important for αIIbβ3 targeting to the plasma membrane. Based on the role of the WASH complex in mediating endosomal cargo trafficking, including of integrins, Strumpellin most likely influences αIIbβ3 recycling back to the cell surface from endosomes in platelets and megakaryocytes (Figure 33).

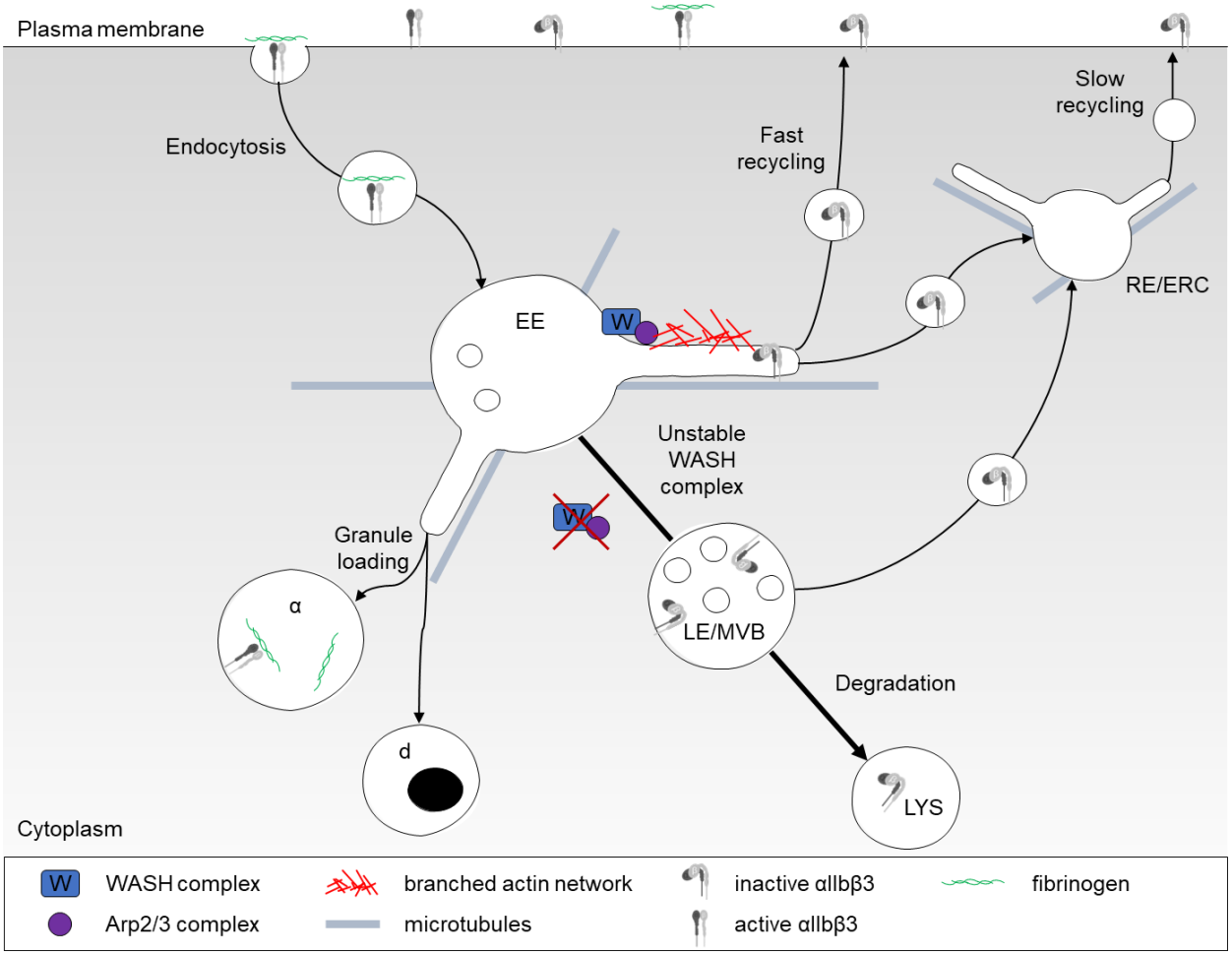

Figure 33: Schematic of how αIIbβ3 might be trafficked through platelets
Ligand-bound or -unbound αIIbβ3 is internalised via clathrin-dependent or -independent mechanisms and incorporated into EE. Here, the WASH complex recruits and stimulates the Arp2/3 complex to promote the generation of a branched actin network. This is necessary to form endosomal tubulations along microtubule tracks. αIIbβ3 is packaged into these tubules and subsequently trafficked back to the plasma membrane. Depletion of Strumpellin leads to an unstable WASH complex and decreased WASH1 protein levels. Recycling of αIIbβ3 to the surface is still possible, but impaired. αIIbβ3 accumulates in endosomal compartments and is rerouted towards degradation. Adapted from (150).

However, many questions remain unanswered. First and foremost, why is there a decrease of only 20% of αIIbβ3 on the megakaryocyte and platelet surface? The results of this thesis demonstrate that Strumpellin deficiency leads to a decrease, but not a loss of WASH1 protein abundance in platelets (Figure 12) – similar to a previous study in murine melanocytes (107). As discussed in Chapter 4.1, this could mean that in the absence of Strumpellin residual WASH complex subunits may still assemble and partially function in αIIbβ3 trafficking.

Another possibility could be that WASP family members substitute for one another. Like WASH1, WHAMM and JMY localise to internal membranes, including *cis*-Golgi, ERGIC and TGN, where they are involved in maintaining organelle morphology and cargo transportation (84, 88, 89). Especially WHAMM displays many similarities with WASH: it not

only activates the Arp2/3 complex to establish a branched actin network; it is also capable of binding to microtubules, thus enabling membrane tubulation (88, 166). Furthermore, N-WASP is not only important for endocytosis, but also endocytic vesicle and endosome movement through the cytoplasm (167, 168). Due to their functionally similar roles in intracellular transportation, it might be possible that WHAMM, JMY or N-WASP are able to compensate for the loss of WASH1 in Strumpellin-deficient platelets by upregulation and/or re-localisation. Compensatory mechanisms have already been shown for some WASP family members (169-172). And very recently, *Verboon et al.* proved that WAVE protein levels are increasingly upregulated in WASH-deficient *Drosophila* oocytes over several generations, where it localises to the oocyte cortex similarly to WASH (173). In addition, RNAi knockdown of WAVE phenocopied WASH complex knockdown in *Drosophila* oocytes (premature ooplasmic streaming and defects in actin structure at the oocyte cortex) (173). This suggests that WAVE proteins may compensate for the loss of WASH in *Drosophila* oocytes. So far, WASP, JMY and members of the WAVE complex have been detected in mouse platelets (101). Further experiments are necessary to determine whether the expression of other WASP family members is upregulated and where exactly they are located in Strumpellin-deficient megakaryocytes and platelets.

Furthermore, it remains to be confirmed whether Strumpellin influences the surface expression of other platelet integrins, such as α5, α6 and αv. Similar to human platelets, αIIbβ3 integrin is the most abundant integrin in murine platelets. There are approximately 106,624 αIIb and 104,066 β3 copies per mouse platelet, whereas integrin subunits α2 (~17,591 copies), α5 (~1,886 copies), α6 (~20 copies), αv (~467 copies) and β1 (~30,855 copies) are all less expressed (101). Altogether, antibodies against α2, αIIb, β1 and β3 were tested in this study with differing results. α2 and β1 surface expression was not affected by the loss of Strumpellin (Table 5, Figure 18A). This suggests that: 1) α2 and β1 are not recycled or are less recycled, or 2) the remaining WASH-complex or other compensatory mechanisms are sufficient for maintaining normal α2 and β1 surface expression, or 3) there is the possibility of specific recycling pathways for different integrins in platelets and megakaryocytes – each integrin subtype may be processed differently due to distinct internalisation and trafficking mechanisms as well as activation state (151).

4.3 Strumpellin deficiency has no effect on αIIbβ3 *in vitro* function

In vitro functional assays did not demonstrate defective αIIbβ3 function in *Strumpellin*$^{-/-}$ platelets despite a 20% decrease in αIIbβ3 surface expression (Table 5, Figure 18). Flow cytometry analysis displayed a significantly impaired αIIbβ3 activation (Table 6, Figure 19) and reduced fibrinogen-binding to αIIbβ3 (Figure 22A) after platelet activation. Furthermore, there was an initial delay in fibrinogen uptake (Figure 22B), but an overall unaltered fibrinogen abundance (Figure 21). Previous studies on WASH1- and Strumpellin-depleted cells demonstrated adhesion and spreading defects on fibronectin, due to defective α5 trafficking (123, 155). But remarkably, αIIbβ3-dependent platelet spreading on fibrinogen (Figure 24) as well as aggregation (Figure 25) were not affected by the loss of Strumpellin. This data indicates that Strumpellin deficiency has no effect on αIIbβ3 function, at least *in vitro*, and the remaining 80% of αIIbβ3 is still sufficient for normal platelet spreading and aggregation. This coincides with results obtained from heterozygous β3-integrin mutant mice, which only express 50% of wild-type αIIbβ3 in platelets (138). These mice did not showcase any bleeding defects; platelet fibrinogen content and platelet aggregation were unaltered (138). Decreased αIIbβ3 activation, reduced fibrinogen-binding to αIIbβ3 as well as initial delay in fibrinogen internalisation of *Strumpellin*$^{-/-}$ platelets are most likely due to the already decreased level of αIIbβ3 expression on the platelet surface and not due to a defective function.

4.4 Concluding remarks and outlook

Increasingly over the last few years, the intricate molecular mechanisms that orchestrate endosomal retrieval and recycling of internalised cargo proteins have been discovered. The identification of effectors, such as the WASH complex and the cargo-retrieval complexes retromer, retriever and the CCC complex, has contributed immensely to the understanding of the endosomal sorting machinery in all manner of cells. This thesis demonstrates that the WASH complex also plays a key role in endocytic trafficking in platelets and megakaryocytes.

The results obtained here provide the first-ever evidence that the WASH complex subunit Strumpellin selectively regulates αIIbβ3 integrin surface expression in platelets and megakaryocytes. Major findings of this study are:

I) a decrease in WASH1 abundance in Strumpellin-deficient platelets,

II) a 20% decrease in αIIbβ3 surface expression in *Strumpellin*$^{-/-}$ platelets and megakaryocytes and consequently, a reduced αIIbβ3 activation after platelet stimulation,
III) an overall decrease in αIIbβ3 content in *Strumpellin*$^{-/-}$ platelets, but functioning αIIbβ3 recruitment after platelet activation,
IV) and lastly, no defect in αIIbβ3 *in vitro* function.

As a member of the WASH complex, Strumpellin most likely plays a role in αIIbβ3 trafficking and recycling back to the cell surface in platelets and megakaryocytes. Residual WASH complex subunits may still assemble and function, at least partially, in the absence of Strumpellin. This could explain the only 20% decrease in αIIbβ3 surface expression in platelets and megakaryocytes under resting conditions.

However, further studies are required to thoroughly investigate the role of the WASH complex in platelets and megakaryocytes and how individual complex members contribute to cargo retrieval and trafficking. Analysis of megakaryocyte and platelet specific *WASH1* knockout mice are of interest to further study αIIbβ3 trafficking in platelets. It could reveal a more severe decrease in surface αIIbβ3. It could also shed some light on whether the remaining subunits in *Strumpellin*$^{-/-}$ platelets are responsible for the residual 80% αIIbβ3 surface expression. *WASH1* knockout in platelets and megakaryocytes could also determine if trafficking of other platelet integrins, such as α2β1, α5β1, α6β1 and αvβ3, is WASH complex-dependent and if α- and possibly dense granule formation is affected.

Furthermore, the cargo-retrieval complex retriever and its adaptor SNX17 have been implemented in integrin trafficking, specifically of α5β1 (37, 174, 175). Both retriever (subunits: VPS29, DSCR3 and C16orf62) and SNX17 were detected in human and mouse platelets (63, 101). Further investigation may give some indication whether the WASH complex is responsible for αIIbβ3 trafficking in concert with retriever and SNX17.

Finally, immunofluorescence studies of platelets and megakaryocytes are imperative. Thus far, immunofluorescence staining of platelets with commercially available antibodies and in-house attempts to generate a functional antibody were not successful. Immunofluorescence staining of platelets and megakaryocytes will shed some light on how the endosomal actin network is affected in Strumpellin-deficient platelets as well as identify precisely how loss of Strumpellin disrupts αIIbβ3 trafficking through Rab4-, Rab11- and vWF-positive compartments (markers for EE, RE and α-granules, respectively).

5 References

1. Machlus KR, Italiano JE, Jr. The incredible journey: From megakaryocyte development to platelet formation. *J Cell Biol*. 2013;201(6):785-96.
2. Patel SR, Hartwig JH*, et al.* The biogenesis of platelets from megakaryocyte proplatelets. *J Clin Invest*. 2005;115(12):3348-54.
3. Junt T, Schulze H*, et al.* Dynamic visualization of thrombopoiesis within bone marrow. *Science*. 2007;317(5845):1767-70.
4. Italiano JE, Jr., Lecine P*, et al.* Blood platelets are assembled principally at the ends of proplatelet processes produced by differentiated megakaryocytes. *J Cell Biol*. 1999;147(6):1299-312.
5. Thon JN, Montalvo A*, et al.* Cytoskeletal mechanics of proplatelet maturation and platelet release. *J Cell Biol*. 2010;191(4):861-74.
6. Kaushansky K, Lok S*, et al.* Promotion of megakaryocyte progenitor expansion and differentiation by the c-Mpl ligand thrombopoietin. *Nature*. 1994;369(6481):568-71.
7. Richardson JL, Shivdasani RA*, et al.* Mechanisms of organelle transport and capture along proplatelets during platelet production. *Blood*. 2005;106(13):4066-75.
8. Schulze H, Korpal M*, et al.* Characterization of the megakaryocyte demarcation membrane system and its role in thrombopoiesis. *Blood*. 2006;107(10):3868-75.
9. Patel SR, Richardson JL*, et al.* Differential roles of microtubule assembly and sliding in proplatelet formation by megakaryocytes. *Blood*. 2005;106(13):4076-85.
10. Bender M, Eckly A*, et al.* ADF/n-cofilin-dependent actin turnover determines platelet formation and sizing. *Blood*. 2010;116(10):1767-75.
11. Varga-Szabo D, Pleines I*, et al.* Cell adhesion mechanisms in platelets. *Arterioscler Thromb Vasc Biol*. 2008;28(3):403-12.
12. Nieswandt B, Pleines I*, et al.* Platelet adhesion and activation mechanisms in arterial thrombosis and ischaemic stroke. *J Thromb Haemost*. 2011;9 Suppl 1:92-104.
13. Nieswandt B, Varga-Szabo D*, et al.* Integrins in platelet activation. *J Thromb Haemost*. 2009;7 Suppl 1:206-9.
14. Falet H. Anatomy of the Platelet Cytoskeleton. In: Gresele P*, et al.* Platelets in Thrombotic and Non-Thrombotic Disorders. Springer; 2017. p. 139-56.
15. Ruggeri ZM. Platelets in atherothrombosis. *Nat Med*. 2002;8(11):1227-34.
16. Rumbaut RE, Thiagarajan P. Platelet-Vessel Wall Interactions in Hemostasis and Thrombosis. In: Granger DN*, et al.* Colloquium Series on Integrated Systems Physiology: From Molecule to Function to Disease. Morgan & Claypool Life Sciences; 2010.
17. Neumüller J, Ellinger A*, et al.* Transmission Electron Microscopy of Platelets from Apheresis and Buffy-Coat-Derived Platelet Concentrates. In: Maaz K. The Transmission Electron Microscope - Theory and Applications. INTECH; 2015. p. 255-84.
18. Heijnen HFG, Korporaal SJA. Platelet Morphology and Ultrastructure. In: Gresele P*, et al.* Platelets in Thrombotic and Non-Thrombotic Disorders. Springer; 2017. p. 21-38.
19. Eckly A, Heijnen H*, et al.* Biogenesis of the demarcation membrane system (DMS) in megakaryocytes. *Blood*. 2014;123(6):921-30.
20. van Nispen tot Pannerden H, de Haas F*, et al.* The platelet interior revisited: electron tomography reveals tubular alpha-granule subtypes. *Blood*. 2010;116(7):1147-56.
21. Rendu F, Brohard-Bohn B. The platelet release reaction: granules' constituents, secretion and functions. *Platelets*. 2001;12(5):261-73.
22. Italiano JE. Megakaryocyte Development and Platelet Production. In: Gresele P*, et al.* Platelets in Thrombotic and Non-Thrombotic Disorders. Springer; 2017. p. 39-53.
23. Hartwig JH, DeSisto M. The cytoskeleton of the resting human blood platelet: structure of the membrane skeleton and its attachment to actin filaments. *J Cell Biol*. 1991;112(3):407-25.
24. Patel-Hett S, Richardson JL*, et al.* Visualization of microtubule growth in living platelets reveals a dynamic marginal band with multiple microtubules. *Blood*. 2008;111(9):4605-16.
25. Sharda A, Flaumenhaft R. The life cycle of platelet granules. *F1000Res*. 2018;7:236.
26. Harrison P, Cramer EM. Platelet alpha-granules. *Blood reviews*. 1993;7(1):52-62.

27. Flaumenhaft R. Platelet Secretion. In: Gresele P*, et al.* Platelets in Thrombotic and Non-Thrombotic Disorders. Springer; 2017. p. 353-66.
28. Maynard DM, Heijnen HF*, et al.* Proteomic analysis of platelet alpha-granules using mass spectrometry. *J Thromb Haemost*. 2007;5(9):1945-55.
29. Simonetti B, Cullen PJ. Actin-dependent endosomal receptor recycling. *Curr Opin Cell Biol*. 2019;56:22-33.
30. Wang J, Fedoseienko A*, et al.* Endosomal receptor trafficking: Retromer and beyond. *Traffic*. 2018;19(8):578-90.
31. Bonifacino JS, Neefjes J. Moving and positioning the endolysosomal system. *Curr Opin Cell Biol*. 2017;47:1-8.
32. Mayor S, Parton RG*, et al.* Clathrin-independent pathways of endocytosis. *Cold Spring Harb Perspect Biol*. 2014;6(6).
33. Cullen PJ, Steinberg F. To degrade or not to degrade: mechanisms and significance of endocytic recycling. *Nat Rev Mol Cell Biol*. 2018;19(11):679-96.
34. Huotari J, Helenius A. Endosome maturation. *Embo j*. 2011;30(17):3481-500.
35. Naslavsky N, Caplan S. The enigmatic endosome - sorting the ins and outs of endocytic trafficking. *J Cell Sci*. 2018;131(13).
36. Podinovskaia M, Spang A. The Endosomal Network: Mediators and Regulators of Endosome Maturation. *Prog Mol Subcell Biol*. 2018;57:1-38.
37. McNally KE, Faulkner R*, et al.* Retriever is a multiprotein complex for retromer-independent endosomal cargo recycling. *Nat Cell Biol*. 2017;19(10):1214-25.
38. Chen KE, Healy MD*, et al.* Towards a molecular understanding of endosomal trafficking by Retromer and Retriever. *Traffic*. 2019;20(7):465-78.
39. Lee S, Chang J*, et al.* FAM21 directs SNX27-retromer cargoes to the plasma membrane by preventing transport to the Golgi apparatus. *Nat Commun*. 2016;7:10939.
40. Temkin P, Lauffer B*, et al.* SNX27 mediates retromer tubule entry and endosome-to-plasma membrane trafficking of signalling receptors. *Nat Cell Biol*. 2011;13(6):715-21.
41. Burd C, Cullen PJ. Retromer: a master conductor of endosome sorting. *Cold Spring Harb Perspect Biol*. 2014;6(2).
42. Harrison MS, Hung CS*, et al.* A mechanism for retromer endosomal coat complex assembly with cargo. *Proc Natl Acad Sci U S A*. 2014;111(1):267-72.
43. Rojas R, van Vlijmen T*, et al.* Regulation of retromer recruitment to endosomes by sequential action of Rab5 and Rab7. *J Cell Biol*. 2008;183(3):513-26.
44. Seaman MN, Harbour ME*, et al.* Membrane recruitment of the cargo-selective retromer subcomplex is catalysed by the small GTPase Rab7 and inhibited by the Rab-GAP TBC1D5. *J Cell Sci*. 2009;122(Pt 14):2371-82.
45. Harbour ME, Breusegem SY*, et al.* The cargo-selective retromer complex is a recruiting hub for protein complexes that regulate endosomal tubule dynamics. *J Cell Sci*. 2010;123(Pt 21):3703-17.
46. Phillips-Krawczak CA, Singla A*, et al.* COMMD1 is linked to the WASH complex and regulates endosomal trafficking of the copper transporter ATP7A. *Mol Biol Cell*. 2015;26(1):91-103.
47. Bartuzi P, Billadeau DD*, et al.* CCC- and WASH-mediated endosomal sorting of LDLR is required for normal clearance of circulating LDL. *Nat Commun*. 2016;7:10961.
48. Wijers M, Zanoni P*, et al.* The hepatic WASH complex is required for efficient plasma LDL and HDL cholesterol clearance. *JCI Insight*. 2019;4(11).
49. Morel E, Parton RG*, et al.* Annexin A2-dependent polymerization of actin mediates endosome biogenesis. *Dev Cell*. 2009;16(3):445-57.
50. Muriel O, Tomas A*, et al.* Moesin and cortactin control actin-dependent multivesicular endosome biogenesis. *Mol Biol Cell*. 2016;27(21):3305-16.
51. Derivery E, Sousa C*, et al.* The Arp2/3 activator WASH controls the fission of endosomes through a large multiprotein complex. *Dev Cell*. 2009;17(5):712-23.
52. Gomez TS, Billadeau DD. A FAM21-containing WASH complex regulates retromer-dependent sorting. *Dev Cell*. 2009;17(5):699-711.
53. Gomez TS, Gorman JA*, et al.* Trafficking defects in WASH-knockout fibroblasts originate from collapsed endosomal and lysosomal networks. *Mol Biol Cell*. 2012;23(16):3215-28.

54. Duleh SN, Welch MD. WASH and the Arp2/3 complex regulate endosome shape and trafficking. *Cytoskeleton (Hoboken)*. 2010;67(3):193-206.
55. Puthenveedu MA, Lauffer B*, et al.* Sequence-dependent sorting of recycling proteins by actin-stabilized endosomal microdomains. *Cell*. 2010;143(5):761-73.
56. Derivery E, Helfer E*, et al.* Actin polymerization controls the organization of WASH domains at the surface of endosomes. *PLoS One*. 2012;7(6):e39774.
57. Zech T, Calaminus SD*, et al.* Actin on trafficking: could actin guide directed receptor transport? *Cell Adh Migr*. 2012;6(6):476-81.
58. Harbour ME, Breusegem SY*, et al.* Recruitment of the endosomal WASH complex is mediated by the extended 'tail' of Fam21 binding to the retromer protein Vps35. *Biochem J*. 2012;442(1):209-20.
59. Banerjee M, Whiteheart SW. The ins and outs of endocytic trafficking in platelet functions. *Curr Opin Hematol*. 2017;24(5):467-74.
60. Huang Y, Joshi S*, et al.* Arf6 controls platelet spreading and clot retraction via integrin alphaIIbbeta3 trafficking. *Blood*. 2016;127(11):1459-67.
61. Walsh TG, Li Y*, et al.* Small GTPases in platelet membrane trafficking. *Platelets*. 2019;30(1):31-40.
62. Yadav S, Storrie B. The cellular basis of platelet secretion: Emerging structure/function relationships. *Platelets*. 2017;28(2):108-18.
63. Burkhart JM, Vaudel M*, et al.* The first comprehensive and quantitative analysis of human platelet protein composition allows the comparative analysis of structural and functional pathways. *Blood*. 2012;120(15):e73-82.
64. Harrison P, Wilbourn B*, et al.* Uptake of plasma fibrinogen into the alpha granules of human megakaryocytes and platelets. *J Clin Invest*. 1989;84(4):1320-4.
65. Handagama PJ, Shuman MA*, et al.* Incorporation of intravenously injected albumin, immunoglobulin G, and fibrinogen in guinea pig megakaryocyte granules. *J Clin Invest*. 1989;84(1):73-82.
66. Lorenz V, Stegner D*, et al.* Targeted downregulation of platelet CLEC-2 occurs through Syk-independent internalization. *Blood*. 2015;125(26):4069-77.
67. Kanamarlapudi V, Owens SE*, et al.* ARF6-dependent regulation of P2Y receptor traffic and function in human platelets. *PLoS One*. 2012;7(8):e43532.
68. Gao W, Shi P*, et al.* Clathrin-mediated integrin alphaIIbbeta3 trafficking controls platelet spreading. *Platelets*. 2018;29(6):610-21.
69. Ferguson SM, De Camilli P. Dynamin, a membrane-remodelling GTPase. *Nat Rev Mol Cell Biol*. 2012;13(2):75-88.
70. Parton RG, Simons K. The multiple faces of caveolae. *Nat Rev Mol Cell Biol*. 2007;8(3):185-94.
71. Banerjee M, Joshi S*, et al.* Cellubrevin/vesicle-associated membrane protein-3-mediated endocytosis and trafficking regulate platelet functions. *Blood*. 2017;130(26):2872-83.
72. Joshi S, Whiteheart SW. The nuts and bolts of the platelet release reaction. *Platelets*. 2017;28(2):129-37.
73. Flaumenhaft R. Platelet Secretion. In: Michelson AD. Platelets, Third Edition. Third ed. Elsevier; 2013. p. 343-66.
74. Heijnen HF, Debili N*, et al.* Multivesicular bodies are an intermediate stage in the formation of platelet alpha-granules. *Blood*. 1998;91(7):2313-25.
75. Youssefian T, Cramer EM. Megakaryocyte dense granule components are sorted in multivesicular bodies. *Blood*. 2000;95(12):4004-7.
76. Chen Y, Yuan Y*, et al.* Sorting machineries: how platelet-dense granules differ from alpha-granules. *Biosci Rep*. 2018;38(5).
77. Handagama P, Scarborough RM*, et al.* Endocytosis of fibrinogen into megakaryocyte and platelet alpha-granules is mediated by alpha IIb beta 3 (glycoprotein IIb-IIIa). *Blood*. 1993;82(1):135-8.
78. Rottner K, Faix J*, et al.* Actin assembly mechanisms at a glance. *J Cell Sci*. 2017;130(20):3427-35.
79. Goley ED, Welch MD. The ARP2/3 complex: an actin nucleator comes of age. *Nat Rev Mol Cell Biol*. 2006;7(10):713-26.

80. Takenawa T, Suetsugu S. The WASP-WAVE protein network: connecting the membrane to the cytoskeleton. *Nat Rev Mol Cell Biol*. 2007;8(1):37-48.
81. Campellone KG, Welch MD. A nucleator arms race: cellular control of actin assembly. *Nat Rev Mol Cell Biol*. 2010;11(4):237-51.
82. Alekhina O, Burstein E*, et al.* Cellular functions of WASP family proteins at a glance. *J Cell Sci*. 2017;130(14):2235-41.
83. Jia D, Gomez TS*, et al.* WASH and WAVE actin regulators of the Wiskott-Aldrich syndrome protein (WASP) family are controlled by analogous structurally related complexes. *Proc Natl Acad Sci U S A*. 2010;107(23):10442-7.
84. Schlüter K, Waschbüsch D*, et al.* JMY is involved in anterograde vesicle trafficking from the trans-Golgi network. *Eur J Cell Biol*. 2014;93(5-6):194-204.
85. Burianek LE, Soderling SH. Under lock and key: spatiotemporal regulation of WASP family proteins coordinates separate dynamic cellular processes. *Semin Cell Dev Biol*. 2013;24(4):258-66.
86. Derry JM, Ochs HD*, et al.* Isolation of a novel gene mutated in Wiskott-Aldrich syndrome. *Cell*. 1994;78(4):635-44.
87. Schurr Y, Sperr A*, et al.* Platelet lamellipodium formation is not required for thrombus formation and stability. *Blood*. 2019;134(25):2318-29.
88. Campellone KG, Webb NJ*, et al.* WHAMM is an Arp2/3 complex activator that binds microtubules and functions in ER to Golgi transport. *Cell*. 2008;134(1):148-61.
89. Blom M, Reis K*, et al.* RhoD is a Golgi component with a role in anterograde protein transport from the ER to the plasma membrane. *Exp Cell Res*. 2015;333(2):208-19.
90. Zuchero JB, Coutts AS*, et al.* p53-cofactor JMY is a multifunctional actin nucleation factor. *Nat Cell Biol*. 2009;11(4):451-9.
91. Shikama N, Lee CW*, et al.* A novel cofactor for p300 that regulates the p53 response. *Mol Cell*. 1999;4(3):365-76.
92. Coutts AS, Boulahbel H*, et al.* Mdm2 targets the p53 transcription cofactor JMY for degradation. *EMBO Rep*. 2007;8(1):84-90.
93. Coutts AS, Weston L*, et al.* A transcription co-factor integrates cell adhesion and motility with the p53 response. *Proc Natl Acad Sci U S A*. 2009;106(47):19872-7.
94. Kast DJ, Zajac AL*, et al.* WHAMM Directs the Arp2/3 Complex to the ER for Autophagosome Biogenesis through an Actin Comet Tail Mechanism. *Curr Biol*. 2015;25(13):1791-7.
95. Dai A, Yu L*, et al.* WHAMM initiates autolysosome tubulation by promoting actin polymerization on autolysosomes. *Nat Commun*. 2019;10(1):3699.
96. Coutts AS, La Thangue NB. Actin nucleation by WH2 domains at the autophagosome. *Nat Commun*. 2015;6:7888.
97. Linardopoulou EV, Parghi SS*, et al.* Human subtelomeric WASH genes encode a new subclass of the WASP family. *PLoS Genet*. 2007;3(12):e237.
98. Schmid EM, Ford MG*, et al.* Role of the AP2 beta-appendage hub in recruiting partners for clathrin-coated vesicle assembly. *PLoS Biol*. 2006;4(9):e262.
99. Jia D, Gomez TS*, et al.* Multiple repeat elements within the FAM21 tail link the WASH actin regulatory complex to the retromer. *Mol Biol Cell*. 2012;23(12):2352-61.
100. Verboon JM, Rincon-Arano H*, et al.* Wash interacts with lamin and affects global nuclear organization. *Curr Biol*. 2015;25(6):804-10.
101. Zeiler M, Moser M*, et al.* Copy number analysis of the murine platelet proteome spanning the complete abundance range. *Mol Cell Proteomics*. 2014;13(12):3435-45.
102. Xia P, Wang S*, et al.* WASH inhibits autophagy through suppression of Beclin 1 ubiquitination. *Embo j*. 2013;32(20):2685-96.
103. Derivery E, Gautreau A. Evolutionary conservation of the WASH complex, an actin polymerization machine involved in endosomal fission. *Commun Integr Biol*. 2010;3(3):227-30.
104. Zech T, Calaminus SD*, et al.* The Arp2/3 activator WASH regulates alpha5beta1-integrin-mediated invasive migration. *J Cell Sci*. 2011;124(Pt 22):3753-9.
105. Hao YH, Doyle JM*, et al.* Regulation of WASH-dependent actin polymerization and protein trafficking by ubiquitination. *Cell*. 2013;152(5):1051-64.

106. Hao YH, Fountain MD, Jr.*, et al.* USP7 Acts as a Molecular Rheostat to Promote WASH-Dependent Endosomal Protein Recycling and Is Mutated in a Human Neurodevelopmental Disorder. *Mol Cell*. 2015;59(6):956-69.
107. Tyrrell BJ, Woodham EF*, et al.* Loss of strumpellin in the melanocytic lineage impairs the WASH Complex but does not affect coat colour. *Pigment Cell Melanoma Res*. 2016;29(5):559-71.
108. Helfer E, Harbour ME*, et al.* Endosomal recruitment of the WASH complex: active sequences and mutations impairing interaction with the retromer. *Biol Cell*. 2013;105(5):191-207.
109. Visweshwaran SP, Thomason PA*, et al.* The trimeric coiled-coil HSBP1 protein promotes WASH complex assembly at centrosomes. *Embo j*. 2018;37(13).
110. Ropers F, Derivery E*, et al.* Identification of a novel candidate gene for non-syndromic autosomal recessive intellectual disability: the WASH complex member SWIP. *Hum Mol Genet*. 2011;20(13):2585-90.
111. Assoum M, Bruel AL*, et al.* Novel KIAA1033/WASHC4 mutations in three patients with syndromic intellectual disability and a review of the literature. *Am J Med Genet A*. 2020;182(4):792-7.
112. Piotrowski JT, Gomez TS*, et al.* WASH knockout T cells demonstrate defective receptor trafficking, proliferation, and effector function. *Mol Cell Biol*. 2013;33(5):958-73.
113. Ding L, Han L*, et al.* WASH Regulates Glucose Homeostasis by Facilitating Glut2 Receptor Recycling in Pancreatic β-Cells. *Diabetes*. 2019;68(2):377-86.
114. Clemen CS, Tangavelou K*, et al.* Strumpellin is a novel valosin-containing protein binding partner linking hereditary spastic paraplegia to protein aggregation diseases. *Brain*. 2010;133(10):2920-41.
115. Meijer IA, Valdmanis PN*, et al.* Spastic Paraplegia 8. In: Adam MP*, et al.* GeneReviews®. University of Washington, Seattle; 2008.
116. Freeman C, Seaman MNJ*, et al.* The hereditary spastic paraplegia protein strumpellin: characterisation in neurons and of the effect of disease mutations on WASH complex assembly and function. *Biochimica et Biophysica Acta*. 2013;1832(1):160-73.
117. Jahic A, Khundadze M*, et al.* The spectrum of KIAA0196 variants, and characterization of a murine knockout: implications for the mutational mechanism in hereditary spastic paraplegia type SPG8. *Orphanet J Rare Dis*. 2015;10:147.
118. Valdmanis PN, Meijer IA*, et al.* Mutations in the KIAA0196 gene at the SPG8 locus cause hereditary spastic paraplegia. *Am J Hum Genet*. 2007;80(1):152-61.
119. Elliott AM, Simard LR*, et al.* A novel mutation in KIAA0196: identification of a gene involved in Ritscher-Schinzel/3C syndrome in a First Nations cohort. *J Med Genet*. 2013;50(12):819-22.
120. Blackstone C. Converging cellular themes for the hereditary spastic paraplegias. *Curr Opin Neurobiol*. 2018;51:139-46.
121. Ginanneschi F, D'Amore A*, et al.* SPG8 mutations in Italian families: clinical data and literature review. *Neurol Sci*. 2020;41(3):699-703.
122. Song L, Rijal R*, et al.* Expression of N471D strumpellin leads to defects in the endolysosomal system. *Dis Model Mech*. 2018;11(9).
123. Lee S, Park H*, et al.* Hereditary spastic paraplegia SPG8 mutations impair CAV1-dependent, integrin-mediated cell adhesion. *Sci Signal*. 2020;13(613).
124. Kolanczyk M, Krawitz P*, et al.* Missense variant in CCDC22 causes X-linked recessive intellectual disability with features of Ritscher-Schinzel/3C syndrome. *Eur J Hum Genet*. 2015;23(5):633-8.
125. Gruner S, Prostredna M*, et al.* Multiple integrin-ligand interactions synergize in shear-resistant platelet adhesion at sites of arterial injury in vivo. *Blood*. 2003;102(12):4021-7.
126. Nieswandt B, Brakebusch C*, et al.* Glycoprotein VI but not alpha2beta1 integrin is essential for platelet interaction with collagen. *Embo j*. 2001;20(9):2120-30.
127. Holtkotter O, Nieswandt B*, et al.* Integrin alpha 2-deficient mice develop normally, are fertile, but display partially defective platelet interaction with collagen. *J Biol Chem*. 2002;277(13):10789-94.

128. Wagner CL, Mascelli MA*, et al.* Analysis of GPIIb/IIIa receptor number by quantification of 7E3 binding to human platelets. *Blood*. 1996;88(3):907-14.
129. Bennett JS. aIIbb3 (GPIIb/IIIa) Structure and Function. In: Gresele P*, et al.* Platelets in Thrombotic and Non-Thrombotic Disorders. Springer; 2017. p. 99-112.
130. Niiya K, Hodson E*, et al.* Increased surface expression of the membrane glycoprotein IIb/IIIa complex induced by platelet activation. Relationship to the binding of fibrinogen and platelet aggregation. *Blood*. 1987;70(2):475-83.
131. Wencel-Drake JD, Plow EF*, et al.* Localization of internal pools of membrane glycoproteins involved in platelet adhesive responses. *Am J Pathol*. 1986;124(2):324-34.
132. Duperray A, Berthier R*, et al.* Biosynthesis and processing of platelet GPIIb-IIIa in human megakaryocytes. *J Cell Biol*. 1987;104(6):1665-73.
133. Kolodziej MA, Vilaire G*, et al.* Study of the endoproteolytic cleavage of platelet glycoprotein IIb using oligonucleotide-mediated mutagenesis. *J Biol Chem*. 1991;266(34):23499-504.
134. Thon JN, Devine DV. Translation of glycoprotein IIIa in stored blood platelets. *Transfusion*. 2007;47(12):2260-70.
135. Coller BS, Shattil SJ. The GPIIb/IIIa (integrin alphaIIbbeta3) odyssey: a technology-driven saga of a receptor with twists, turns, and even a bend. *Blood*. 2008;112(8):3011-25.
136. Moser M, Nieswandt B*, et al.* Kindlin-3 is essential for integrin activation and platelet aggregation. *Nat Med*. 2008;14(3):325-30.
137. Nurden AT. Glanzmann thrombasthenia. *Orphanet J Rare Dis*. 2006;1:10.
138. Hodivala-Dilke KM, McHugh KP*, et al.* Beta3-integrin-deficient mice are a model for Glanzmann thrombasthenia showing placental defects and reduced survival. *J Clin Invest*. 1999;103(2):229-38.
139. Tiedt R, Schomber T*, et al.* Pf4-Cre transgenic mice allow the generation of lineage-restricted gene knockouts for studying megakaryocyte and platelet function in vivo. *Blood*. 2007;109(4):1503-6.
140. Skarnes WC, Rosen B*, et al.* A conditional knockout resource for the genome-wide study of mouse gene function. *Nature*. 2011;474(7351):337-42.
141. Tucker KL, Wang Y*, et al.* A transgenic mouse strain expressing four drug-selectable marker genes. *Nucleic Acids Res*. 1997;25(18):3745-6.
142. Nagy A, Gertsenstein M*, et al.* Manipulation the Mouse Embryo: A Laboratory Manual. Third ed. New York, USA: Cold Spring Harbor; 2003.
143. Rodríguez CI, Buchholz F*, et al.* High-efficiency deleter mice show that FLPe is an alternative to Cre-loxP. *Nat Genet*. 2000;25(2):139-40.
144. Kawamoto T. Use of a new adhesive film for the preparation of multi-purpose fresh-frozen sections from hard tissues, whole-animals, insects and plants. *Arch Histol Cytol*. 2003;66(2):123-43.
145. Schurr Y. Studies on the role of cytoskeletal-regulatory and -crosslinking proteins in platelet function [Doctoral thesis]. Würzburg: Julius-Maximilians-Universität Würzburg; 2020.
146. Kasirer-Friede A, Shattil SJ. Regulation of Platelet Adhesion Receptors. In: Gresele P*, et al.* Platelets in Thrombotic and Non-Thrombotic Disorders. Springer; 2017. p. 69-84.
147. Boulaftali Y, Ho Tin Noé B*, et al.* GPVI. In: Gresele P*, et al.* Platelets in Thrombotic and Non-Thrombotic Disorders. Springer; 2017. p. 113-27.
148. Rayes J, Hardy AT*, et al.* The Role of CLEC-2 in and Beyond the Vasculature. In: Gresele P*, et al.* Platelets in Thrombotic and Non-Thrombotic Disorders. Springer; 2017. p. 129-38.
149. Zhao J, Hedera P. Strumpellin and Spartin, Hereditary Spastic Paraplegia Proteins, are Binding Partners. *Journal of Experimental Neuroscience*. 2015;9:15-25.
150. De Franceschi N, Hamidi H*, et al.* Integrin traffic - the update. *J Cell Sci*. 2015;128(5):839-52.
151. Moreno-Layseca P, Icha J*, et al.* Integrin trafficking in cells and tissues. *Nat Cell Biol*. 2019;21(2):122-32.
152. Wencel-Drake JD, Frelinger AL, 3rd*, et al.* Arg-Gly-Asp-dependent occupancy of GPIIb/IIIa by applaggin: evidence for internalization and cycling of a platelet integrin. *Blood*. 1993;81(1):62-9.
153. Schober JM, Lam SC*, et al.* Effect of cellular and receptor activation on the extent of integrin alphaIIbbeta3 internalization. *J Thromb Haemost*. 2003;1(11):2404-10.

154. Wencel-Drake JD. Plasma membrane GPIIb/IIIa. Evidence for a cycling receptor pool. *Am J Pathol*. 1990;136(1):61-70.
155. Duleh SN, Welch MD. Regulation of integrin trafficking, cell adhesion, and cell migration by WASH and the Arp2/3 complex. *Cytoskeleton (Hoboken)*. 2012;69(12):1047-58.
156. Kristó I, Bajusz I*, et al.* Actin, actin-binding proteins, and actin-related proteins in the nucleus. *Histochem Cell Biol*. 2016;145(4):373-88.
157. Kelpsch DJ, Tootle TL. Nuclear Actin: From Discovery to Function. *Anat Rec (Hoboken)*. 2018;301(12):1999-2013.
158. Verboon JM, Sugumar B*, et al.* Wiskott-Aldrich syndrome proteins in the nucleus: aWASH with possibilities. *Nucleus*. 2015;6(5):349-59.
159. Wu X, Yoo Y*, et al.* Regulation of RNA-polymerase-II-dependent transcription by N-WASP and its nuclear-binding partners. *Nat Cell Biol*. 2006;8(7):756-63.
160. Sadhukhan S, Sarkar K*, et al.* Nuclear role of WASp in gene transcription is uncoupled from its ARP2/3-dependent cytoplasmic role in actin polymerization. *J Immunol*. 2014;193(1):150-60.
161. Miyamoto K, Teperek M*, et al.* Nuclear Wave1 is required for reprogramming transcription in oocytes and for normal development. *Science*. 2013;341(6149):1002-5.
162. Hochheimer A, Zhou S*, et al.* TRF2 associates with DREF and directs promoter-selective gene expression in Drosophila. *Nature*. 2002;420(6914):439-45.
163. Xia P, Wang S*, et al.* WASH is required for the differentiation commitment of hematopoietic stem cells in a c-Myc-dependent manner. *J Exp Med*. 2014;211(10):2119-34.
164. Deng ZH, Gomez TS*, et al.* Nuclear FAM21 participates in NF-kappaB-dependent gene regulation in pancreatic cancer cells. *J Cell Sci*. 2015;128(2):373-84.
165. Bentfeld-Barker ME, Bainton DF. Identification of primary lysosomes in human megakaryocytes and platelets. *Blood*. 1982;59(3):472-81.
166. Shen QT, Hsiue PP*, et al.* Structural insights into WHAMM-mediated cytoskeletal coordination during membrane remodeling. *J Cell Biol*. 2012;199(1):111-24.
167. Taunton J, Rowning BA*, et al.* Actin-dependent propulsion of endosomes and lysosomes by recruitment of N-WASP. *J Cell Biol*. 2000;148(3):519-30.
168. Benesch S, Lommel S*, et al.* Phosphatidylinositol 4,5-biphosphate (PIP2)-induced vesicle movement depends on N-WASP and involves Nck, WIP, and Grb2. *J Biol Chem*. 2002;277(40):37771-6.
169. Veltman DM, King JS*, et al.* SCAR knockouts in Dictyostelium: WASP assumes SCAR's position and upstream regulators in pseudopods. *J Cell Biol*. 2012;198(4):501-8.
170. Davidson AJ, Amato C*, et al.* WASP family proteins and formins compete in pseudopod- and bleb-based migration. *J Cell Biol*. 2018;217(2):701-14.
171. Zhu Z, Chai Y*, et al.* Functional Coordination of WAVE and WASP in C. elegans Neuroblast Migration. *Dev Cell*. 2016;39(2):224-38.
172. Isaac BM, Ishihara D*, et al.* N-WASP has the ability to compensate for the loss of WASP in macrophage podosome formation and chemotaxis. *Exp Cell Res*. 2010;316(20):3406-16.
173. Verboon JM, Decker JR*, et al.* Wash exhibits context-dependent phenotypes and, along with the WASH regulatory complex, regulates Drosophila oogenesis. *J Cell Sci*. 2018;131(8).
174. Steinberg F, Heesom KJ*, et al.* SNX17 protects integrins from degradation by sorting between lysosomal and recycling pathways. *J Cell Biol*. 2012;197(2):219-30.
175. Böttcher RT, Stremmel C*, et al.* Sorting nexin 17 prevents lysosomal degradation of β1 integrins by binding to the β1-integrin tail. *Nat Cell Biol*. 2012;14(6):584-92.

6 Acknowledgements

I would like to express my sincere gratitude to the following people, who helped and supported me during my time at the Institute of Experimental Biomedicine, University Hospital Würzburg and writing my doctoral thesis:

- my supervisor and working group leader Dr. Markus Bender. Thank you for giving me the opportunity to work on this project and accomplish my medical doctoral thesis. You provided me with constant support, critical input and advice during this entire time.
- Prof. Dr. Antje Gohla and Prof. Dr. Andreas Beilhack. Thank you for being part of my thesis committee and for your valuable input into my work during our committee meetings.
- Yvonne. Thank you for welcoming me into the laboratory world of D16, for teaching me all these methods and for all your constructive input into my thesis.
- Hendrikje and Ruth. Thank you for having my back and making this experience so much more fun.
- Franzi, my old friend and confidant. Thank you for staying up all night to help me practice my talks. It must have sounded like gibberish to you!
- Simon. Thank you for constantly supporting me and making me laugh with your crazy thoughts and ideas. Even though we did not have our big adventure this year, I am sure we will have thousands to come!
- And last but not least, my dear, dear family. Thank you for your constant support, incredibly helpful pep talks, proof-reading, etc. And thank you for just being the most incredible, crazy family you are. I would not be here without you!

7 Publication and poster presentation

Co-author publication

Schur Y, Sperr A, Volz J, Beck S, Reil L, Kusch C, Eiring P, Bryson S, Sauer M, Nieswandt B, Machesky L, Bender M; *Platelet lamellipodium formation is not required for thrombus formation and stability*, *Blood*, 2019, 134 (25): 2318-2329.

International poster presentation

EUREKA 2017, 12th International Symposium organised by the Doctoral Researchers of the Graduate School of Life Sciences in Würzburg, Germany, October 2017; *WASH complex subunit Strumpellin selectively regulates integrin αIIbβ3 expression*.

8 Curriculum vitae

9 Affidavit

I hereby confirm that my thesis entitled *The role of WASH complex subunit Strumpellin in platelet function* is the result of my own work. Some of the results represented in this thesis were obtained in collaboration with Dr. Yvonne Schurr and can also be found in her doctoral thesis (145). They are indicated accordingly. I did not receive any help or support from commercial consultants. All sources and/or materials applied are listed and specified in the thesis.

Furthermore, I confirm that this thesis has not yet been submitted as part of another examination process neither in identical nor in similar form.

Place, date	Lucy Reil

Eidesstattliche Erklärung

Hiermit erkläre ich an Eides statt, die Dissertation *Die Rolle der WASH-Komplex-Untereinheit Strumpellin in der Thrombozytenfunktion* eigenständig, d.h. insbesondere selbstständig und ohne Hilfe eines kommerziellen Promotionsberaters angefertigt und keine anderen als die von mir angegebenen Quellen und Hilfsmittel verwendet zu haben. Einige Daten wurden gemeinsam mit Dr. Yvonne Schurr erhoben und finden sich in ihrer Doktorarbeit wieder (145). Diese Daten sind entsprechend gekennzeichnet.

Ich erkläre außerdem, dass die Dissertation weder in gleicher noch in ähnlicher Form bereits in einem anderen Prüfungsverfahren vorgelegen hat.

Ort, Datum	Lucy Reil